Estimation of Load Carrying Capacity for Girder Bridges under a Moving Vehicle by Radar-based Displacement Measurements

レーダーを用いた変位計測に基づく走行車両による桁橋の耐荷性能評価

A Dissertation
Submitted to the Department of Civil Engineering,
Graduate School of Urban Innovation
for the Doctoral Degree,
By Zhen Sun

Yokohama National University
February 2020

Abstract

Safety of in-service bridges plays an important role in sustainable economic development and societal functioning. According to Road Maintenance Report in 2019, around 10% of the highway bridges are rated as Level 3 and 4 in Japan, which need early action or emergent action. In bridge management and maintenance, load carrying capacity evaluation of severely damaged bridges is significant to determine the repair, strengthening or traffic weight regulation countermeasures. However, traditional static proof-load test method is labor-extensive and time consuming. For expressway and rural bridges, this can rarely be conducted because of traffic closure time and budget respectively.

In this research, a displacement-based load carrying capacity estimation method is proposed for deficient girder bridges under a moving vehicle. The method is applicable for girder bridges with a span of 20~50 meters, which could be simply supported or continuous. Though only PC girder bridges are used as the examples of verification in Chapter 5, the method can be applied to steel bridges too. And bridge types include T girder bridges, void slab bridges and box girder bridges. It is also noted that the method is mainly based on bending theory, so shear load carrying capacity and shear load related defects are beyond the scope of this dissertation. The objectives of this dissertation are twofold. The first is local stiffness loss estimation caused by severe damages, based on which the bridge operators can make repair or strengthening plans. The second is load carrying capacity evaluation with displacements obtained from a truck-pass-by test, based on which the bridge operators can determine the truck weight limitation of severely damaged bridges. It serves as a more efficient substitute for traditional static load proof

test.

In Chapter 1, the background and previous relevant studies are reviewed. The displacement-based load carrying capacity estimation method is proposed with two objectives, the first is to estimate stiffness loss due to severe local damage, and the second is to evaluate the bridge load carrying capacity. At last, the outline of the whole dissertation is presented.

In Chapter 2, firstly, the load carrying capacity estimation method is described. Secondly, the correlation between curvature and stiffness loss is deducted based on beam bending theory, and the difficulties for its application in practice are summarized. Thirdly, the dynamic displacement components in truck pass-by test are investigated, and a numerical example is used to verify the idea of estimating stiffness loss from bridge dynamic displacement. This chapter mainly provides the theoretical basis of this dissertation.

In Chapter 3, the effect of measurement noise on curvature is studied with laboratory experiment of a beam model. A noise/damage effect ratio is defined to evaluate the level of noise. Two approaches are proposed to reduce the effect of measurement noise. The first one uses averaged multiple displacement measurement to minimize the noise level, and the other selects appropriate curvature calculation interval based on the noise/damage effect ratio. At last, the approach was verified on a three dimensional bridge model.

In Chapter 4, firstly, principle of the Radar device for displacement measurement is introduced, which can measure multiple points at high sampling frequency. Laboratory experiment and field test verified the precision of the displacement measurement device.

And the multi-point measurements of displacements were also utilized to predict displacement at one point to illustrate its merit.

In Chapter 5, the proposed load carrying capacity estimation method is applied on two pre-stressed concrete bridges to verify its reliability and efficiency. In the first bridge, truck pass-by test was conducted and curvature results showed no stiffness loss. The measurements were used to calibrate a finite element model, on which artificial damage of concrete spalling and prestressed tendon rupture was created. Stiffness loss estimation is performed on the calibrated bridge model, which indicated that the artificial damage is equivalent to 22.3 % of stiffness loss. In the second bridge, both static proof load test and truck pass-by test were performed, and the proposed method is applied, which showed that the proposed method with truck pass-by test can be a substitute for the static proof load test.

In Chapter 6, conclusions are drawn for this dissertation, and recommendations of future work are discussed as well for application of the proposed method in practice.

論文要旨

2019 年 8 月に国土交通省が発表した「道路メンテナンス年報」によると、722,942 連の道路橋梁のうち、多くは 1960～1980 年代に建設され、供用後 50 年を経過したのも 27%となっている。点検結果による健全性の診断では、うち 10%が段階３（早期措置段階）か段階４（緊急措置段階）に区分されている。劣化した橋梁の耐荷性能評価は、維持管理において極めて重要である。その結果に基づき、橋梁維持管理者は補修、補強あるいは交通荷重規制の手段を決める。しかし、一般的な静的荷重試験は交通規制が必要とされ、人手や時間がかかる。

本研究はこのような現状に対して、健全性診断の段階３と段階４の中小桁橋を対象に、まずレーダー装置を用いて走行車両による橋梁変位を高周波数で計測する。次に、計測した変位のノイズの影響と動的成分を分析し、処理を行う。こうした処理方法に得られた変位結果により最終的に、橋梁の耐荷性能の評価することを目的とする。この耐荷性能評価手法では、局部的に激しい損傷位置の剛度低下を評価することで、総合的に橋梁の耐荷力を判断することができる。

本論文は 6 章で構成され、内容は以下の通りである。

第 1 章「Introduction （緒論）」では、本研究の背景を述べた上で、橋梁耐荷性能評価に関する先行研究や問題点の整理を行い、本研究の位置づけを説明し、論文の目的と全体構成を示す。

第 2 章「Displacement-based load carrying capacity estimation method for girder bridges （変位による桁橋の耐荷性能評価手法）」では、本研究で提案している耐荷性能評価手法を実施する方法とプロセスについて論述する。次に、梁の曲げ理

論に基づき、曲率と橋梁の剛度低下の関係を求め、実用の際に伴う問題点をまとめた。走行車両による橋梁の変位には動的成分が含まれている。したがって、数値解析により曲率の変化から局部的な剛度低下を評価し検証した。

第 3 章「Investigation and treatment of noise in displacement measurement （変位計測に伴うノイズの考察と処理方法)」では、変位計測ノイズが曲率計算にもたらす影響を実験で調べ、処理する方法を提示する。実験室の梁の試験でノイズの影響を考察し、ノイズ/損傷影響係数を定義し、ノイズの影響を定量的に評価する。ノイズの影響を減らすために、まずは多回計測の平均変位で曲率を計算し、その有効性を示す。つぎはノイズ/損傷影響係数を基準にし、曲率計算（$\kappa(x) = \frac{w(x-\Delta x) - 2w(x) + w(x+\Delta x)}{\Delta x^2}$）の歩幅 Δx を選択する方法でノイズの影響を減らす。最後に、三次元 FE モデルでこの方法を検証する。

第 4 章「Displacement measurement with Radar device （レーダー装置による変位計測)」では、レーダー装置の変位計測の適用性を検証する。この装置は周波数変調連続波の技術を利用し、多点のターゲット距離差を 1.1 メートル分離できる。干渉原理を利用し、送信信号と受信信号の位相差の変動で観測対象点の変位を 200Hz まで計測できる。実験室で 0.03 ㎜の精度、現場の橋梁試験で 0.06 ㎜の精度を検証した。さらに、多点計測のメリットを利用し、橋梁の変位推測方法も提示する。

第 5 章「Load carrying capacity estimation for girder bridges: applications （桁橋の耐荷性能評価：実例の応用)」では、本研究で提案した耐荷性能評価手法を二つの PC 橋で検証する。一つ目の橋梁は、走行試験による変位から計算した曲率に、局部的な剛度低下がなかった。計測データで橋梁の FE モデルを校正し、人

為的な損傷（PC 鋼材の破断とコンクリートの剥離）を与え、数値解析で 22.3%の剛度低下を評価した。二つ目の橋梁は静的載荷試験と走行試験を行い、提案した方法で得られた変位と静的載荷試験で得られた変位を比較し、その有効性と適用性を明らかにする。

第 6 章「Conclusions and future work （結論）」では、本研究で得られた結果を総括するとともに、今後の研究すべき方向について述べる。

Acknowledgements

First and foremost, I would like to express my sincere gratitude to my supervisor, Prof. Yozo Fujino. I am very lucky to do research under his guidance, which is the treasure I am proud of in my life. I have learnt a lot from him in different aspects, which will inspire me in future.

I also want to thank the other dissertation committee members, Prof. Yamada, Prof. Katsuchi, Prof. Hayano, Prof. Tamura, Prof. Nagayama, Prof. Nishio and Prof. Dion. Their constructive comments and advices have improved much of this dissertation.

The help and kindness from Prof. Ishihara, Prof. Sudi and other members in Bridge and Structure Laboratory are deeply appreciated. I am also grateful to Mrs. Yokoyama and Mrs. Ootsuka, who helped with preparation of the defense.

I wish to thank my Japanese language teacher, Mrs. Shirai, who helped me to improve my Japanese. I had the valuable opportunity to have a host family, Ikeya family. I hope health and happiness for all of them. I also met many good friends in Japan, which I cherish a lot. I would like to thank the kind Japanese society to provide such chances for foreign students. Financial support from Ministry of Education, Science and Technology, Japan is gratefully acknowledged.

At last, I want to thank my family for their love and support during the past years. Their trust and understanding are indispensable in the completion of the dissertation.

Zhen Sun

February, 2020

Contents

Chapter 1 Introduction

1.1 Background

Bridges play an important role in sustainable economic development and societal functioning. By 2019, there were totally 722,942 bridges (longer than 2 m) in Japan, most of which were completed between 1960s and 1980s. According to statistics of Ministry of Land, Infrastructure, Transport and Tourism (MLIT) of Japan, 27% of the bridges are more than 50 years old, and this number will increase to 52% in 2029. As aged bridges increase, they pose a lot of challenges for bridge maintenance.

Generally, routine inspection of bridges is conducted in most countries, and condition rating is given based on the inspection results. According to the rating level, bridge operators may implement repair or strengthening on severely damaged bridges. If some defects in a bridge became more and more severe and not repaired in time, it may cause sudden collapses. United States and China are two countries which have experienced generally more bridge failures than other countries. Harik et al. (1990) conducted a study on 114 bridge failures in the United States between 1951 and 1988,

and found that more than 20 % of the failures were due to overweight, and 5% were caused by bridge aging. Wardhana and Hadipriono (2003) studied over 500 bridge failures in the United States between 1989 and 2000, revealing that 386 of them occurred in the service stage. The results also showed that 44 of the failures were due to overloading, and 43 were maintenance related, they account for 22.5 % of the bridge failures during service life. Xu et al. (2016) analyzed 302 highway bridge catastrophic collapses in China between 2000 and 2014, out of which 171 bridge collapses were during the service stage. They had an average service life of 18.7 years. Almost half of the collapses were due to overloaded trucks, and other causes include performance degradation, lack of maintenance, etc.

In Japan, there were relatively rare reports of collapsed PC bridges. On June 15, 1989, Shinsuge Bridge in Nagano Prefecture, a 25 m simply supported prestressed concrete (PC) box girder bridge collapsed after 24 years of operation. On July 16, 1990, Shimada Bridge in Gifu Prefecture, a 38 m PC cantilever cable-stayed bridge, collapsed after opening for 27 years (寺田典生, 2015). In both cases, trucks were running over the bridges, and they fell down with the bridges. It could be concluded that both bridges did not have enough live load carrying capacity, but this cannot be revealed by routine inspection.

In order to ensure that bridges are in a healthy condition, a maximum interval is regulated for routine inspection of bridges. For example, the routine inspection interval is 2 years, 3 years and 5 years in US, China and Japan respectively. Special inspection may also be scheduled by the bridge owner to investigate a particular known or suspected deficiency. In these inspections, visual observation and nondestructive techniques (NDTs)

are the main techniques which are used. Visual observation is usually the first step for bridge condition assessment, which confirms visible defects such as concrete cracking, delamination, concrete spalling, exposed corroded reinforcement etc. Size and location of these defects are recorded, and photographs are taken as documents. After that, NDTs are used to investigate the defects in more details, which can be categorized as surface testing methods and sampling methods. Surface testing includes rebound hammer, half-cell potentials, resistivity, ultrasonic pulse velocity, corrosion rate measurements etc. The procedure and limitations of these NDTs are introduced with details in most bridge inspection manuals, and have been adopted in engineering practice.

Visual inspection and NDTs can provide basic information of the bridge health condition. Though labor-intensive and time-consuming, they are the existing practice in most countries, and are specified in maintenance codes. Frankly speaking, there are very few defects which can escape detection. However, the most critical shortcoming of these methods is that they could not relate the defects with bridge stiffness loss, hence could not give any hints on load carrying capacity of bridges. This is fine for bridges with moderate defects, because the defects could be easily repaired with existing methods available. However, load carrying capacity evaluation is of significant value for bridges with severe defects. Even the defects are repaired, bridge operators care about the bridge load carrying capacity after retrofitting. Such information would be important to determine whether a weight regulation is necessary for passing trucks. If the load carrying capacity of severely damaged bridges is not determined and no traffic weight regulation is performed, in worst cases, sudden bridge collapse may occur without any warning (Woodward and Williams, 1988).

From the viewpoints of bridge operators, they care about two questions. The first is where is the defects, which could be generally answered with existing visual inspection and NDTs in engineering practice. Based on the inspection results, the bridge conditions are rated as Level 1~4, in which Level 3 and 4 bridges needs early or emergent maintenance actions. The second question is that, for bridges rated as Level 3 and 4, how much is the local stiffness loss at damaged locations, and how much is the load carrying capacity of these bridges. By answering the former, decisions on repair or strengthening plans can be made. By answering the latter, truck weight limitations can be posted on severely damaged bridges with load carrying capacity lower than design. In this way, further damages or bridge collapses can be avoided. However, the current practice of visual inspection and NDTs cannot provide answer to this question. According to statistics of MLIT, Japan, among the 722, 942 bridges (longer than 2 m), almost 10 % falls into bridge condition rating level 3 and 4, which needs for early action or emergent action. By 2022, almost 40 % of all the bridges in Japan will become more than 50 years old, which poses more and more challenges for bridge management and maintenance.

Apart from condition rating, which is usually conducted based on results of visual inspection and NDTs, there are also load rating requirements in bridge maintenance codes in US (AASHTO, 2011) and China (JTG /TJ21, 2011). However, there is no such requirement in bridge maintenance codes in Japan. This is probably due to the fact that the emphasized bridge seismic load capacity in design can largely improve the real bridge live load carrying capacity compared with the bridges in US and China. However, as bridges age, they become more deteriorated and the load carrying capacity is decreasing. In US and China, the load carrying capacity is evaluated with static proof load test. During

the test, more than 10 personnel are often allocated, and traffic closure is often required which lasts 5 to 8 hours. This is indeed expensive considering the necessary labor forces and traffic closure time. In Japan, static proof load test is not in the bridge maintenance code, but is sometimes conducted by the bridge operators to confirm load carrying capacity of severely damaged bridge. For example, proof load test was conducted on Myoko Bridge in Niigata Prefecture, which is a severely damaged PC box girder bridge. This kind of load test is rarely performed in Japan because of high cost, especially for expressway bridges and rural bridges. In the former, traffic closure is almost impossible, and in the latter, there is often very little budget available to perform such tests.

From the viewpoint of bridge maintenance, the bridge operators care about the following questions.

First, where are the defects in a bridge? This question can already be answered by the existing condition rating practice, which mainly uses visual inspection and non-destructive methods such as infrared thermography method, impact elastic wave method, acoustic emission method, supersonic method, etc. There are already maintenance codes or manuals in most countries around the world.

Second, suppose a bridge is rated as in a poor condition, such as Level 3 or Level 4 in the bridge condition rating system in Japan (Table 1.1).

In a local scale, how much is the stiffness loss at the location of damages? Knowing this will help bridge operators to decide repair or strengthening countermeasures. Results from the current condition rating cannot answer this question yet.

In a global scale, how much is the load carrying of the damaged bridge? Knowing

this question will provide reference for posting truck weight limitations, which can prevent further damage or even collapse of the bridge when a very heavy truck passes over.

To address these questions, in this dissertation, a displacement-based load carrying capacity estimation method is proposed for damaged girder bridges, with Radar-based displacement measurements under a moving truck. .

1.2 Literature review

1.2.1 Introduction

The cornerstone of bridge preservation is inspection. In Japan, bridge inspection is conducted by experienced bridge inspectors, and the condition rating of the bridge is determined as one of the four levels shown in Table 1. 1.

Table 1.1 Four level of bridge condition rating (国土交通省道路局, 2019)

Level	Condition	Description
I	Healthy	No adverse effect on bridge function
II	Preventive maintenance	No adverse effect on bridge function, but action is required from point of view of preventive maintenance
III	Early action	Possible adverse effect on bridge function, and early
IV	Emergent action	Adverse effect or probable adverse effect on bridge function, emergent action required

In Japan, rating for load carrying capacity is not required in bridge maintenance codes. In comparison, load rating is required in US and China codes. It is conducted for bridges designed with old design standards, bridges with severe visual damages and retrofitted bridges. Field test is often performed when bridge design documents are not

available, or analytical computation methods are not able to determine the load carrying capacity. Static load test is implemented step by step, which costs a lot of time and labor.

In addition to the aforementioned methods used in bridge standards or guidelines, there are also other methods to assess the structure properties based on response such as displacement, acceleration, strain, etc. Damage is often simplified as changes in material and geometric properties or boundary conditions (Farrar and Worden, 2007). In recent years, different damage estimation techniques have been developed to avoid sudden and premature failure of bridges.

Vibration-based damage estimation has attracted interests from researchers for a long time. The basic idea behind vibration-based methods is that localized structural damage will cause change in dynamic parameters of structures. These dynamic parameters include mode frequency, mode shape and mode shape curvature (Pandey et al., 1991). Detailed review of these methods can be found in some previous literature (Salawu 1997; Doebling et al. 1998, Farrar et al. 2001). The methods utilizing modal parameters need analytical models or test data of undamaged structure as a baseline, which is often unavailable. Environment conditions such as temperature or humidity also contribute to changes in structural mode properties, making damage identification difficult (Sohn et.al. 1999, Sohn 2007; Xia et.al. 2011). Generally, global modes reflect the whole performance of the structure, and they are not sensitive to local damage. Local modes are very difficult to excite, and many sensors are needed to capture the local behavior in measurement, which is costly in time and labor work. .

1.2.2 Review on load rating and proof load test

Generally, periodic inspection is specified in codes of most countries, with visual inspection and non-destructive techniques as the main methods. Conditions of bridges are rated into different levels, and the deficient bridges are payed more attention by bridge operators. In order to determine rational and economic countermeasures such as repair, strengthening or traffic weight regulation, load carrying capacity evaluation of severely damaged bridges is often needed.

Bridge load carrying capacity evaluation could be carried out by computation based on design drawings and simplified boundary conditions. Inspection results on local damages are also incorporated to achieve a more realistic modeling of the bridges. Ghosn *et al*. (1986) proposed an approach to incorporate field test results in the load rating process. The collected data of traffic weights and volume, stress and girder distribution factors could improve the accuracy of load rating. Nowak and Tharmabala (1988) used bridge load test data to evaluate the actual load carrying capacity more accurately, and it is demonstrated with an example of a steel truss bridge. Chajes *et al*. (1997) conducted tests which showed that the girders were acting compositely with the concrete deck, and that the support was having significant restraints. A numerical model of the bridge was developed to determine the bridge load rating. Brownjohn *et al*. (2001) described a sensitivity-analysis-based finite element model updating method, and applied it to condition assessment of real bridges. Jauregui and Barr (2004) performed a load rating analysis on the I-40 Bridge, and field test data and finite element analysis results were considered to obtain a more realistic rating result. Rens *et al*. (2005) proposed a methodology to integrate non-destructive field test with bridge evaluation using a Markovian deterioration model. Ding et al. (2012) incorporated model updating with field

test data in a nonlinear finite element analysis to predict the behavior of a slab-girder bridge. Nonlinear analysis is performed on the updated model to evaluate the bridge load carrying capacity, which verified its effectiveness.

It is believed that computation methods may not reflect the real status of the bridge, due to the variation in factors such as material properties, boundary conditions and composite action (Bakht and Jaeger, 1990; Saraf and Nowak, 1998). In addition, design documents may not be available for some bridges. As such, static proof load test is sometimes adopted for deficient bridges in engineering practice (Faber et al., 2000; Wisniewski et al., 2012; Casas and Gomez, 2013). The proof load test is often preferred as it can demonstrate the resistance of the tested bridge with reduced uncertainty (Fujino and Lind 1977). There are codes and guidelines for assessment of load carrying capacity in UK (Highway Agency, 2006), Denmark (Danish Road Directorate, 1996; 2004.), US (AASHTO, 2003) and China (Ministry of Transport, China, 2011).

In bridge maintenance codes, load rating is often defined to determine the live-load carrying capacity of an existing bridge. In US, highway bridge load rating is conducted with the AASHTO specification *Manual for Bridge Evaluation (2011).* A rating factor (RF) is used to demonstrate the live load carrying capacity, which is the ratio of available live load carrying capacity to the live load demand due to passing truck loadings.

$$\mathrm{RF} = \frac{C - A_1(DL)}{A_2(LL)(1+I)} \tag{1.1}$$

In which, C denotes the capacity of the bridge; DL and LL denote the dead load and live load effects respectively; A_1 and A_2 are magnification factors for dead load and live load respectively; I is the impact factor for the live load.

In a load rating analysis procedure, RF can be calculated for each bridge member under specified truck loading. If RF is smaller than 1, it indicates that the bridge cannot satisfy the designed live load carrying capacity. Proof-load test is often used to evaluate the realistic live load carrying capacity of a bridge, as it directly provides the bridge member responses under truck loading. Based on the test result, an adjustment factor is incorporated into the load carrying capacity evaluation procedure. It may also permit utilization of possible sources of strength that are neglected or not revealed in the analysis (Fujino Y., and Lind N.C, 1977).

1.2.3 Review on stiffness loss estimation methods using displacement

As widely known, displacement is directly correlated with stiffness and load carrying capacity of a bridge. Besides, displacement is an important indicator for bridge behavior, which is specified in bridge evaluation codes or guidelines (AASHTO, 2011). There have been a lot of efforts by researchers to utilize bridge displacement response for quantitative bridge condition assessment. Compared with other damage evaluation methods, displacement curvature-based methods have been recognized as more sensitive to damage (Wenzel H. 2009).

Some researchers have concluded that static deflection is a local phenomenon related to damage or stiffness loss, while dynamic response is a global or distributed phenomenon (Jekins et al. 1997). Numerical and experimental investigations have shown that it is more sensitive to local damage than natural frequency.

For plate-like structures, deflection curvature was proved to be the most sensitive in numerical and experiment study by Yam et al. (2002). They investigated static parameters

such as out-of-plane deflection, and its slope and curvature. In comparison with dynamic parameters and strain frequency response function, deflection curvature was shown to be most sensitive among analyzed parameters. Another advantage of curvature for damage estimation is that a baseline model of undamaged structure is not needed. Sanayei and Onipede (1991) estimated structural stiffness at the element level from applied static forces and displacement measurements through an algorithm to solve sensitivity matrix. Banan et al. (1994) proposed algorithms for estimating member constitutive properties of a bridge model from measured displacements under known static loading. They were based on the concept of minimizing an index of discrepancy between model and measurements. These methods deal mainly with space structure such as truss, and damage estimation is at member level. Choi et al. (2004) utilized static displacement changes between undamaged and damaged states for damage identification of bridges. Maxwell-Betti Reciprocal Theorem was suggested as an alternative to obtain more deflection measurement with limited displacement transducers. Effect of measurement noise was not studied, and damage extent was not assessed.

Compared with the methods based on mode properties, the advantages of displacement-based methods are as follows. First, baseline of structure under undamaged state is not needed. Second, displacement curvature could reflect change in stiffness, which leads to quantitative assessment of damage extent. However, dense displacement measurements are needed to obtain curvature. In reality, bridges are often built over rivers or highways. Linear Variable Differential Transformer (LVDT), the most frequently used contact-type sensor for displacement measurement, needs stable fixed reference point. This makes field measurement work very difficult, if not impossible.

To cope with this difficulty, Maxwell-Betti reciprocal theorem can be utilized to obtain dense measurement. Instead of measuring displacement with dense displacement transducers, vehicle can run across the bridge and displacement is measured at a single point. The displacement measurements are equivalent to deflection of the bridge under a concentrated load.

Stohr et al. (2006) measured inclination influence line with an inclinometer at the left support in laboratory test of a girder under moving load. The moving load was applied by weights and pushed by hands. Simulation of damage was made by stiffening some cross sections with plates. Difference before and after damage was calculated to detect the damage. Field test on a pedestrian bridge was also conducted, and location of stiffness modification was successfully located. In case of lack of reference of undamaged state, a finite element model (FEM) was proposed.

Cheng et al. (2012) evaluated stiffness of a uniform simply supported beam using dynamic displacement influence line under moving load. Displacement response was calculated from theoretical model. Empirical mode decomposition (EMD) and window smoothing are applied to displacement response to obtain the quasi-static influence line. Comparison results showed EMD cannot effectively remove all the modal vibration part of the response. Using quasi-static displacement filtered by window smoothing, curvature is calculated as second derivative of the displacement. By dividing moment diagram, the flexural stiffness was recovered. Through parameter study of moving speed, it is concluded that reducing moving speed leads to larger range of steady recovered stiffness. With speed at 10 km/h, stiffness distribution at central 80% of the span can be reasonably assessed.

1.2.4 Review on stiffness loss evaluation using a moving vehicle

Regarding condition assessment of bridges in the long run, the need to reduce the dependence upon excitation forces is noted by many researchers (Doebling et al. 1998). The use of operating loads such as a vehicle will reduce the cost in the field investigation. Stiffness loss evaluation methods utilizing dynamic responses under a moving vehicle are reviewed in this section.

Mazurek and Dewolf (1990) conducted experimental study on a two-span aluminum plate-girder bridge model with vehicular excitation. The effects of roadway roughness (bumps using different thicknesses and spacing of duct tape strips), vehicle velocity, and damage on resonant frequencies and mode shapes were investigated. The results show that resonant frequencies and mode shapes are not influenced by vehicle velocity or roadway roughness. Mass of vehicle has significant effect on resonant frequency, but minimal influence on mode shapes. Released support and crack damage (29%, 32% and 33% at mid-span) cause change in frequency and mode shapes, and change in mode shape is used to determine the damage location. Mahamound (2001) presented a procedure for determining stress intensity factors (SIF) for single and double edge cracks in simply supported undamped Bernouli-Euler beams under a moving load. The approach is based on using modal analysis to determine the equivalent load on the beam, with results showing (a) SIF of moving load is larger than same static load; (b) it is largest when the crack is near mid-span, and the load is at or shortly after it reaches mid-span. Mahamound and Zaid (2002) developed an iterative modal analysis approach to determine the effect of transverse crack on the dynamic behavior of simply supported undamped Bernouli-Euler beams subject to a moving mass. The presence of crack results in larger

displacements and alters the beam response patterns. Huang (2001) applies HHT to a model of simply supported bridge with loading of three axle truck. Damage is simulated as reduction in cross section. The research used undamaged model as baseline, and used the variation of local frequency and deformation to detect the damage. The research claimed that HHT could deal with non-stationary and nonlinear time series. However, there is limitation that a baseline of undamaged model is needed, and the damage extent is 50% reduction of cross-section, which is not realistic. The use of variation in displacement is very vague, and accurate detection is not optimistic. The use of variation in frequency still has the same problem as wavelet analysis, as the author criticized, shorter local time sub-series would make frequency resolution worse. Lee et al. (2002) investigated the feasibility of detecting structural deterioration in highway bridges using vehicular excitation in laboratory. The damage assessment is carried out based on the estimated modal parameters using the neural networks technique. Simply supported bridge model is built in laboratory, which is loaded by moving vehicle model. Damage was inflicted by cutting of bottom flange. Because frequency changes according to weight of vehicle model, the frequency ratio before and after damage is chosen as parameter and input to neural network. Majumder and Manohar (2003) proposed a time-domain approach for damage estimation using vibration data with moving oscillator as excitation source. Effects such as dynamic interaction between vehicle and the bridge, bridge deck unevenness, spatial incompleteness of measured data and presence of measurement noise are incorporated into analysis. A validated finite element model for the bridge structure in its undamaged state is assumed to be available. Bilello and Bergman (2004) conducted theoretical and experimental study of response of a damaged Euler-Bernoulli beam traversed by a moving mass. Damage is modeled through rotational springs connecting

two intact sections. The analytical solution is based on the series expansion in the basis of beam eigen-functions. And it is validated through experimental tests on a small-scale bridge model. Experimental results of natural frequency and deflection agrees well with theoretical predictions, with experimental response being larger. Compared with natural frequency, deflection showed larger difference between undamaged and damaged case, indicating higher sensitivity of deflection to damage. Law and Zhu (2004) studied the dynamic behavior of damaged reinforced concrete bridge structures under moving vehicular loads. The vehicle is modeled as a moving mass or moving oscillator, and bridge is modeled as a simply supported Euler-Bernoulli beam. A damage function representing either the open crack model or breathing model is used to model the crack zone in the reinforced concrete beam. An experimental study is performed on a reinforced concrete beam with T-section subjected to vehicular loadings. Effects of parameters like moving speed, road surface roughness and oscillator parameters are studied. Dynamic displacement, relative frequency change (RFC), absolute frequency change (AFC) and phase plot of the responses are studied, showing dynamic displacement and RFC can be sensitive indicator of damage in bridge structures. Gonzalez and Hester (2009) performed wavelet transform on response of damaged bridge under moving load, and investigated feasibility of this method to detect the damage. It is concluded that multiple measurement points need to be used to detect and accurately locate damage, mainly due to the fact that closer measurement location to damage will provide best result. However, from the paper it is found that sensor location causes clear peak in wavelet coefficient line rather than damage. The influence of damage on peak is totally lost compared with that caused by sensor location. Hester and Gonzalez (2012) applied wavelet-based approach to acceleration signal of bridge under moving vehicle. Wavelet energy content, proving to

be more sensitive than wavelet coefficient line, is used at each bridge section. Higher vehicle speed is found to weaken the method to detect damage, due to shorter singularity at damage location. Meredith and Gonzalez (2012) used empirical mode decomposition to detect and locate damage in a bridge using acceleration response to the crossing of a vehicle. Damage is identified through a distinctive peak in decomposed signal. Damage is simulated as localized loss of stiffness. The influence of damage size and location, road surface smoothness, vehicle speed sensor location is studied. The limitations are (1) weight of the vehicle should be increased for rough road surface, while the increased weight 50 ton or 200 ton is unavailable in reality; (2) sensor location also causes peak in the signal, whose effect cannot be distinguished from that caused by damage.

In the previous studies, very few have tried to evaluate damage effects using dynamic displacement of bridges under a moving vehicle. In those few literatures which did, limitation is summarized as: (1) simplified analytical beam model is used, which is not practical; (2) a baseline of undamaged bridge state is needed.

The previous curvature-based studies were not used much in engineering practice, which is mainly due to the following reasons.

First, dense measurement of displacement through the bridge span is necessary to calculate curvature, but such measurement is impossible with traditional LVDT or dial gages.

Second, according to Maxwell-Betti Theorem, the dense measurement could be equivalent to dynamic displacement under a moving vehicle. However, there is dynamic component in obtained dynamic displacement, which should be treated in curvature

calculation. Besides, new type of displacement sensor with high-frequency measurement is needed.

Third, curvature calculation is very sensitive to measurement noise, and its effects should be investigated and treated.

1.3 Research objectives and outline

1.3.1 Research objectives

In this dissertation, a displacement-based capacity estimation method is proposed for girder bridges. It has the potential to estimate the local stiffness loss due to severe defects more reliably and evaluate bridge load carrying capacity more efficiently, which are from local and global scales respectively. The method is applicable for girder bridges with a span of 20~50 meters, which could be simply supported or continuous. It is also noted that the method is mainly based on bending theory, so shear load carrying capacity and shear load related defects are beyond the scope of this dissertation. The objectives of the research are as follows.

1) To develop a load carrying capacity estimation method using moving-vehicle-induced displacement for damaged girder bridges, which includes local stiffness loss estimation and live load carrying capacity evaluation;

2) To propose a dynamic displacement treatment approach for curvature based stiffness loss estimation;

3) To investigate the effect of measurement noise on application of the displacement-based method, and propose approaches to reduce noise effects;

4) To verify the method on real bridges, with a moving truck as the loading condition, and a Radar device for displacement measurement.

1.3.2 Research outline

Organization of the dissertation is as follows.

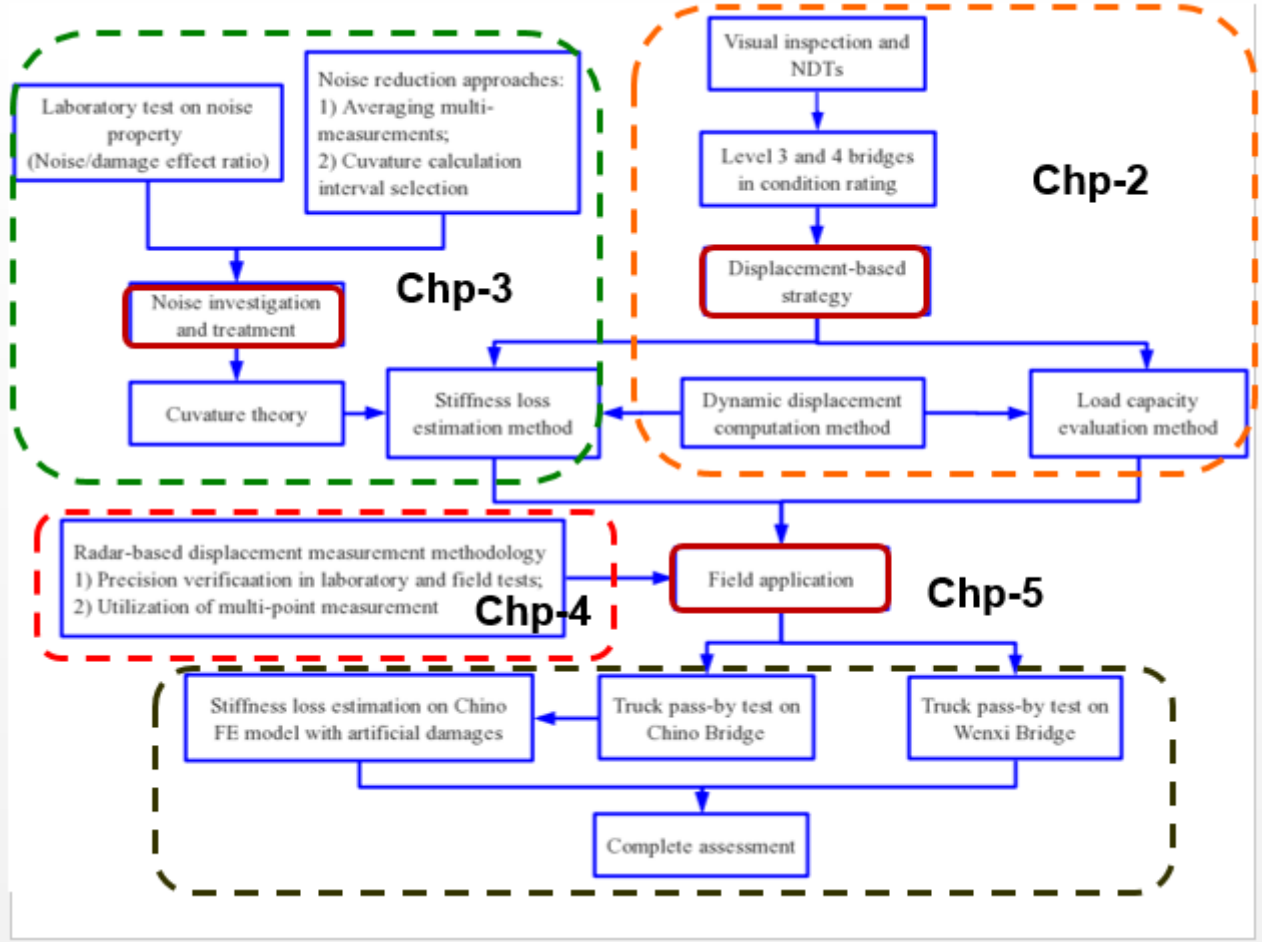

Fig 1.2 Outline of the dissertation

In Chapter 1, the background and previous research on current studies are reviewed. The displacement-based load carrying capacity estimation method is proposed with two objectives, the first is to estimate stiffness loss due to severe local damage, and the second is to evaluate the bridge load carrying capacity. At last, the outline of the whole dissertation is presented.

In Chapter 2, firstly, the load carrying capacity estimation method is described. Secondly, the correlation between curvature and stiffness loss is deducted based on beam bending theory, and the difficulties for its application in practice are summarized. Thirdly, the dynamic displacement components in truck pass-by test are investigated, and a numerical example is used to verify the idea of estimating stiffness loss from bridge dynamic displacement. This chapter mainly provides the theoretical basis of this dissertation.

In Chapter 3, the effect of measurement noise on curvature is studied with laboratory experiment of a beam model. A noise/damage effect ratio is defined to evaluate the level of noise. Two approaches are proposed to reduce the effect of measurement noise. The first one uses averaged multiple displacement measurement to minimize the noise level, and the other selects appropriate curvature calculation interval based on noise/damage effect ratio. At last, the approach was verified in a three dimensional bridge model.

In Chapter 4, firstly, principle of the Radar device for displacement measurement is introduced, which can measure multiple points at high sampling frequency. Laboratory experiment and field test verified the precision of the displacement measurement device. And the multi-point measurements of displacements were also utilized to predict displacement at one point to illustrate its merit.

In Chapter 5, the proposed load carrying capacity estimation method is applied on two pre-stressed concrete bridges to verify its reliability and efficiency. In the first bridge, truck pass-by test was conducted and curvature results showed no stiffness loss. The measurements were used to calibrate a finite element model, on which artificial damage of concrete spalling and prestressed tendon rupture was created. Stiffness loss estimation is performed on the calibrated bridge model, which showed 22.3 % of stiffness loss. In the second bridge, both static proof load test and truck pass-by test were performed, and the proposed method is applied, which showed that the proposed method with truck pass-by test can be a substitute for the static proof load test.

In Chapter 6, conclusions are drawn for this dissertation, and recommendations of future work are provided as well for application of the proposed method in practice.

Chapter 2 Displacement-based load carrying capacity estimation method for girder bridges

In recent year, there is more and more concern over load carrying capacity of aging bridges, based on which maintenance plan such as repair or strengthening can be made. In addition, traffic weight limitation can also be regulated for severely damaged bridges with load carrying capacity lower than design. In this chapter, the load carrying capacity estimation method is proposed for bridges rated as Level 3 and 4, and it has two goals. They are stiffness loss estimation and load carrying capacity evaluation, which are in local and global scales respectively. The estimation result provides information of health condition of existing bridges in light of ability to bear live loads.

2.1 Description of the proposed method

2.1.1 Background

In engineering practice, bridge condition assessment often requires rating of the bridge status, which involves periodic bridge inspection and load carrying capacity evaluation. In US and China, proof load test is required to evaluate load carrying capacity of bridges. The relevant guidelines are The Manual for Bridge Evaluation (AASHTO, 2011) and Highway Bridge Maintenance standards (China, 2011) respectively. A flowchart of the bridge condition assessment is illustrated in Fig 2.1.

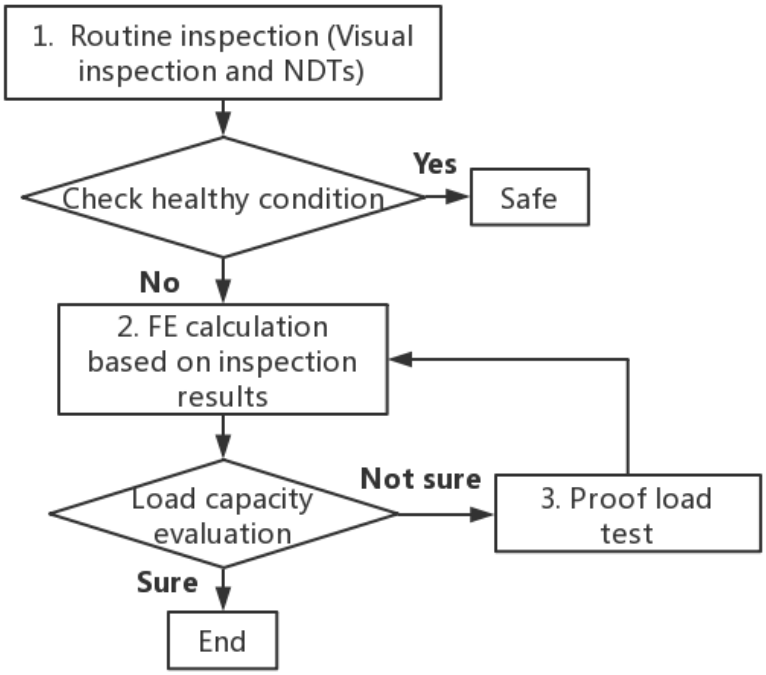

Fig 2.1 Flowchart of bridge condition assessment in US and China

In Japan, bridge condition rating is mainly based on bridge member rating. Proof load test is not required, but in some rare cases, static proof load test can be performed as reference for load carrying capacity evaluation. For example, static proof load test was performed on Myokyo Bridge in 2011 in Niigata prefecture as shown in Fig 2.2.

Fig 2.2 Static proof load test on Myoko Bridge in Nov, 2011

2.1.2 The displacement-based load carrying capacity estimation method

In August, 2019, Road Maintenance Report was published by MLIT of Japan, as shown in Fig 2.3. It is observed that Level 1 and 2 bridges take up 41 % and 49 % respectively, while Level 3 and 4 account for 10 % and 0.1 %. Therefore, early action and emergent action are needed for the 68,369 and 682 bridges respectively. Considering the large volume of these bridges, it is a big challenge for bridge management and maintenance, and determination on repair, strengthening or traffic weight regulation is not an easy job.

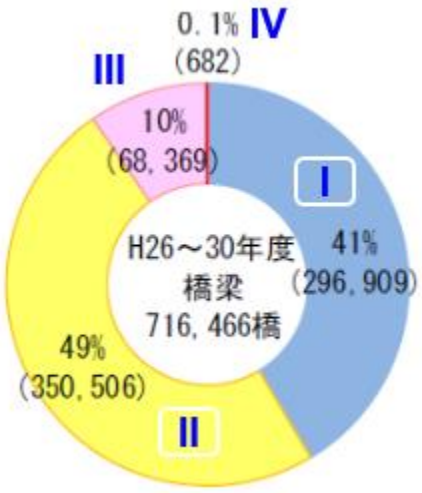

Fig 2.3 Percentage of bridges in different level of condition rating
(From 'Road Maintenance Report', 2019)

Static proof load test is a main method to assess the load carrying capacity of existing bridges (Faber et al., 2000; Wisniewski et al., 2012; Casas and Gomez, 2013) with increasing load steps. The actual load carrying capacity of a bridge is often higher than the analysis result, which may be due to system effects, load redistribution or variation in material property (Bakht and Jaeger, 1990; Saraf and Nowak, 1998). Therefore, a proof load test is often preferred as it can demonstrate the resistance of the tested bridge with

reduced uncertainty (Fujino and Lind 1977). However, a complete static proof load test is very expensive to perform. For example, for a short or medium span bridge, one test costs up to 6% of the bridge replacement cost in New South Wales, Australia (Faber et al., 2000). In addition, it takes almost 1 day to install the instrumentation of strain gauges and displacement sensors, and another half a day to conduct the test. Closure of all traffic lanes is required, which is very difficult to implement, and almost impossible on expressways.

The proposed method uses displacement in the bridge girder under a pass-by truck, and it is applicable for short or medium span damaged girder bridges. After finishing the preparation work, the bridge load carrying capacity estimation with the proposed method can be performed as described in the following flowchart. And the procedure can be implemented in seven steps.

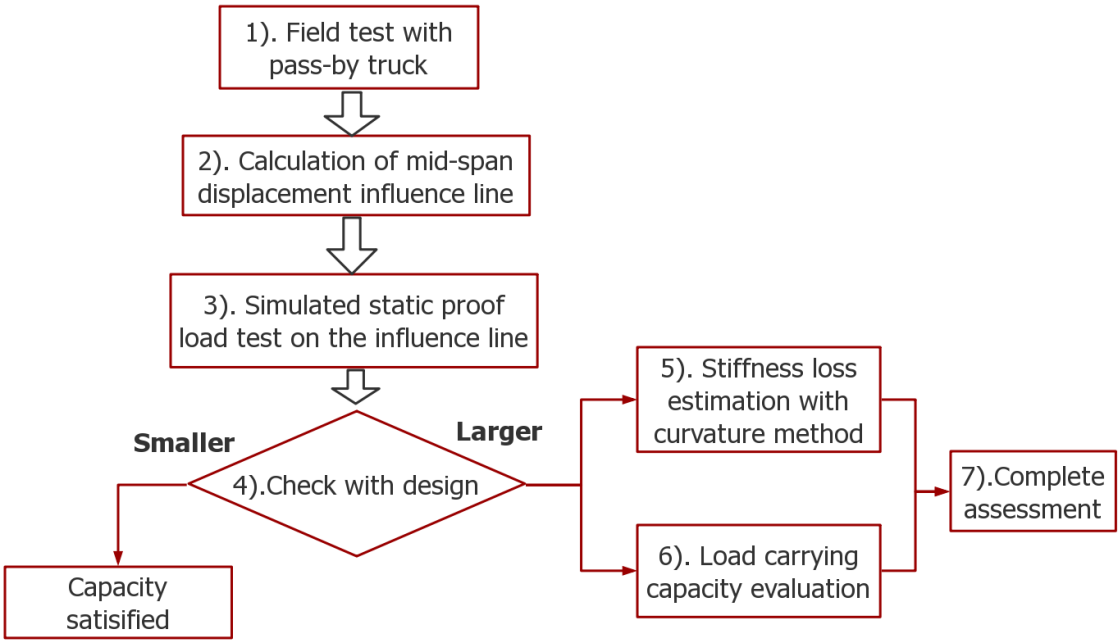

Fig 2.4 Procedure for condition assessment of girder bridges

Step 1—Execution of the test, with Radar device for measurement. The procedure includes: 1) Measurement of relative displacement between the Radar device and the reflectors. 2) Traffic regulation with road cones and two persons for traffic control. During the truck pass-by test, public vehicles and pedestrians are not allowed to enter the testing area.

Step 2—Processing of the displacement measurements during the truck pass-by test, and calculation of mid-span displacement influence line.

Step 3—Conduction of simulated static proof load test on the influence line.

Step 4—Check with the design documents. If the displacement is smaller than design, it indicates that the bridge is in a healthy condition and the load carrying capacity can be satisfied. The load carrying capacity estimation procedure is completed. If the displacement is larger than design, step 5, 6 and 7 are performed.

Step 5—Stiffness loss estimation is performed with the curvature method.

Step 6—Load carrying capacity evaluation is performed and the load rating factor is obtained as follows.

$$LF = \frac{y_d}{y_t} \times RF_0$$

In which y_t is the displacement obtained with the proposed method, and y_d is the displacement under the same condition according to design. RF_0 is the load carrying capacity based on calculation with Equation 1.1. If LF is larger than 1, the bridge cannot satisfy the designed load carrying capacity, and countermeasures should be taken.

Step 7—Complete assessment of the bridge, and determination on repair,

strengthening or truck weight limitation countermeasures.

2.1.3 Maxwell-Betti Reciprocal Theorem

In order to explain the proposed method using dynamic displacement under truck pass-by test, Maxwell-Betti Reciprocal Theorem (Timoshenko and Goodier, 1951) adopted as the basis for the concept of influence line. The theorem is explained as follows. Consider a beam in two states; it is loaded by P1 and P2 in state 1 and state 2 respectively. Maxwell-Betti Reciprocal Theorem states that the work of the forces of the first state on the displacements of the second state is equal to the work of forces of the second state on the displacements of the first state.

This is illustrated in Fig 2.5. In case 1, the beam is first loaded by P1 at position 1, which causes displacement d11 at position 1. Then keeping P1 in position, load P2 is applied at position 2, which causes displacement d12, d12 at position 1 and 2 respectively. The total work done on the beam is

$$W_1 = P_1(d_{11} + d_{12}) + P_2 d_{22} \tag{2.1}$$

Where the first subscript i in d_{ij} denotes displacement position, and second subscript j denotes the load.

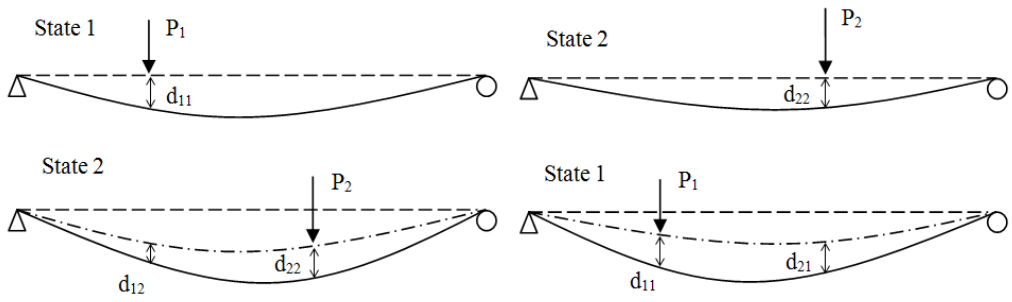

(a) Case 1: loading sequence P_1, P_2 (b) Case 2: loading sequence P_2, P_1

Fig 2.5 Illustration of Maxwell-Betti Theorem: beam loaded in two cases

In case 2, oppositely, the beam is first loaded by P2 at position 2, which causes displacement d22 at position 2. Then keeping P2 in position, load P1 is applied at position 1, which causes displacement d11, d21 at position 1 and 2 respectively. The total work done on the beam is:

$$W_2 = P_2(d_{22} + d_{21}) + P_1 d_{11} \tag{2.2}$$

As the beam is loaded in elastic stage, changing the loading sequences will not affect the work of the forces on the beam. Therefore the work done in two states are the same, $W_1 = W_2$, it is derived that

$$P_1 d_{12} = P_2 d_{21} \tag{2.3}$$

If amplitudes of P1 and P2 are the same, d12 and d21 will have the same value. Therefore as an important application, the displacement of a beam can be obtained at high density under moving load P, as shown in Fig 2.6. When load P is applied on each position on the beam at time t1, t2, t3, t4, t5 …, displacement are measured. The result is equivalent to displacement under load P applied at the position of measurement, which is also the basis of the concept of influence line.

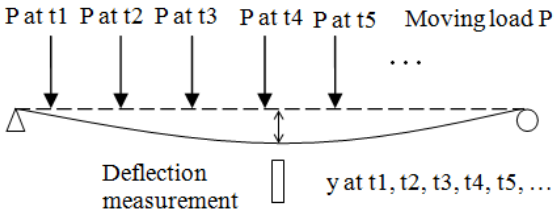

Fig 2.6 Maxwell-Betti Theorem for dense displacement measurement

2.2 Curvature based local stiffness loss estimation method

2.2.1 Comparison between different displacement-based parameters

For a beam type structure, local stiffness loss estimation can be conducted with

different displacement characteristics, which are displacement, slope (first derivative) and curvature (second derivative) respectively. For example, Choi et al. (2004) used static difference between displacement amplitude in undamaged and damaged states for damage estimation.

In the following example, a simply supported beam is used for comparing the feasibility of the three characteristics in stiffness loss estimation. The beam is 1 m long with the bending stiffness $EI = 93\,\mathrm{N}\cdot\mathrm{m}^2$. The load $F = 5N$, applied at 0.6 m position. Stiffness loss of 15 % is simulated at range between 0.31 m and 0.36 m, as shown in Fig 2.7. Displacement amplitude, slope and curvature of the beam were obtained in Fig 2.8 (a), (b) and (c).

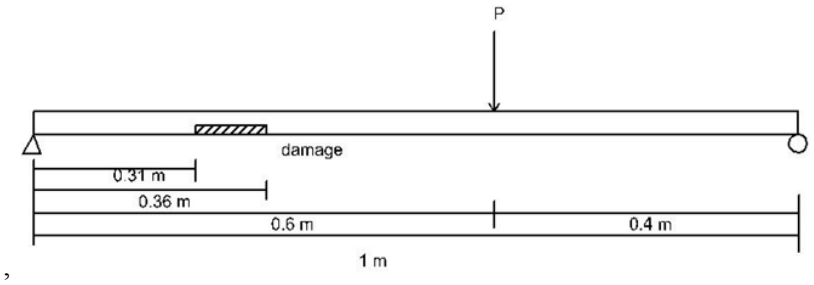

Fig 2.7 Damaged beam for analysis

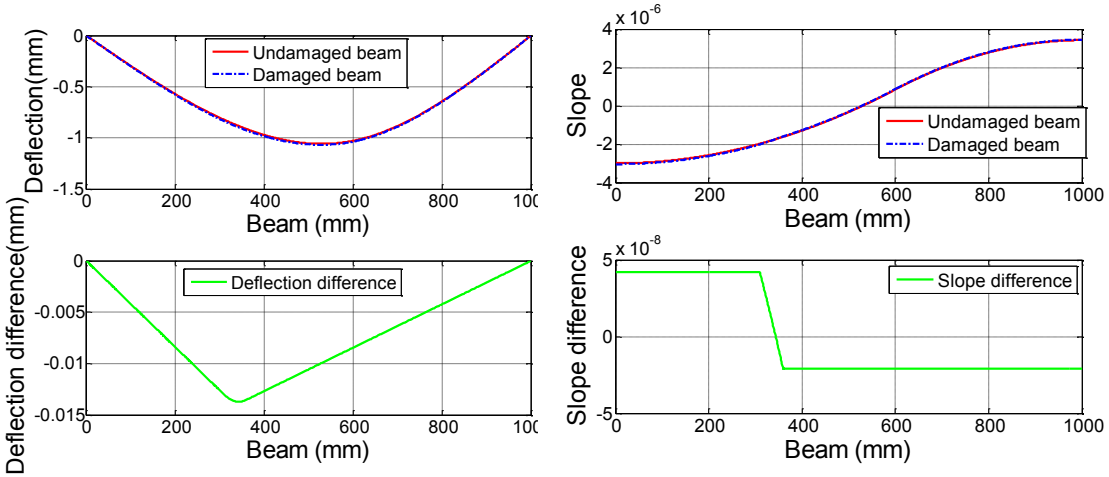

(a) Change in deflection (b) Change in slope

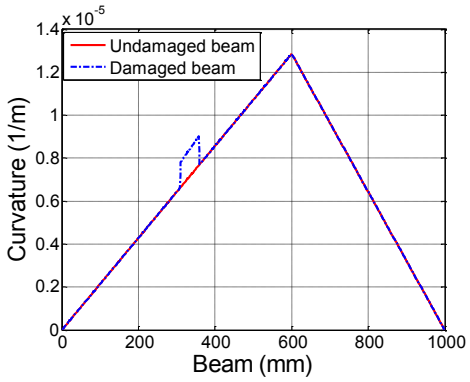

(c) Change in Curvature

Fig 2.8 Changes in displacement, slope and curvature due to local damage

It can be observed that for displacement and slope, baseline of undamaged state is needed to detect and estimate the local stiffness loss. In addition, it is obvious that the amplitude difference between undamaged and damaged state is less than 2 % of the maximum value for displacement and slope respectively. For real bridges, baseline of undamaged state is often unavailable, and analytical model or finite element model is often used as baseline. However, analytical model or finite element model is only an approximation, and modeling inaccuracy could be larger than 2 %. As a result, stiffness loss using displacement or slope is unpractical. In contrast, stiffness loss can be evaluated from curvature change without baseline of undamaged state. This could lead to better understanding of bridge health condition from a practical perspective.

2.2.2 Theoretical explanation

Stiffness loss estimation with displacement curvature can find its origin from bending theory of beam. Based on theory on strength of materials (Timoshenko, 1955), bending moment of a beam is expressed as

$$\mathrm{M(x)} = -EI(x)\frac{\mathrm{d}^2 w(x)}{dx^2} \qquad (2.4)$$

In which, E is Young's modulus of the material, I is the second moment of area of beam cross-section, w(x) is displacement of the beam, x is the beam length coordinate, M(x) is the bending moment.

Curvature $\kappa(x)$ of the beam, can be expressed as

$$\kappa(x) = \frac{\mathrm{d}^2 w(x)}{dx^2} = -\frac{\mathrm{M(x)}}{EI(x)} \tag{2.5}$$

For a uniform beam, with flexural rigidity invariant along the length, the curvature $\kappa(x)$ should have the same distribution as bending momentM(x). If there is stiffness loss in some location, there will be abrupt change of curvature at corresponding location. As curvature can be calculated from second derivative of displacement, it is possible to use displacement measurements of a beam to detect any curvature change and estimate stiffness loss.

Local stiffness loss is defined as follows.

$$\alpha = \frac{EI_i - EI_d}{EI_i} \tag{2.6}$$

Where EI_i and EI_d denote the stiffness in damage range under intact and damage state.

From aforementioned equations, stiffness loss could be calculated.

$$\alpha = 1 - \frac{\kappa_i}{\kappa_d} \tag{2.7}$$

Where κ_d is directly obtainable from curvature figure; κ_i is obtained from linear fitting of curvature results at non-damaged range.

2.3 Stiffness loss estimation using dynamic displacement

In truck pass-by tests of bridges, however slow the vehicle is, there is dynamic component in the displacement, and its effect should be investigated. The vehicle bridge interaction problem is shortly introduced, and a computation method is proposed and used in this research. Then a numerical example is used to illustrate application of the curvature method for stiffness loss estimation.

2.3.1 The vehicle-bridge interaction analysis

The dynamic problem of moving vehicle and bridge has been a subject of interest for a long time. From theoretical point of view, the system contains the vehicle and the bridge, which interact with each other through a contact force. The force is time dependent, and acts at the contact point between the wheel and road surface. It varies in amplitude as a result of vibration of two subsystems. Depending on accuracy of the models used, this problem has been studied by many researchers.

The problem of vehicle bridge interaction can date back to more than one century ago. On May 24, 1847, Dee Railway Bridge collapsed with five fatalities in Chester, England (Simmons,1847). After the accident, Willis (1849) and Stokes (1849) investigated the failure, and the bridge was loaded under a moving vehicle with constant velocity.

For an undamaged beam under a moving force at constant velocity, the closed-form

solution is available. Timoshenko studied the case in which the moving load has no mass, and the bridge was modeled with a uniform simply supported beam. Dynamic displacement of the bridge is obtained as follows (Weaver et al., 1990).

$$v = -\frac{2Pl^3}{m\pi^2}\sum_{i=1}^{\infty}\frac{\sin\left(\frac{i\pi x}{l}\right)}{i^2\left(i^2\pi^2a^2-\dot{u}^2l^2\right)}\sin\left(\frac{i\pi it}{l}\right)+\frac{2Pl^4\dot{u}}{m\pi^3a}\sum_{i=1}^{\infty}\frac{\sin\left(\frac{i\pi x}{l}\right)}{i^3\left(i^2\pi^2a^2-\dot{u}^2l^2\right)}\sin\omega_n t \qquad (2.8)$$

In which,

$$a=\sqrt{\frac{EI}{m}}\;;\quad \omega_n=\frac{i^2\pi^2}{l^2}\sqrt{\frac{EI}{m}}$$

l : Length of the bridge;

P : Amplitude of the moving force;

m : Mass per unit length;

EI : Flexural rigidity of the bridge;

$\dot{u}$: Velocity of the moving force;

ω_n : Natural frequency of the bridge.

Inglis (1934) studied the problem extensively with different practical cases using harmonic analysis. Detailed review of the early analytical work can be found in (Timoshenko, 1953) and (Fryba, 1999). Before the advent of computers, investigations were mainly on developing analytical or approximate solutions with simplifications. From the 1970s, the computer facilitated numerical methods based on FE model with a large number of degrees of freedom.

Depending on the purpose of investigation, mathematical models of bridge with different accuracy are used to describe the dynamic response of a bridge under a moving load. One dimensional model can be used in preliminary study of the problem, in which bridge can be modeled with continuous or discretized finite beam elements. As 1-D model cannot accurately represent 2-D and 3-D bridge behavior, more refined models are used such as plate elements or solid elements. Plate bridge models have been used to investigate the problem by Henchi et al. (1998) and Zhu and Law (2002). 3-D solid elements were used by Kwasniewski et al. (2006) and Deng and Cai (2010).

Vehicle can be modeled as a moving constant force, mass or mass with spring. The simplest vehicle model is a constant force that ignores interaction between vehicle and bridge. This model gives good result when vehicle mass is negligible compared with bridge. The mass models allow for inertial forces of moving load, but are unable to incorporate the effect of road surface on vehicle and bridge response. The model of mass with spring can incorporate the frequency of the vehicle, and varies in complexity depending on assumption of performance of suspensions and tires.

A single-DOF model was used by Green and Cebon (1997) for preliminary study of dynamic interaction between heavy vehicles and highway bridges. A two-DOF model can be employed to represent the body bouncing and axle hop behavior of the vehicle (Green and Cebon, 1997). The vehicle can also be modeled in 3-D to allow for rolling and twisting motions (Kim et al. 2005; Kwasniewski et al. 2006).

The main interest of these studies is to obtain the maximum displacement under a moving load, and provide a dynamic amplification factor for designing. In this dissertation, it will be utilized to verify the curvature-based method of estimating local

stiffness loss.

2.3.2 Stiffness loss estimation from dynamic displacement

Moving vehicle is very convenient for implementation in field tests. The proposed method utilizing dynamic displacement is illustrated in Fig 2.9. Displacement transducer is installed at one position, and it will supply the information of structure damage.

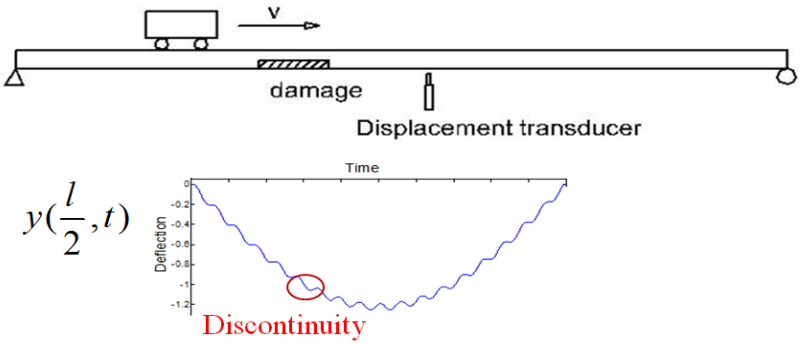

Fig 2.9 Idea of stiffness loss estimation from dynamic displacement

The basic assumption is that there is corresponding discontinuity in recorded dynamic displacement when a vehicle passes the damage range. Therefore, dynamic displacement under vehicle loading is extracted to stiffness loss due to the damage.

According to analytical solution of the dynamic displacement response in equation (0.8), it could be noticed that the first part is related to vehicle speed. It refers to the quasi-static component, which is contributed from moving vehicle; the second part containing bridge natural frequency refers to dynamic part, which comes from the vibration of the bridge. Other characteristics are: (1) contribution of higher modes is negligible, because the coefficients of them are much smaller; (2) for middle span displacement, contribution of even number modes is zero.

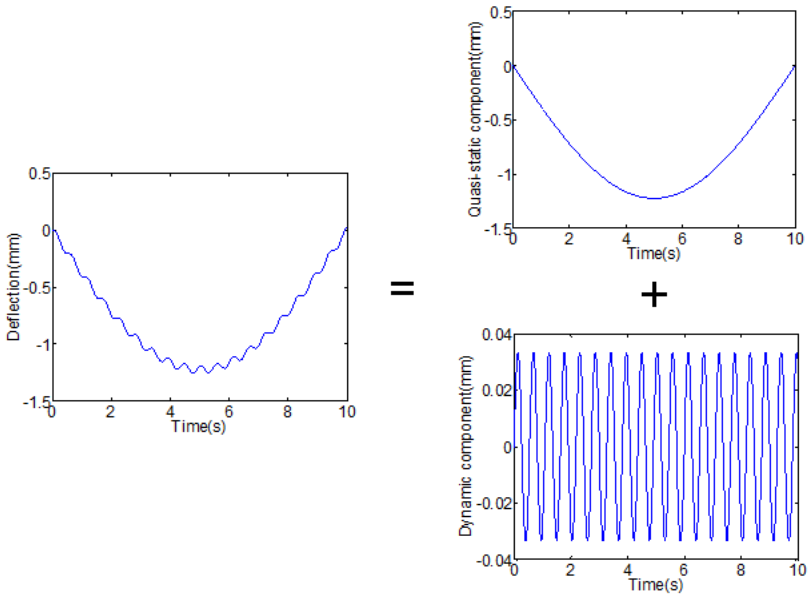

Fig 2.10 Static and dynamic components in displacement signal

In Fig 2.10, it is illustrated that the dynamic displacement at mid-span is composed of static and dynamic components. As introduced in static displacement case, curvature is calculated to estimate the stiffness loss. Similarly, curvature can be calculated using dynamic displacement to obtain the stiffness loss.

$$\kappa(x) = w''(x) = \frac{w(x-\Delta x) - 2w(x) + w(x+\Delta x)}{\Delta x^2}$$

where $w(x)$ denotes displacement.

For dynamic displacement of a damaged bridge under vehicle loading, it contains three parts: quasi-static component, dynamic component and damage component. Therefore curvature can be expressed as below.

$$\kappa(x) = \frac{w_{static}(x-\Delta x) - 2w_{static}(x) + w_{static}(x+\Delta x)}{\Delta x^2} + \frac{w_{dynamic}(x-\Delta x) - 2w_{dynamic}(x) + w_{dynamic}(x+\Delta x)}{\Delta x^2} + \frac{w_{damage}(x-\Delta x) - 2w_{damage}(x) + w_{damage}(x+\Delta x)}{\Delta x^2} \tag{2.9}$$

Noticing that dynamic component is periodic function (Fig 2.10), in curvature calculation formula, calculation interval Δx can be chosen as the length of natural period.

$$\Delta x = T_n \times f_s \tag{2.10}$$

In which T_n denotes fundamental natural period of the bridge; f_s denotes sampling frequency of data acquisition. In this way, three terms in the numerator of dynamic component will be canceled out, while contribution from damage is still kept in calculated curvature. For beam, the fundamental natural period is integer times of higher bending mode periods. Therefore higher bending mode components are also incorporated.

In fact, in equation of the dynamic displacement

$$v = -\frac{2Pl^3}{m\pi^2}\sum_{i=1}^{\infty}\frac{\sin\left(\frac{i\pi x}{l}\right)}{i^2\left(i^2\pi^2a^2 - \dot{u}^2l^2\right)}\sin\left(\frac{i\pi\dot{u}t}{l}\right) + \frac{2Pl^4\dot{u}}{m\pi^3 a}\sum_{i=1}^{\infty}\frac{\sin\left(\frac{i\pi x}{l}\right)}{i^3\left(i^2\pi^2a^2 - \dot{u}^2l^2\right)}\sin\omega_n t\,,$$

The first part represents the static component. And when velocity is very small, $\dot{u}$ is seen as 0. Then the quasi-static component becomes

$$v_{qs} = -\frac{2Pl^3}{\pi^4 EI}\sum_{i=1}^{\infty}\frac{1}{i^4}\sin\left(\frac{i\pi x}{l}\right)\sin\left(\frac{i\pi\dot{u}t}{l}\right) \tag{2.11}$$

Taking $x = x_1$, t from 0 to $\frac{l}{\dot{u}}$, the static component is obtained at point x_1. It is noted that this expression is equivalent to static deflection of the beam when load P is applied

at x_1 from the left support.

2.3.3 Calculation algorithm

In uncoupled system, vehicle model can be established using Matlab, and contact force could be obtained and applied to the bridge. Bridge model can be established in FEM software such as ABAQUS, which facilitates the computation with good accuracy and high efficiency. For different vehicles, only updating in Matlab codes is needed. As a result, an uncoupled vehicle and bridge system is established, to investigate stiffness loss estimation utilizing dynamic displacement of bridge under moving vehicle loading.

The main problem of vehicle-bridge interaction modeling is that the contact points move with time, and at each contact point, displacements of vehicle and bridge affect each other. The connection is contact force, which couples vehicle and bridge together. The detailed modeling procedures are introduced below.

Equations of motion can be established for bridge and vehicle, and they should satisfy compatibility of displacements at the contact points. The contact points of the vehicle and the bridge move from time to time. In this way, they interact with each other. Except for case in which simple vehicle model of moving constant force is adopted, closed-form solution is unavailable. Numerical method is necessary for solving this vehicle-bridge interaction problem.

For uncoupled system, interaction between the bridge and the vehicle is realized through contact force. At the contact points between vehicle wheel and bridge, contact force causes deformation of bridge; in the other way, bridge response affects dynamic behavior of vehicle, hence changes the contact force. Convergence should be satisfied at

each contact points.

Mainly two algorithms are available for the computation: step by step method (Wyss et al. 2011) in which the vehicle moves through the bridge, and iteration is conducted at each contact location to achieve convergence.

Another computation procedure is global iteration method (Gonzalez, 2010). Instead of conducting iterations step by step at each contact points, iteration is realized on contact force history. First, road profile is supposed as input force for vehicle, and contact force history is calculated for each contact points. Then bridge response is incorporated in the vehicle dynamic equation as input together with road profile, and a new contact force history is generated. This procedure will be repeated until convergence between two successive computed contact force histories is achieved.

2.3.4 Investigation with a finite element model

In order to verify the proposed curvature-based method, investigation is conducted on a vehicle-bridge model using Matlab and finite element software ABAQUS. In the analysis, the vehicle model is established using Matlab, and the contact force at the wheel is calculated with Newmark's Method. The bridge is modeled as a simply supported beam in ABAQUS, and contact force is imported from Matlab calculation result. The analysis scheme can be used to compute the bridge behavior with good accuracy and high efficiency.

(1) Vehicle model

Equation of motion for the vehicle is obtained using principle of virtual work. The

vehicle loading is simulated with a quarter-car model (Fig 2.11), composed of a spring with stiffness coefficient of $8\times10^3 N/m$, and a damper with damping coefficient of $1.44\times10^3 N\cdot s/m$. The mass of vehicle body is 100 kg. Considering the mass of tire is much smaller than the vehicle body, it is neglected in the calculation.

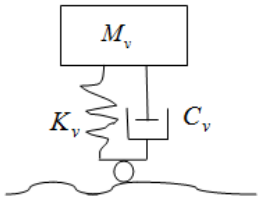

Fig 2.11 Quarter car model

The equation of motion for vehicle is

$$M_v\ddot{w}_v + C_v\dot{w}_v + K_v w_v = f_v \tag{2.12}$$

In which, M_v, C_v, K_v are mass, damping coefficient, stiffness of the vehicle respectively; $\ddot{w}_v, \dot{w}_v, w_v$ are acceleration, velocity and displacement of vehicle motion respectively; f_v is the vertical contact force on the vehicle, assuming constant speed and straight vehicle path.

The dynamic equation is calculated in Matlab with Newmark method. The contact force on the bridge is calculated as

$$F_b = f_v + M_v g - C_v\dot{w}_v - K_v w_v \tag{2.13}$$

(2) Bridge model

Steel beam model is established with three dimensional beam element B31 in commercial finite element software ABAQUS, and the schematic view is shown in Fig

2.12. It is 15m long and 1 m wide, with a thickness of 0.06 m, and the boundary condition is specified as simply supported. The beam is modeled totally with 200 beam elements.

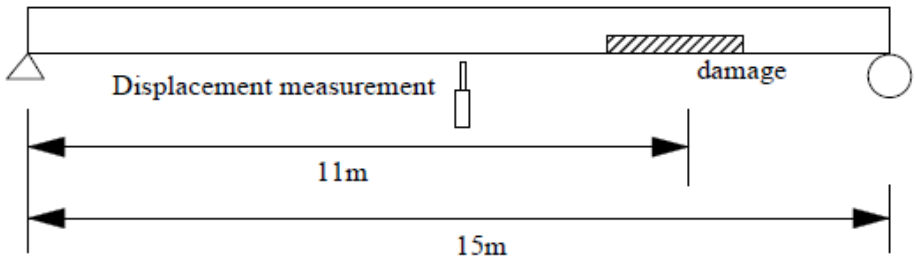

Fig 2.12 Schematic view of the bridge model

The bridge specifications are provided in Table 2.1. Stiffness loss of 42% is simulated by reduction of cross section, which is 11 m away from the left end, with a length of 0.75m and the thickness reduced to 0.05m. In analysis, vehicle passes at a constant speed of 1 m/s, so totally it takes 15 s to pass the bridge. Rayleigh damping is defined for the model.

Table 2.1 Properties of the beam model

Density	7800 kg/m^3
Young's Modulus	$2.1\times10^{11} N/m^2$
Poisson's Ratio	0.3
Damage location	11m from the left support

Road surface is continuously distributed in random fashion, which affects dynamic behavior of both vehicle and bridge. It is usually assumed to be a stationary Gaussian random process and generated from power spectral density functions (Dodds and Robson, 1973). The power spectra basically describe the distribution of mean square amplitude of road geometry deviations as a function of the spatial frequency of the irregularities.

When modeled as a stationary Gaussian random process, the road pavement profile can be generated by an inverse Fourier transform as

$$r(x) = \sum_{k=1}^{N} \sqrt{2G_d(n_k)\Delta n}\cos\left(2\pi n_k x - \theta_k\right) \tag{2.14}$$

Where $G_d(n_k) = \dfrac{a}{(2\pi n_k)^2}$: PSD function, and a has different values according to the road condition; here it is chosen as 2×10^{-6}, good condition.

Δn: Frequency interval, $\Delta n = \dfrac{n_{\max} - n_{\min}}{N}$, where $n_{\max}$ and $n_{\min}$ are the upper and lower cut-off frequencies respectively; here they are chosen as 5 Hz and 0.1 Hz;

n_k: Wave number;

θ_k: Random phase angle uniformly distributed from 0 to 2π.

When calculating the dynamic behavior of the vehicle, the space function is transformed to time function according to the vehicle speed. The generated road profile is shown in Fig 2.13, with the largest amplitude of roughness below 2 mm.

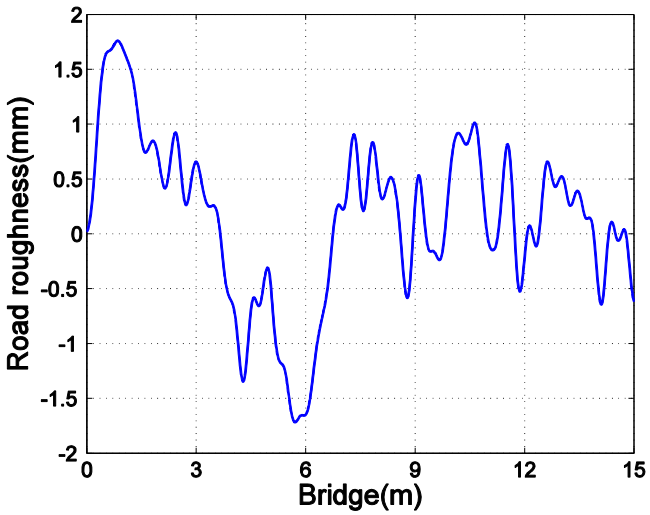

Fig 2.13 Bridge surface profile

(3) Calculation algorithm

In this analysis, interaction between the bridge and the vehicle is realized through contact force. At the contact points between the vehicle wheel and the bridge, displacement of the vehicle and the bridge should satisfy compatibility at the contact points, where the same deformation of both the vehicle and the bridge should be maintained. Convergence should be satisfied at every contact point.

Computation procedure is conducted in a global manner presented as illustrated in Fig 2.14, and interaction between the vehicle and the bridge is realized through the contact force time history. First, road profile is used as the initial input for the vehicle, and the contact force history is calculated for each contact points. The contact force history is then applied to the bridge model in ABAQUS, which leads to bridge response. Then the bridge response is incorporated in the vehicle dynamic equation as input, together with the road profile, and a new contact force time history is generated. This procedure is

repeated until a user defined convergence criteria is satisfied. Particularly the convergence criterion is set that the maximum displacement difference between successive iterations is smaller than 0.01% of the dynamic displacement at mid-span. Once the convergence criterion is satisfied, displacement response of the bridge is extracted for stiffness loss estimation.

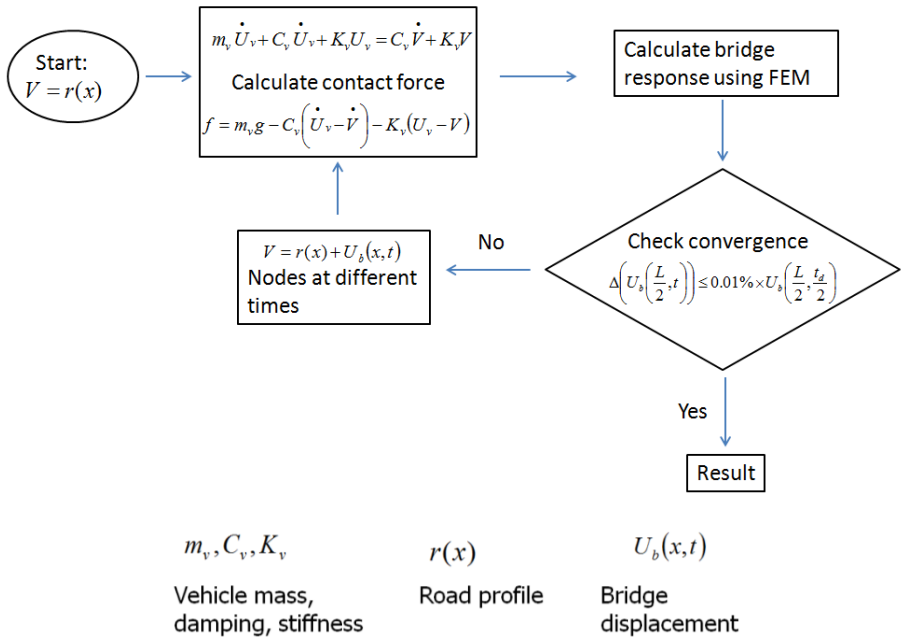

Fig 2.14 Calculation algorithm for vehicle-bridge model

(4) Analysis result

Analysis is conducted until convergence is satisfied. The difference of dynamic displacement at the mid-span point is shown in Fig 2.15. It indicates that after three iterations, the maximum difference between two iterations is $5\times10^{-7}m$, around 0.0025% of the mid-span displacement of the bridge. It satisfies the convergence criterion that the displacement difference is smaller than 0.01% of the mid-span displacement.

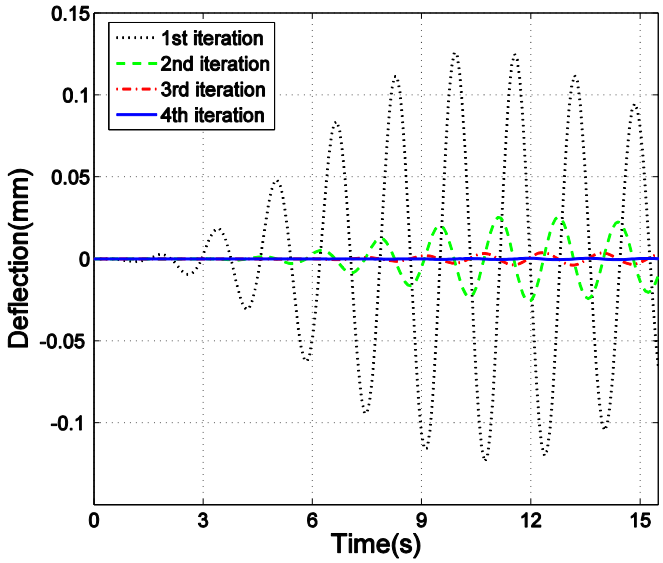

Fig 2.15 Convergence of displacement at contact points

Dynamic displacement at the mid-span point is extracted for stiffness loss estimation, as shown in Fig 2.16. The natural frequencies of the bridge were also extracted, which shows that the fundamental natural frequency is 0.61 Hz. Hence the fundamental natural period is obtained as 1.648 s. In data processing, the second derivatives of the dynamic displacement data are taken, at an interval of the natural period of the bridge. The vehicle passes the bridge in 15 s, and displacement is recorded. Therefore, f_s is calculated as 13.4 Hz. For the calculation of dynamic curvature, Δx is chosen as $\Delta x = T_n \times f_s$. Δx is then rounded to an integer value, which is 22.

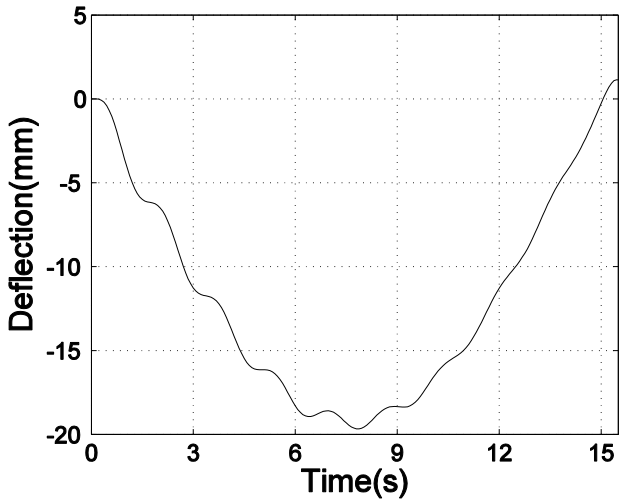

Fig 2.16 Dynamic displacement at the center of the bridge span

The curvature is illustrated in Fig 2.17. When the vehicle bridge interaction is not considered, the dynamic curvature is also presented for comparison, given by the red dashed line. In the curvature figure, there are no calculated curvature values at both ends of the bridge span, because the second derivative was taken at an interval Δx. It can be indicated from the figure that when interaction is not considered, curvature plot is smoother, and peak caused by damage is more apparent. In contrast, there are more fluctuations on the curvature result which incorporated interaction between the vehicle and the bridge. But even considering the interaction effect, the damage location is clearly confirmed.

Apparent peak at the location of 11m on the dynamic curvature plot indicates the damage location. Using the calculation equation Eqn (9), the stiffness loss is obtained as 39.98%. Compared with the actual stiffness loss of 42 %, the difference is around 2%. It demonstrates that even with the effects from road roughness and vehicle-bridge interaction, the curvature method can evaluate the stiffness loss with good accuracy.

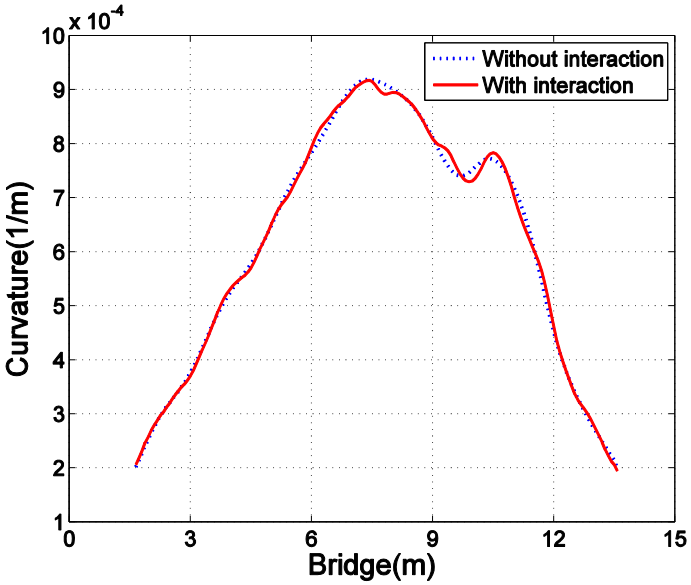

Fig 2.17 Curvature of bridge at mid-point of the span

(5) Effect of damage location and extent

In order to investigate the effect of damage location and extent, different damage locations and extents are analyzed. Damage is assumed at location of 3m (L/5), 5m (L/3) and 12m (4L/5) respectively, and damage length is 0.75m with thickness reduced to 0.05m. The displacement with measurement noise is calculated as the formula below (Zhu and Law, 2006; Nguyen and Tran, 2010).

$$w = w_c + E_p N\sigma(w_c)$$

Where w is the polluted bridge displacement with measurement noise. E_p is the noise level and N is a standard normal distribution with zero mean value and unit standard deviation. w_c is the calculated displacement at mid-point of bridge span, and $\sigma(w_c)$ is its standard deviation.

Noise level is assumed as 0.1%, and it is added to calculated displacement in the same way as in the last subsection. The curvature results are illustrated in Fig 2.18. It is

shown that damage can be detected reliably regardless of its location. Damage extent is identified as stiffness loss of 36.8%, 32.9% and 33.9% respectively.

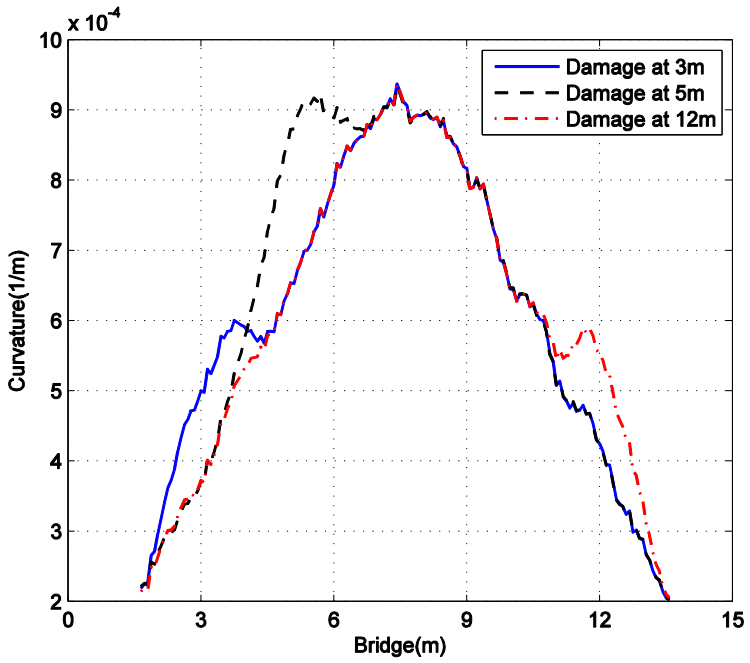

Fig 2.18 Curvature at mid-span with different damage location

Effect of damage extent is also studied, by assuming stiffness loss of 20%, 40% and 60%. Noise level is assumed as 0.1%. The curvature results are plotted in Fig 2.19, which shows that the peak caused by damage increases as stiffness loss increases from 20% to 60%, which were estimated as 17.9%, 32.2% and 49.6% respectively. The discrepancy can be attributed to the road surface roughness and measurement noise.

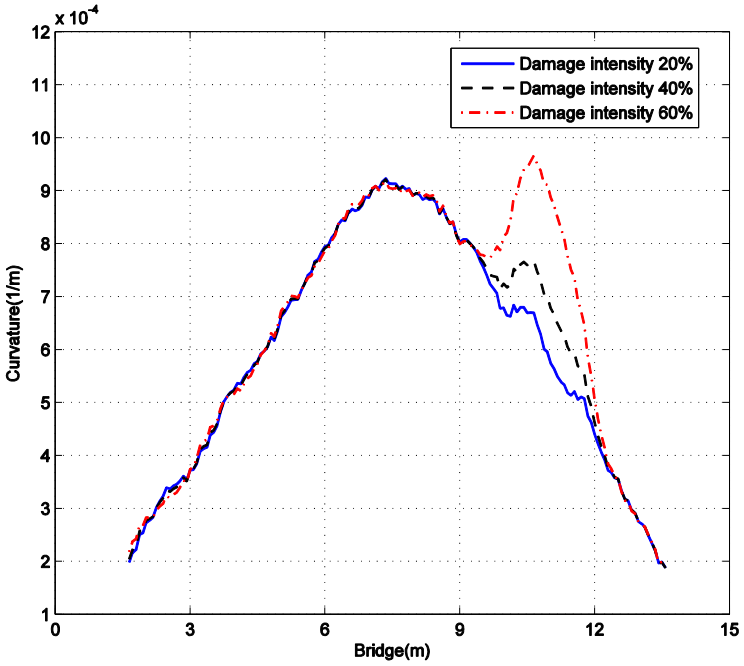

Fig 2.19 Curvature at mid-span with different damage extent

2.3.5 Conclusion on the curvature base method using dynamic displacement

A local stiffness loss estimation method is proposed based on dynamic displacement of bridge under the loading of a moving vehicle. Through the investigation, several conclusions are drawn as follows.

(1) Closed-form solution of the vehicle-bridge problem shows the idea of decomposing dynamic displacement into quasi-static component and dynamic component, and curvature of the quasi-static component can be used to estimate stiffness loss.

(2) In curvature calculation using dynamic displacement, the calculation interval is chosen as natural period of the beam, by which dynamic component can be canceled out, while stiffness loss is estimated with quasi-static component.

(3) Numerical simulation of a beam model is investigated, in which road surface

roughness, vehicle-bridge interaction and measurement noise are considered. Parametric study on damage location and extent verified the reliability and efficacy of this method. It is also shown that the estimated stiffness loss level could be less accurate due to measurement noise.

2.4 Conclusions

In this chapter, a displacement-based method is proposed for load carrying capacity estimation of damaged girder bridges, which includes two goals. The first goal is to estimate the local stiffness loss for damaged bridges, which is important for decision making on repairing and strengthening methodologies. The second goal is to evaluate the load carrying capacity for severely damaged bridges. The conclusions of this chapter are drawn as follows.

(1) The proposed load carrying capacity estimation method is described, and theoretical basis of Maxwell-Betti Reciprocal Theorem is presented.

(2) The curvature-based stiffness loss estimation method is theoretically explained. Curvature is proposed as a parameter to estimate the stiffness loss at damaged location of a bridge.

(3) An approach is proposed to eliminate the dynamic part in displacement curvature calculation under a moving vehicle, which was validated with numerical investigation.

Chapter 3 Investigation and treatment of noise in displacement measurement

In any experiment, measurement noise is inevitable and may be caused by different reasons. In practice, noise mainly arise from the following sources.

1) Instrumental error, caused by measurement device precision.

2) Environmental effect, caused by variation of temperature, humidity, wind, etc.

3) Experiment condition, caused by experiment arrangement, for example, loading condition may not be exactly the same as planned.

In this chapter, the property of measurement noise is investigated, and a noise/damage effect ratio is proposed to evaluate noise effects. Then two approaches are proposed to reduce noise effects. Firstly, a laboratory experiment is conducted to investigate the properties of noise and its effects on the curvature calculation results. A noise/damage effect ratio is defined to evaluate the effect of noise on curvature calculation. Secondly, two approaches are proposed to reduce the effects of noise, and effect of measurement noise on curvature calculation is illustrated analytically. Both approaches are verified with the laboratory test measurements. Thirdly, a three-dimensional bridge FE model is established, which verified the proposed approach for noise reduction.

3.1 Laboratory experiment on noise properties

3.1.1 Introduction

In laboratory, experiments were conducted on an aluminum beam specimen to investigate the property of noise in displacement measurements and its effects on curvature calculation.

The experiment setup is illustrated in Fig 3.1 (a) and (b). The length of the beam is 900 mm with gross cross-section of 20mm×3mm. Damage was created through saw cut of cross section at range between 237 mm and 313mm, which is about 60% stiffness loss. Load was applied using a 5 N weighed mass, which was moved on the beam with 25 mm interval. When the mass was at each position, static displacement was measured at mid-point of the beam with Laser displacement meter LK-H050. Based on Maxwell-Betti reciprocal theorem, the measured displacement is equivalent to deflection under concentrated load at mid-point of the span. Experiment conditions are summarized in Table 3.1.

Table 3.1 Experiment conditions

Specimen dimension (mm)	Length: 90; Beam cross section: 20×3
Boundary condition	Fixed-fixed
Load (N)	5
Loading interval (mm)	25
Damage	60% , between 237mm and 313mm

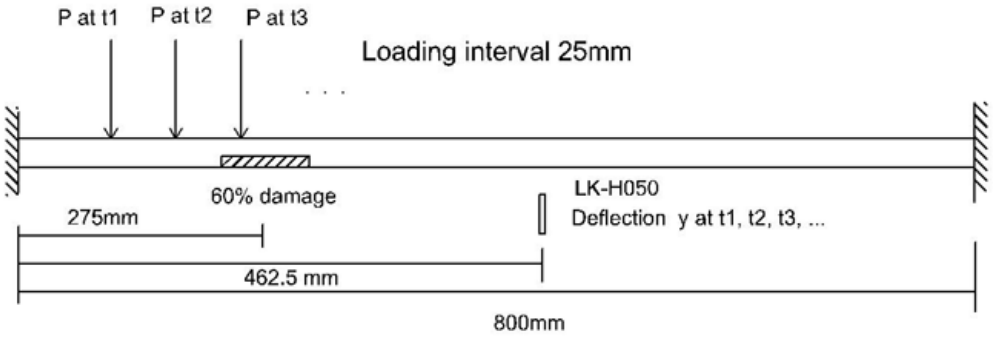

(a)Schematic view of experiment

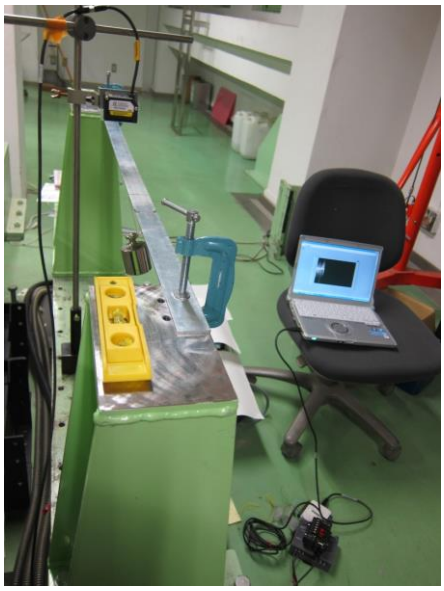

(b) Experiment photo

Fig 3.1 Laboratory experiment set-up

The test was conducted three times under the same experiment condition, and the displacement results are shown in Fig 3.2. It is observed that the three displacement measurements almost coincide with each other, and the damaged location cannot be distinguished from the figure.

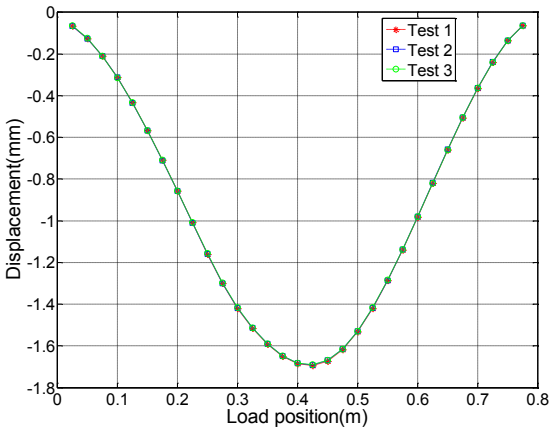

Fig 3.2 Displacement of the test beam

3.1.2 Curvature calculation results

Curvature is calculated using the following formula.

$$\kappa(x) = \frac{w(x-\Delta x) - 2w(x) + w(x+\Delta x)}{\Delta x^2}$$

In which, w(x) is displacement of the beam;

x is the measurement position;

Δx is curvature calculation interval. It is taken as 25 mm here.

Fig 3.3 shows curvature calculation results of the beam in three tests. A linear fitting is plotted in a least squares sense, and curvature change is computed as original curvature subtracted by the linear fitted curvature, as shown in Fig 3.4. The largest discrepancy is at 0.275 m for all three tests, which agrees with the damage location. It is observed from Fig 3.4 that the curvature change is not zero even for undamaged positions. Instead, the curvature change values vary around zero. This result is caused by noise in the test.

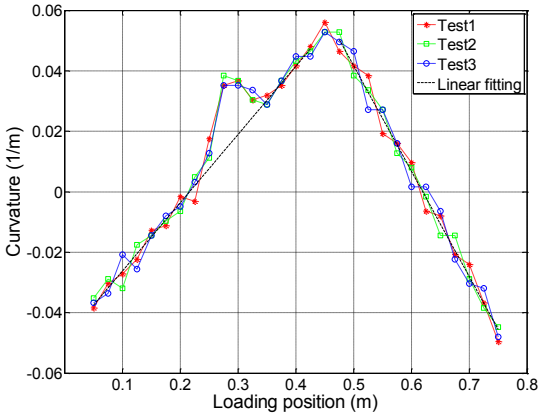

Fig 3.3 Displacement and curvature for 25mm measurement interval

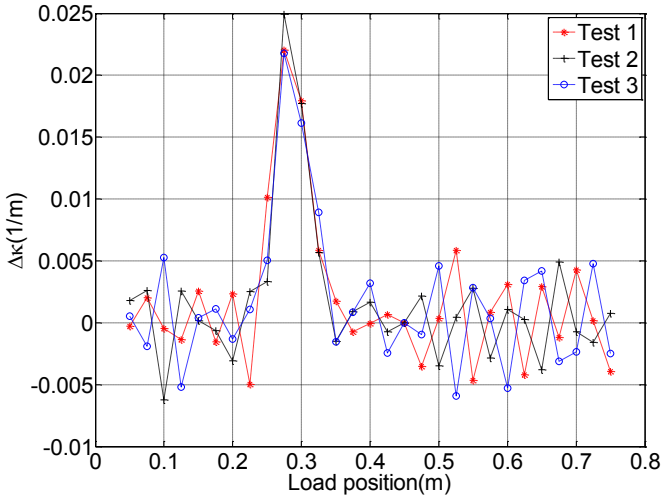

Fig 3.4 Curvature change with respect to linear fitted curvature

As introduced in Chapter 2, stiffness loss be calculated from curvature change.

$$\alpha=1-\frac{\kappa_i}{\kappa_d}$$

In which, κ_i and κ_d are obtained from linear fitted curvature and the original curvature value at 0.275 m.

The identified stiffness loss results of the tests are demonstrated in Table 3.2. It is indicated that identified results agrees well with actual damage extent of 60%.

Table 3.2 Identification results of specimen damage extent

Measurement	Test 1	Test 2	Test 3
Damage extent	62.66 %	64.88 %	61.88 %

As shown in Fig 3.4, curvature in intact state $\kappa_{in}(x)$ can be obtained approximately through linear fitting, and curvature change $\Delta\kappa(x) = \kappa(x) - \kappa_{in}(x)$ is calculated. Noise/damage effect ratio $s = \frac{\sigma}{\Delta\kappa_{\max}}$ is defined as noise/damage effect ratio, in which σ denotes standard deviation of calculated curvature variation in intact range. $\Delta\kappa_{\max}$ denotes the largest curvature change, for example, 0.275 m in Fig 3.4.

3.2 Approaches for noise reduction

In order to minimize the effect of noise on the proposed method, techniques are required to cope with the measurements.

3.2.1 Noise reduction with multi-measurement averaging

It is widely known that random measurement noise can be minimized through averaging multiple measurements under the same experiment condition. The average displacement of three tests in Fig 3.2 is plotted in Fig 3.5. This averaged displacement is used to calculate curvature, as shown in Fig 3.6. And the curvature change is obtained in Fig 3.7. Table 3.3 shows the noise/damage effect ratio for the three different tests and the averaged displacement. It is noticed that the noise/damage ratio is reduced effectively.

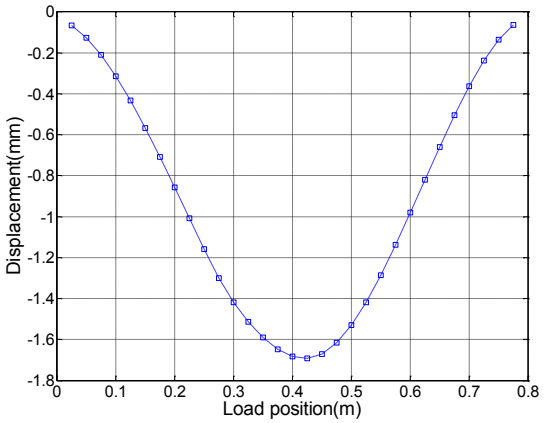

Fig 3.5 Average of dispalcement in three tests

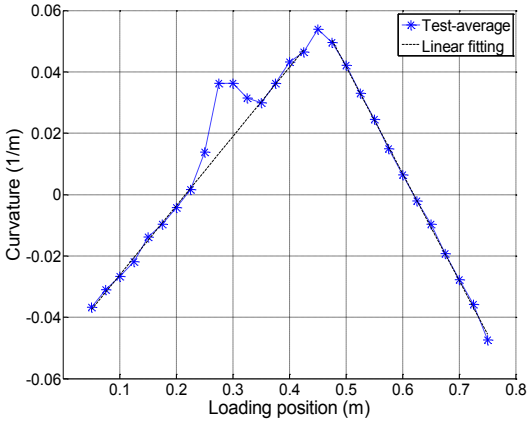

Fig 3.6 The curvature result from average of dispalcement in three tests

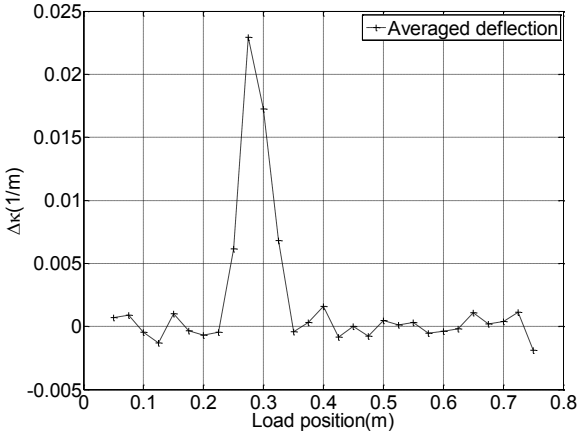

Fig 3.7 Curvature change for averaged displacement

Table 3.3 Noise/damage ratio for three tests and averaged displacement (25 mm)

Test	Test 1	Test 2	Test 3	Average
Noise/damage effect ratio	16.19 %	10.60 %	17.84 %	3.63 %

3.2.2 Effect of curvature calculation interval on noise and damage

It is shown in the last sub-section that noise can be effectively reduced through taking the average displacement value of multi-measurements. However, tests in multi-times in a bridge field experiment is time-consuming, and the same experimental condition should be ensured. In this sub-section, effects of curvature calculation interval on noise and damage are investigated to find an approach to reduced noise-induced variation in curvature calculation.

As already introduced, measurement noise and damage both cause peaks in curvature results. Measurement noise is intrinsically uncertain, and should be treated as a random variable. In the discussion below, the effect of measurement noise in curvature is described using standard deviation in curvature, and denoted as σ_κ. The curvature change caused by damage is denoted as $\Delta\kappa_d$, which is the largest curvature change and it should stays at the same position even different curvature calculation intervals are used.

It is noticed that increasing curvature calculation interval will lower these peaks. Suppose measurement noises in displacement are independent at different points, and with same standard deviation, denoted as σ_e.

Curvature is calculated as below.

$$\kappa = \frac{w(x-\Delta x) - 2w(x) + w(x+\Delta x)}{\Delta x^2}$$

In which, w(x) is the displacement;

x is the measurement position;

Δx is interval of measurement.

According to error propagation (Philip R. Bevington, D. Keith Robinson, 2003), standard deviation of a function $f(x, y, z)$ is as follows.

$$s_f = \sqrt{\left(\frac{\partial f}{\partial x}\right)^2 s_x^2 + \left(\frac{\partial f}{\partial y}\right)^2 s_y^2 + \left(\frac{\partial f}{\partial z}\right)^2 s_z^2} \tag{3.1}$$

For curvature κ, the standard deviation can be calculated as follows.

$$\sigma_\kappa = \frac{\sqrt{6}}{\Delta x^2}\sigma_e \tag{3.2}$$

If curvature calculation interval increases to $2\Delta x$, the standard deviation decreases to 1/4. Three sets of measurement are conducted in the experiment described in Section 3.1, and curvature are obtained using different calculation interval 25 mm, 50 mm, 75 mm and 100 mm. The curvature under undamaged state is plotted through linear fitting. The standard deviations with different curvature calculation intervals are shown in Fig 3.8. It is illustrated that the noise level decrease agrees with the theoretical deduction.

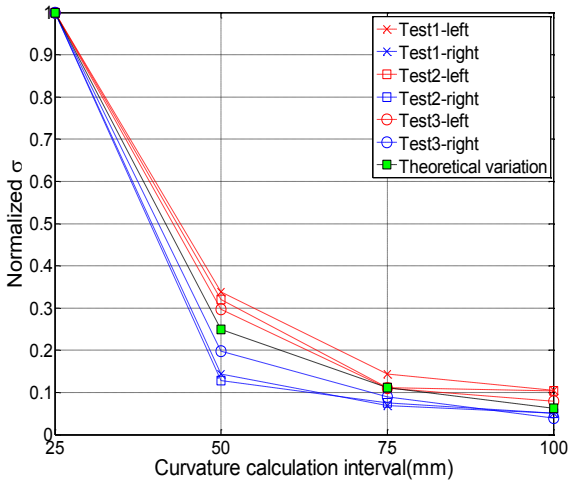

Fig 3.8 Standard deviation of curvature with different calculation interval

On the other hand, the displacement of damaged beam can be seen as two parts: one part of undamaged beam and the other caused by damage: $w(x) = w_i(x) + w_d(x)$. In which, $w_i(x)$ denotes displacement of undamaged beam; $w_d(x)$ denotes displacement caused by damage. In curvature calculation $\kappa(x) = \frac{w(x-\Delta x) - 2w(x) + w(x+\Delta x)}{\Delta x^2}$, it can be decomposed into these two parts, shown as below.

$$\kappa(x) = \frac{w_i(x-\Delta x) - 2w_i(x) + w_i(x+\Delta x)}{\Delta x^2} + \frac{w_d(x-\Delta x) - 2w_d(x) + w_d(x+\Delta x)}{\Delta x^2}$$

In which, $x-\Delta x$, x, $x+\Delta x$ denote the three coordinates of displacements used for curvature calculation at x. Therefore, curvature change caused by damage is

$$\Delta\kappa_d = \frac{w_d(x_d-\Delta x) - 2w_d(x_d) + w_d(x_d+\Delta x)}{\Delta x^2}.$$

In which x_d denotes damage location. If curvature calculation interval increases to $2\Delta x$,

$$\Delta\kappa_d = \frac{w_d(x_d-2\Delta x) - 2w_d(x_d) + w_d(x_d+2\Delta x)}{4\Delta x^2}.$$

For a simply supported beam, closed-form displacement caused by damage can be obtained analytically (Appendix A),

$$w_d = \begin{cases} \frac{\alpha}{1-\alpha}\frac{Pb}{EI}\left(\frac{1}{3l^2}(x_b^3 - x_e^3) - \frac{1}{2l}(x_b^2 - x_e^2)\right)x & 0 < x \le x_b \\ -\frac{\alpha}{1-\alpha}\frac{Pb}{6lEI}x^3 + \frac{\alpha}{1-\alpha}\frac{Pb}{EI}\left(\frac{1}{3l^2}(x_b^3 - x_e^3) + \frac{1}{2l}x_e^2\right)x - \frac{\alpha}{1-\alpha}\frac{Pb}{3lEI}x_b^3 & x_b < x \le x_e \\ \frac{\alpha}{1-\alpha}\frac{Pb}{EI}\left(\frac{1}{3l^2}(x_b^3 - x_e^3)\right)x - \frac{\alpha}{1-\alpha}\frac{Pb}{3l}(x_b^3 - x_e^3) & x_e < x \le l \end{cases}.$$

An example of beam displacement caused damage is shown in Fig 2.8(a). It can be deducted that $w_d(x_d - 2\Delta x)$ and $w_d(x_d + 2\Delta x)$ are larger than $w_d(x_d - \Delta x)$ and $w_d(x_d + \Delta x)$

respectively. Therefore, when curvature calculation interval increases to $2\Delta x$, the decrease in amplitude is smaller than 1/4. For the five different scenarios in Fig B.2, the relation between curvature change and stiffness loss level is summarized.

When curvature calculation interval changes from Δx to $2\Delta x$, possible scenarios are explained here. Note that case 1 would not correspond to the largest curvature change, so it is excluded. And in Case 3 to Case 3, the curvature calculation results is the same. Then the other possible scenarios are Case 2 to Case 2, Case 2 to Case4, Case 3 to Case2, Case 3 to Case4, Case 4 to Case4 and Case 5 to Case5 respectively. In a numerical example, when calculation interval changes from Δx to $2\Delta x$, curvature value results for noise and the six scenarios are illustrated in Fig 3.9. It is demonstrated that the damage induced curvature change decreases much smaller than that of the noise level (1/4).

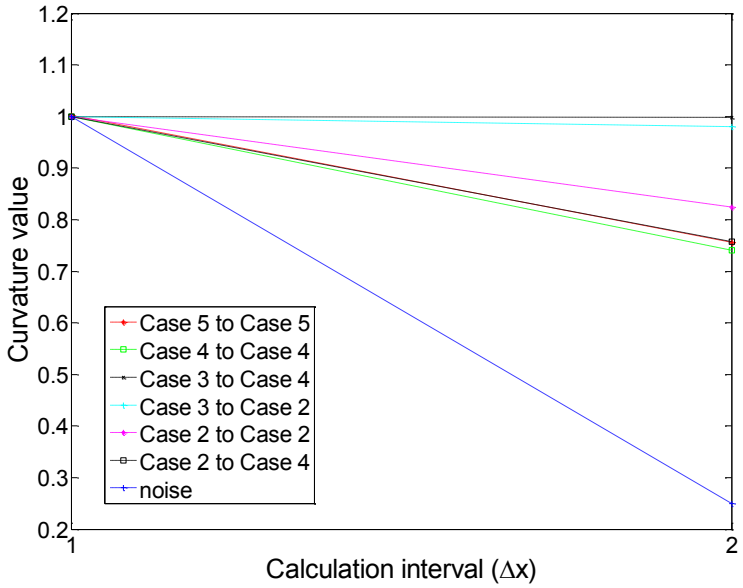

Fig 3.9 Curvature change with different curvature calculation interval

As the decrease of peaks caused by damage is faster than measurement noise, curvature calculation interval is chosen to ensure that noise/damage effect ratio is smallest.

3.2.3 Noise reduction with selection of curvature calculation interval

In this sub-section, a new approach is proposed to reduce noise effect with selection of curvature calculation interval.

Noise-induced curvature variation is described as standard deviation of curvature change, $\Delta\kappa(x) = \kappa(x) - \kappa_{un}(x)$, in which $\kappa_{un}(x)$ denotes curvature in undamaged state obtained from linear fitting in least square sense. Damage-induced increase is described as largest curvature change $\Delta\kappa_{\max}$. The curvature calculation interval is determined through an approach, as shown in Fig 3.10.

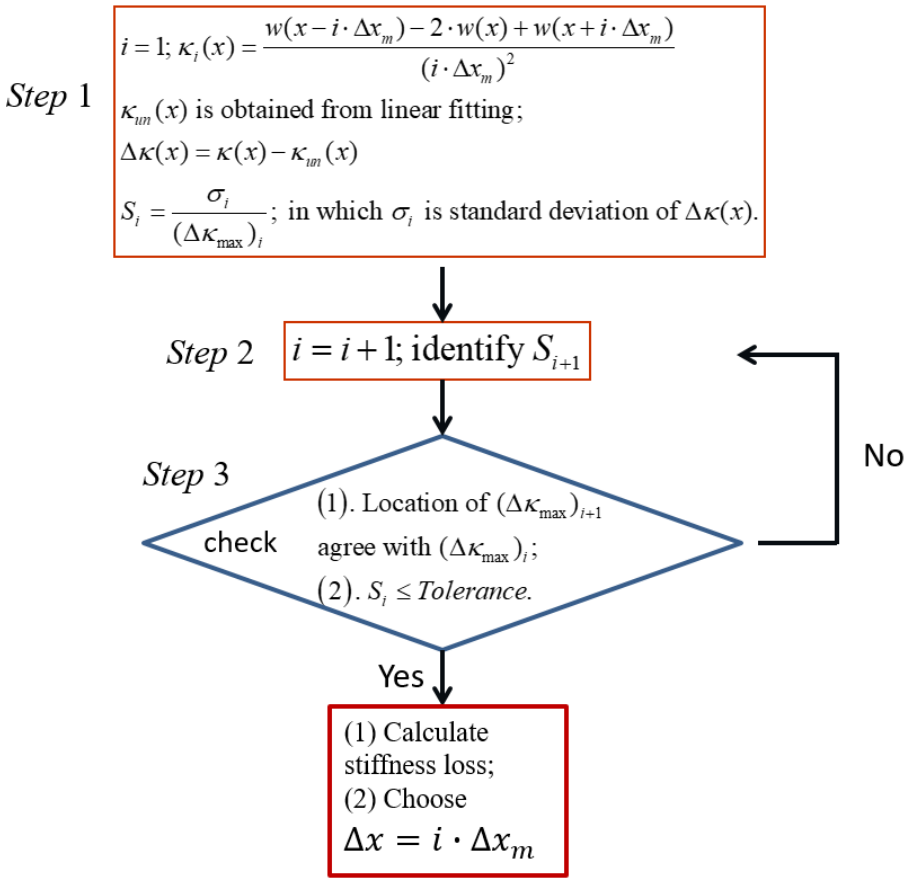

Fig 3.10 Iteration process for determining optimum curvature calculation interval

Suppose displacement measurement interval is Δx_m, In the first step, the curvature calculation interval is chosen as $1 \times \Delta x_m$, and curvature figure is plotted. It is then used as the length of curvature calculation interval in the first step. In the second step, the calculation interval is chosen as $2 \times \Delta x_m$ and the same process is repeated as the previous step. After calculation for several steps, the curvature change $\Delta\kappa_{\max}$ stays at the same location, corresponds to the damage location. If $s = \dfrac{\sigma}{\Delta\kappa_{\max}}$ satisfies the tolerance, the curvature figure is plotted. In this research, the tolerance for the noise/damage effect ratio is chosen as 15%. It is noted that the purpose of the study is for local stiffness loss estimation of severe damage in a bridge, and the damage location is already known in advance.

In this experiment, curvature is calculated with 50 mm interval, and the result is shown in Fig 3.11. And the curvature changes in the three tests are plotted in Fig 3.12. It is calculated as original curvature subtracted by linear fitted curvature.

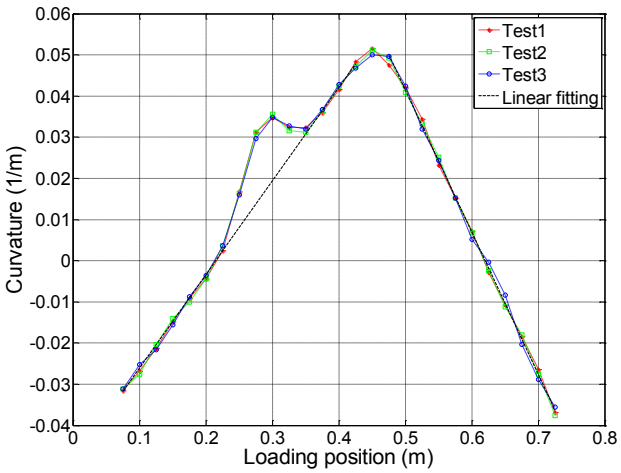

Fig 3.11 Curvature results with 50 mm calculation interval

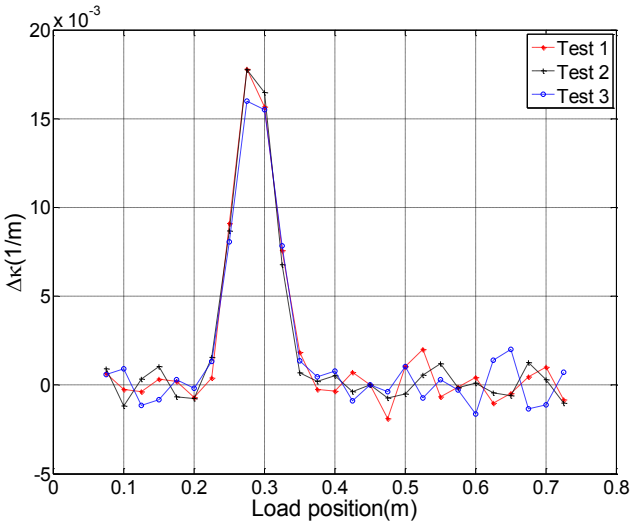

Fig 3.12 Curvature change for calculation interval 50 mm

The noise/damage effect ratios of the results in three tests are listed in Table 3.4. It shows that noise effect is reduced when curvature calculation interval increases from 25 mm to 50 mm.

Table 3.4 Noise/damage effect ratio for three tests (50 mm)

Test	Test 1	Test 2	Test3
Noise/damage effect ratio with 25 mm calculation interval	16.19 %	10.60 %	17.84 %
Noise/damage effect ratio with 50 mm calculation interval	6.31 %	4.36 %	7.52 %

The effectiveness of selection of curvature calculation interval can also be explained from another viewpoint. It is known that beam deflection formula is a three-order polynomial, which could be expressed as below.

$$w(x) = ax^3 + bx^2 + cx + d \tag{3.31}$$

Four coefficients a,b,c,d could be determined from displacement measurement

data at four positions. Taking four displacement data along the beam axis, and move the origin of coordinate to the first of the four data, then d is zero. The other three coefficients could be calculated with the following equations.

$$\begin{cases} a = \left(\frac{1}{2} w_2 - \frac{1}{2} w_3 + \frac{1}{6} w_4 \right) \frac{1}{\Delta x^3} \\ b = \left(-\frac{5}{2} w_2 + 2 w_3 - \frac{1}{2} w_4 \right) \frac{1}{\Delta x^2} \\ c = \left(3 w_2 - \frac{3}{2} w_3 + \frac{1}{3} w_4 \right) \frac{1}{\Delta x} \end{cases} \tag{3.4}$$

Curvature could be calculated from second derivative as follows.

$$\kappa = \frac{d^2 w}{dx^2} = 12 a \Delta x + 2b \tag{3.5}$$

As it is a linear function, coefficient a should be the same for the undamaged portion of the beam. As a result, estimated of a from a least squares sense could indicate the noise effect. Table 3. shows average of a in one test with different curvature calculation interval.

Table 3.5 Average of coefficient a from different calculation interval

Calculation interval	25mm	50mm	75mm	100mm
Average of a	3.8564×10^{-8}	4.8148×10^{-8}	4.9053×10^{-8}	4.8056×10^{-8}

It is noticed that a changed largely from 25 mm interval to 50mm interval, but stayed stable from 50 mm to 100 mm interval.

3.3 Numerical example of a three-dimensional bridge

To verify the feasibility of this method on actual bridges, investigation is conducted on a detailed 3-D bridge model established in finite element software ABAQUS.

3.3.1 Model introduction and calibration

The bridge is a single span bridge, with a length of 25m and width of 8.5m, as shown in Fig 3.13. The concrete deck is supported by five I-shape steel girders. In transverse direction, there is X-type cross frame which consists of top and bottom chords made of 100×100×9.5 angles and diagonals of 75×75×9.5 angles. The thickness of deck is 0.2 m, and concrete cover is 35 mm. The height, width and thickness of the I-shape girder are 1.2m, 0.6m and 0.05m respectively. The boundary conditions are specified as simply supported at two ends of the five I-shape girders on bearings. Both concrete and steel are specified as elastic. The properties are illustrated in Table 3.6. Stiffness loss of 30% is simulated with reduced cross section on the girder 4 at range 7 ~ 9 m, which is realized through reduced section area.

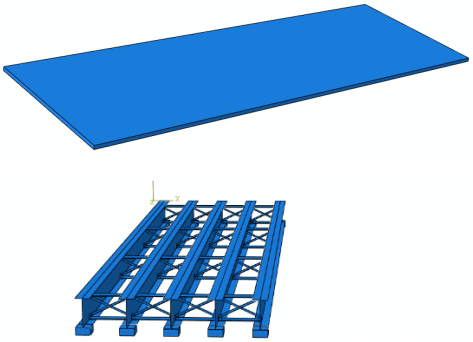

(a) Finite element bridge model (deck and girder with X-bracing)

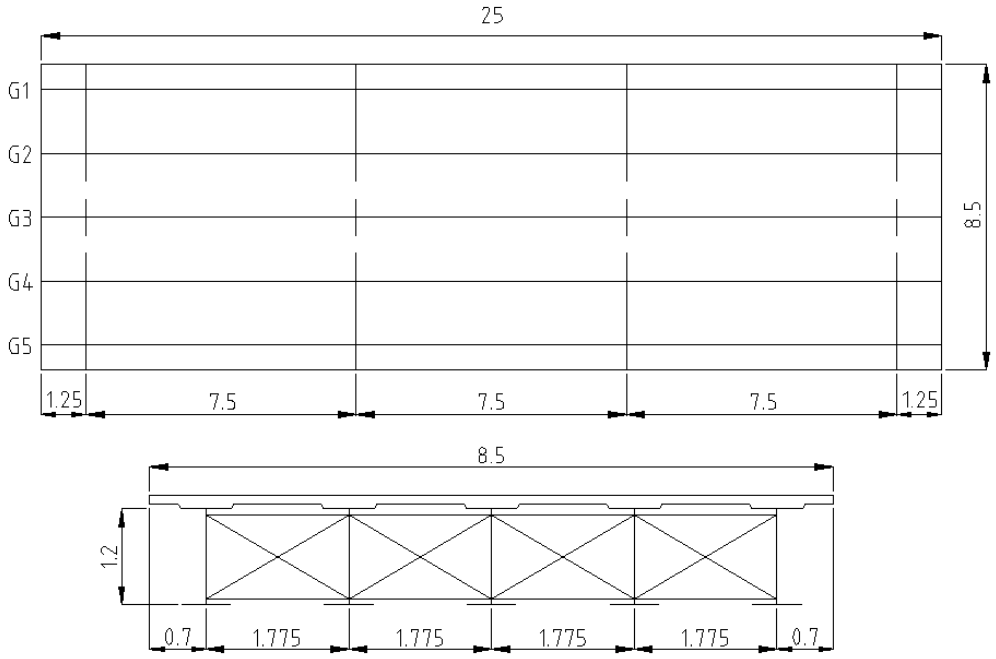

(b) Bridge profile and cross section (Unit:m)

Fig 3.13 Bridge model

Table 3.6 Concrete and steel properties

Material	Concrete	Steel
Density (kg/m^3)	2400	7890
Young's modulus (Pa)	2.8×10^{10}	2.1×10^{11}
Poisson's ratio	0.2	0.3

Surfaces between deck and girders, girders and bearings are connected together with tie constraint, which defines that contact surfaces have the same motion. Reinforced bars are embedded in the concrete deck, which specify same translational degrees of freedom at adjacent nodes. The bridge model contains totally 11067 elements and 15897 nodes. The mesh type and size are illustrated in Table 3.7.

Table 3.7 Element property of bridge model

Member	Mesh type	Mesh size (m)
Deck	Solid element C3D8R	$0.25\times0.25\times0.2$

Rebar in the deck	Truss element T3D2	0.5
I shape Girder	Shell element S4R	0.125×0.15
Bearing	Solid element C3D8R	0.3

It is noted that the mesh size is calibrated before the analysis. Two other models with mesh sizes as 0.5 times and 2 times the chosen model are also established, which are denoted as model A and Model C respectively. The chosen model is denoted as model B, and mode frequency is chosen as the parameter for calibration. Mode analysis is conducted, and first four frequencies are obtained as summarized in Table 3.8. It is indicated difference between Model B and Model A is less than 1% for all the first four modes. The difference between Model A and Model C is small for the first mode frequency, but quite large for other three modes. Therefore Model B is chosen as the calibrated model for consequent analysis.

Table 3.8 Element mesh calibration

Models	Model A	Model B /Difference	Model C /Difference
1 st bending frequency (Hz)	9.4573	9.4449/0.13%	9.4000/0.61%
1 st torsion frequency (Hz)	9.5824	9.5620/0.21%	9.2452/3.52%
2 nd torsion frequency (Hz)	29.682	29.516/0.56%	29.019/2.23%
2 nd bending frequency (Hz)	34.775	34.591/0.53%	32.856/5.52%

In the finite element analysis, vehicle loading is simulated with concentrated load of 100 kN. The load moves along the deck an interval of 0.5 m, and static displacement is obtained at mid-span point of damaged girder. Effect of noise is studied through adding the randomly generated noise, which is selected with zero mean and standard deviation as 0.05% of mid-span displacement. After obtaining the contaminated displacement data, they are used for stiffness loss estimation with the curvature based method. The calculation intervals are chosen as 0.5 m, 1 m and 1.5m. Stiffness loss estimation is

conducted and explained in the following subsection.

3.3.2 Curvature calculation with different intervals

In this subsection, effect of curvature calculation interval is studied. Load moves over girder 4 with an interval of 25 mm. Displacement is obtained at centre of girder 4. According to Maxwell-Betti theorem, interval for obtained displacement is 25 mm. Damage severity of 50 % stiffness loss is considered. Measurement noise is considered in a similar way as in (Shi et al., 1998), and it is selected with zero mean and standard deviation as 0.05% of mid-span displacement. In order to investigate effect of measurement noise, displacement $w(x)_m$ is generated as below.

$$w(x)_m = w(x)_{actual} + e(x) \tag{3.6}$$

Where, $w(x)_{actual}$ is obtained from FEM analysis; $e(x)$ is measurement noise which follows normal distribution. The noise is selected with zero mean and standard deviation as 0.05% of mid-span displacement.

Noise/damage effect ratio $s = \dfrac{\sigma}{\Delta\kappa_{\max}}$ is calculated for different calculation intervals, which are 0.5 m, 1 m and 1.5m. The results of the ratio are 27.93 %, 7.61 % and 9.23 % respectively. Curvature plots are shown in Fig 3.14 with corresponding calculation intervals. It is indicated that noise effect is obvious when calculation interval is 0.5 m, and 1 m is the most appropriate calculation interval to restrain the noise effect while highlighting damage effect.

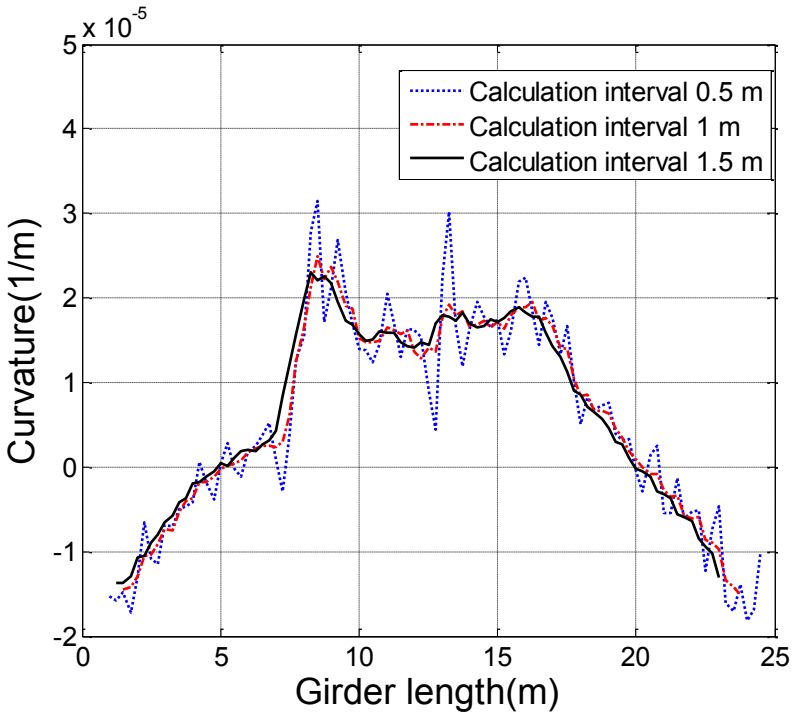

Fig 3.14 Curvature plots with three different calculation intervals

In this numerical example, a realistic detailed Finite Element bridge model is used to verify applicability of the proposed method. Measurement noise exists in any field test, and its effect should be treated carefully when using curvature-based stiffness loss estimation method. It is illustrated in this example that the proposed damage/noise effect ratio can be a good indicator to evaluate the noise effect when choosing an appropriate curvature calculation interval.

3.4 Conclusions

In this chapter, investigation is conducted on effect of measurement noise curvature-based stiffness loss estimation method for bridges. Laboratory experiment and numerical study both indicate capability of the method with the presence of measurement noise. Based on the study, some conclusions can be drawn as follows.

(1) Laboratory experiment was performed to investigate the property of noise. A noise/damage effect ratio is defined to evaluate the noise level with regard to curvature calculation.

(2) Two approaches are studied to reduce effect of measurement noise. The first one is to average multiple displacement measurements, and the other one is to choose appropriate curvature calculation interval. They are verified with the laboratory experiment results.

(3) Numerical study on a detailed 3-D bridge model is conducted to validate the applicability of selecting curvature calculation interval based on noise/damage effect ratio in realistic bridges.

Chapter 4 Displacement measurement with Radar device

Displacement is an important indicators to evaluate the live load carrying capacity of bridges, and it is widely used in static proof load tests. In engineering practice, traditional displacement sensors, such as linear variable differential transformers (LVDTs) and dial gages, are widely used in field tests. However, these sensors require a stationary fixed point to measure the displacements. In many circumstances, it is impossible because bridges are often constructed over highways/deep valleys. Even such fixed point is feasible, the installation often requires traffic regulation and cost much time and labor work.

Another common approach is to perform a double integration on acceleration measurements. This integration process, however, requires filtering selection, baseline correction and manual judgment if anomalies exist in the records (Hudson, 1979). Furthermore, this process may introduce difference with the actual displacement. Displacement could also be inferred from mathematical models using strains measured by fiber sensors, but the accuracy of the obtained displacement is still a concern. The global position system (GPS), which obtains the position of a receiver using a satellite ranging method, is a displacement measurement technique is widely adopted in health monitoring systems of long-span cable supported bridges (Xu et al., 2002; Yi et al., 2010; Sun et al., 2017). Current GPS technology is capable of providing an accuracy of ±1 cm, which is applicable for cable-supported bridges with larger displacement, but not feasible for small or medium span bridges. The existing displacement sensors used in

engineering practice is shown in Table 4.1.

Table 4.1 Existing displacement sensors

Device	Precision (mm)	Static/dynamic	Measuring point
LVDT	0.1	Static	One point
Total station	0.1	Static	One point
Digital level	0.1	Static	One point
Laser-based sensor	0.003	Static/dynamic	One point
GPS	5	Static/dynamic	One point
Radar device	0.01	Static/dynamic	Multi-point

In the proposed load carrying capacity estimation method, a non-contact radio detection and ranging wave (Radar) device is used for displacement measurement. This chapter describes the new interferometric radar device, which can measure displacement at multiple points simultaneously with high sampling frequency. First, the technical mechanism and the characteristics of the Radar device is described briefly. Subsequently, a laboratory test and a field test were introduced which verified precision of this device. At last, its merit of multi-point measurement is also illustrated.

4.1 Introduction on the Radar device

Recent development in radar technology has led to the development of a microwave interferometer, which is suitable for non-contact displacement measurement of bridges. When it is used in truck pass-by test of a bridge, it will not interrupt the traffic. Labor work is only required for reflector installation, which is more efficient than traditional LVDTs or dial gages.

Development of such device could date back to more than 20 years ago. In 1993, Lawrence Livermore National Laboratory in the United States developed a micro-power

impulse radar (MIR), which is a low-cost noncontact ranging sensor (Fraden, 2010). The application was mainly in automation systems, intrusion alarms etc. (Farrar et al, 1999) developed a non-contact Radar system using microwaves, and measured the vibration response of I-40 Bridge. The precision was found to be 0.1mm in the field. The identified modal frequencies agreed well with that from conventional accelerometers.

In this study, a commercial interferometric Radar device (Gentile, 2010) is used for non-contact displacement measurement in truck pass-by tests. The device mainly utilizes two techniques: the SF-CW technique and the interferometric technique. The first is for distinguishing multiple targets, and the second is for high frequency measurement. They are introduced in the following sections.

4.1.1 The SF-CW technique

Stepped Frequency Continuous Wave (SF-CW) technique is used in the Radar device, as shown in Fig 4.1. The signal has a large bandwidth of increasing frequency in discrete steps, and the waveform at each frequency corresponds to a measurement range. In a test with the Radar device, the signal at each frequency will be recorded for all the ranges, no matter there is a moving object in the range or not. In this way, multi-point displacements are measured simultaneously.

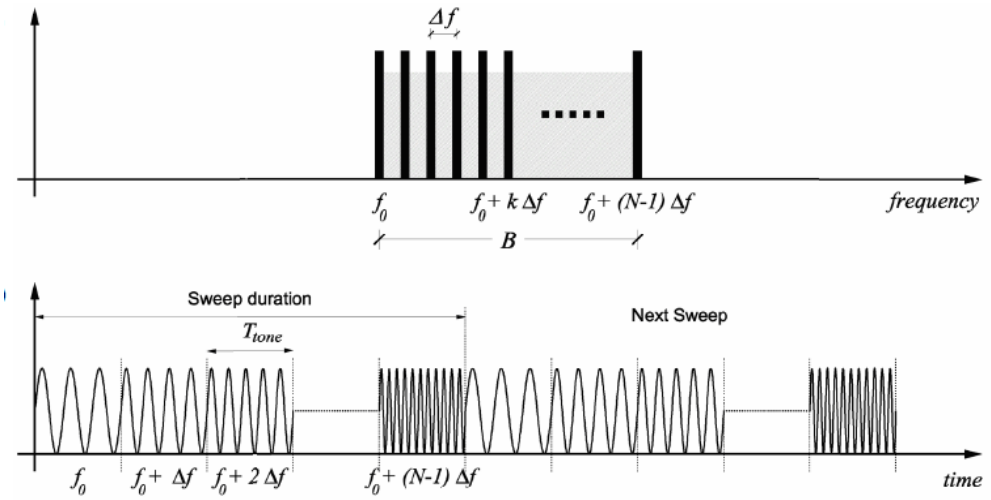

Fig 4.1 Representation of SF-CW waveform in time and frequency domain (Reprinted from (Gentile, 2010))

Suppose that 100 sampling frequency and range resolution of 1 m is set. During measurement, SF-CW waveform of 0.01s (composed of the stepped frequency signals) is sent and received continuously, in which wave of each frequency component is taking information of every 1 m range. The distance from Radar to target can be determined as follows.

$$R = \frac{c \cdot T_0}{2} \tag{4.1}$$

In which, c denotes speed of the radar wave transmission, T_0 denotes the delay of echo signal compared with the original sent signal.

A typical range profile for measurement of cable displacement in a cable-stayed bridge is shown in Fig 4.2, where six clear peaks correspond to six cable targets in the ranges. And ranges longer than 25 m have weaker signal, which means that there is no moving objects which could reflect the signal.

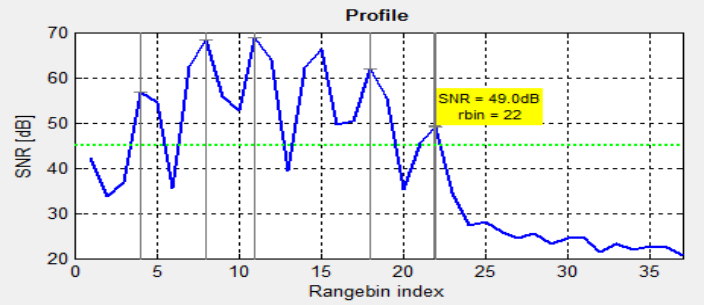

Fig 4.2 Range profile of a cable-stayed bridge

4.1.2 The interferometric technique

This technique enables measurement of the displacement response of each target at high frequency. Electro-magnetic waves reflected by a target differ in the phase information (Henderson and Lewis, 1998). Displacement of the target along the radar wave direction can be computed from difference of phases, as indicated in Fig 4.3.

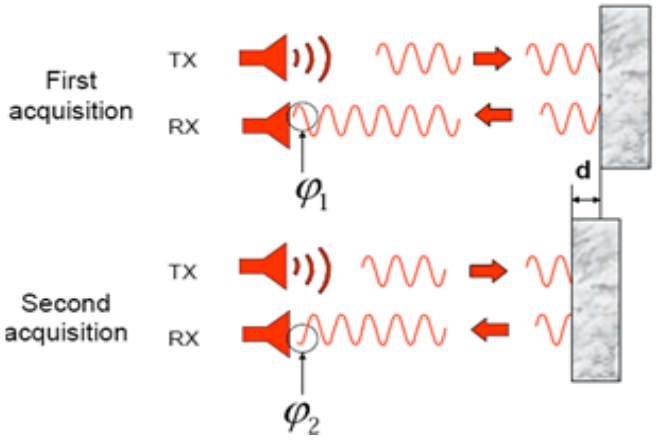

Fig 4.3 Phase change for echo wave at different time

The displacement is obtained as follows.

$$d = -\frac{\lambda}{4\pi}(\varphi_2 - \varphi_1), \tag{4.2}$$

In which, λ is the wave length.

It is noted that the measured displacement is the component in the Radar wave transmission direction, and the actual displacement of targets should be calculated after conversion. For example, bridge displacement is vertical in Fig 4.4, and it should be calculated with equation (4.3) based on geometry relation of Radar and target on the bridge. Geometry information should be measured accurately in field tests to obtain the actual displacement.

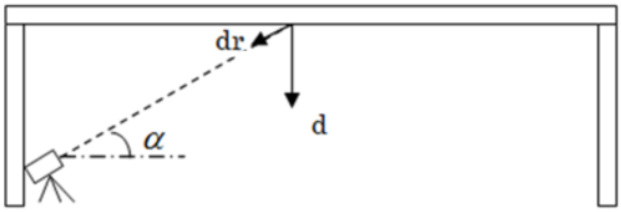

Fig 4.4 Measured displacement and actual displacement

$$d = \frac{d_r}{\sin \alpha} \tag{4.3}$$

4.1.3 Reflector in displacement measurement

Reflection is a general term for the process by which the incident flux leaves a stationary surface of medium from the incident side, without change in frequency. Reflection of electromagnetic waves by the target is the basis for radar operation (David et al., 1998). There are several reasons which affect the reflectivity in the echo signal.

(1) Material. Metal especially aluminum, is strongly radar reflective, while wood and concrete are less reflective. Therefore in measurement of concrete bridges, it is needed to attach reflectors at measurement positions. Aluminum is often chosen as the material for a reflector.

(2) Absolute size. Generally, the larger object has the stronger reflection. However, if a

reflector is too big, the weight of it may change the local mass property of the structure. When the reflectivity is enough in the tests, a relatively smaller reflector is preferred. In this research, corner reflector with side length of 15cm is used.

(3) Incidence angle. If the incidence angle is too large, the echo signal may be reflector away from the receiver.

Reflector is a device designed to redirect the wave from a source. Typically, reflectors have simple geometric shapes. Among them, corner reflector is widely used, especially trihedral reflector (Fig 4.5). It is chosen in this research due to its broad beam-width in both vertical and horizontal direction, and simplicity of installation on structures.

Fig 4.5 Corner reflectors in trihedral shape

4.1.4 Description of the Radar device

The radar equipment (Fig 4.6) consists of a sensor module, a control PC and a power supply unit. The sensor module, weighing 12 kg, includes two horn antennae for transmission and reception of the Radar wave and is installed on a tripod with a rotating head. It is noted that corner reflectors shown as Fig 4.5 are needed for concrete bridges to reach an acceptable reflectivity.

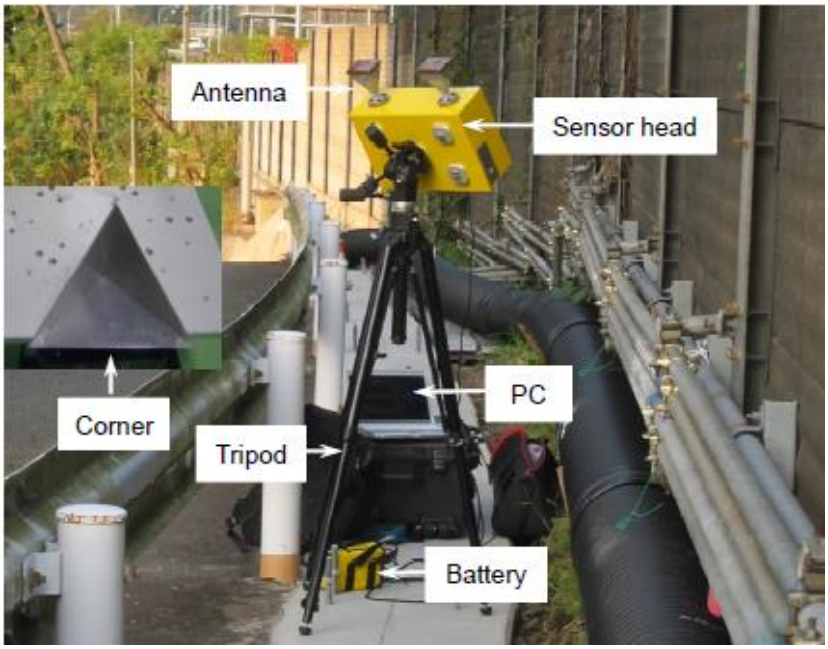

Fig 4.6 View of the Radar device

The equipment radiates at a central frequency of 17.175 GHz with a maximum bandwidth of 140 MHz. The main technical and operational characteristics of the device are summarized in Table 4.2. It can work at a long distance from the bridge (if no other objects are obstructing in the range), which will not interrupt the daily traffic. For expressway bridges or other bridges with busy traffic, this is quite important.

Table 4.2 Specification of the Radar device

Parameters	Amplitude
Maximum Operation distance	1000 m for static; 500 m for dynamic
Displacement precision	0.01 mm
Distance resolution	1.1 m
Sampling frequency	200 Hz
Weight	12 kg

Power supply	12 VDC
Central frequency and frequency band	17.175 GHz, 140 MHz

Compared with other existing displacement measurement devices, the Radar device has the advantage of multi-point measurement. The merits could be illustrated through measurement in two directions with regard to the bridge axis. In transverse direction, the result is shown in Section 5.4 in next chapter. Mid-span displacements of two T-girders were measured simultaneously with the Radar device, which can significantly reduce the testing time in comparison of one-point measurement device such as laser-based sensors. In longitudinal direction, the multi-point measurements could be utilized to improve the displacement measurement precision, as described in Section 4.3.4.

Limitations of the Radar device are also shown here, which should be taken into account in a field test.

(1) Space resolution. Measurement error will occur when different target points are in the same range. In field tests, it is preferable that two targets are at least 1.1 m away from each other in the Radar range.

(3) The precision of the measurements depend on reflectivity of the target. In a field test, the accuracy decrease obviously if signal to noise ratio is low.

In order to verify the reliability of Radar device, laboratory test and field measurement were conducted. Results are illustrated below respectively.

4.2 Laboratory experiment for the Radar precision verification

The performance and precision of the Radar device was investigated in a laboratory

experiment. A vibrating shake table was measured using the Radar device and Laser displacement sensor, as shown in Fig 4.7 (a) and (b). The corner reflector was fixed on the shaking table, at a distance of 3.8 m from the Radar device. The sensor control program was set to measure targets up to a distance of 100.0 m, with a sampling frequency of 200 Hz. The vertical angle between radar transmission wave and horizontal direction is measured as 10.8 degree. At the same time, horizontal movement of the shake table was measured by a laser displacement sensor IL-S100 (produced by Keyence Corporation) for comparison. The nominal accuracy level of IL-S100 is 0.004 mm with a sampling frequency of 1000 Hz. It was mounted about 10 cm away from the shaking table. Specification for the laser sensor is listed in Table 4.3.

(a) View of the experiment

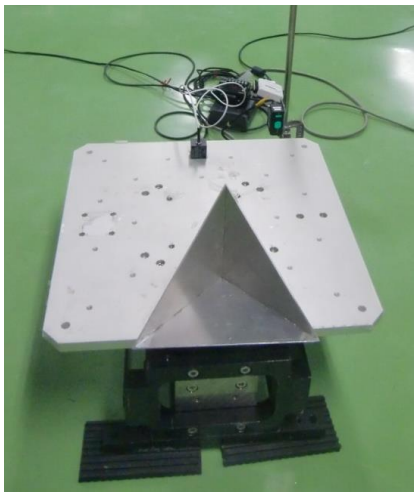

(b) Shake table

Fig 4.7 Radar and Laser measurement of the shake table

Table 4.3 Specifications for Laser sensor IL-S 100

Model	IL-S 100
Mounting distance (mm)	100
Measurement range (mm)	70 to 130
Sampling frequency (Hz)	1000
Accuracy (mm)	0.004
Weight (g)	75

Input signals were chosen as three types: random signal, sine wave at 1 Hz, and sine wave at 5 Hz, which are described in the following sections.

4.2.1 Input of random signal

The whole time history is shown in Fig 4.8. The period from 20 s to 40 s is triangle signal which was used for synchronizing radar measurements and laser measurements.

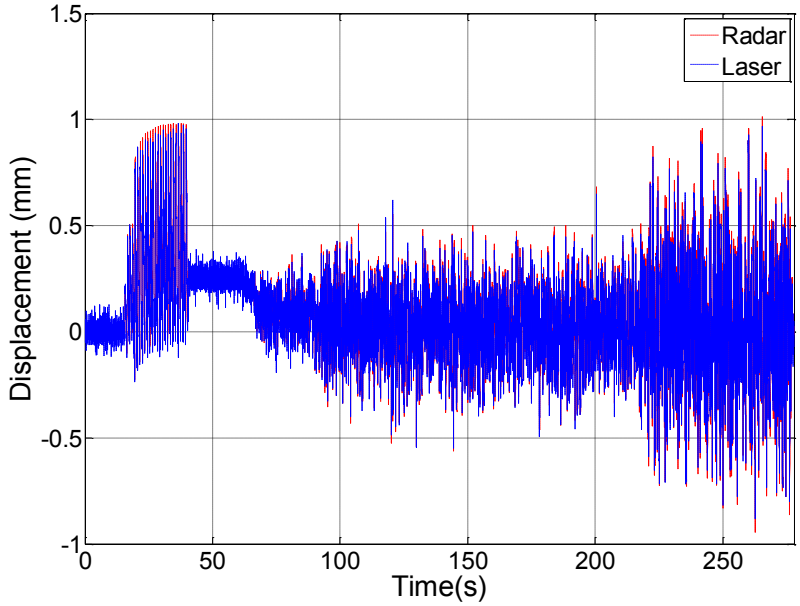

Fig 4.8 Time history of displacement response

The detailed response comparison is illustrated in Fig 4.9. The largest discrepancy between measurements of the two sensors is 0.02 mm. Noticing that the measured original displacement results are in the Radar wave transmission direction, it can be said that they showed good agreement with each other, and Radar measurements captured all the important information of response.

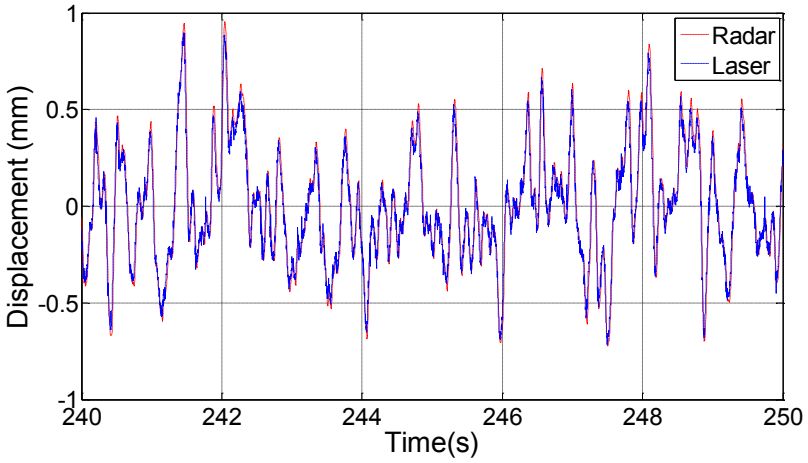

Fig 4.9 Detailed comparison of Radar and Laser measurements

4.2.2 Input of sine wave at 1 Hz

The whole time history and detailed comparison are shown in Fig 4.10 and Fig 4.11 respectively. Still radar measurements agree well with laser measurements. The largest difference is around 0.03mm.

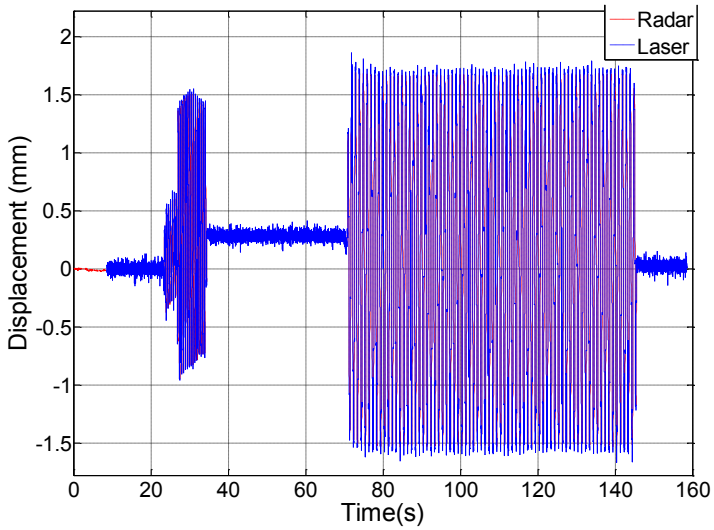

Fig 4.10 Time history of displacement response

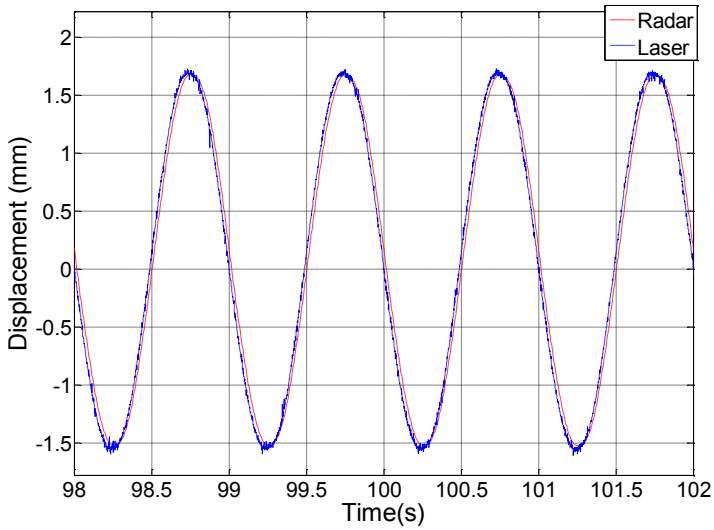

Fig 4.11 Detailed comparison of Radar and Laser measurements

4.2.3 Conclusion for laboratory experiment

In the laboratory experiment, the Radar device can capture structural behavior of the displacement amplitude with a precision of 0.03 mm. It is verified that the device can be used for measurement with in bridge field tests high reliability and accuracy. The difference between Radar and Laser sensor were resulted from two reasons. First, Radar device measures the center of the trihedral reflector, while Laser sensor measures the other side on the shake table. Second, Radar device measures the displacement in the wave transmission direction, which should be converted to the horizontal direction.

4.3 Field test for the Radar precision verification

4.3.1 Introduction on the bridge

Chino viaduct (Fig 4.12) is a four-span continuous PC viaduct, located in Chino city, Nagano prefecture in middle area of Japan. Each span is 24.75 m long and 8.5 m wide with two lanes. The bridge deck is supported by five I-shaped PC girders, each of which has a height of 1.35 m.

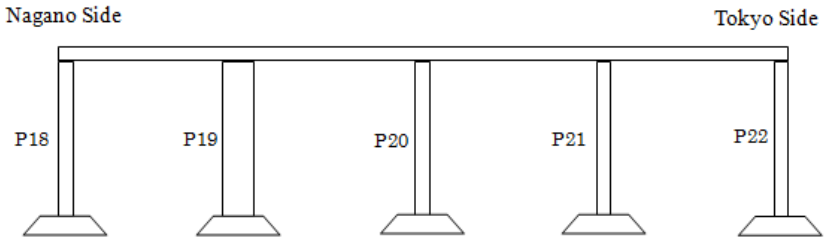

Fig 4.12 Profile of Chino viaduct

The picture and cross-section of the bridge is shown in Fig 4.13 (a), (b) and (c). The viaduct is between Suwa interchange and Suwa-minami interchange, part of ChuO Expressway, which connects Tokyo with Nagano Prefecture, managed by Central Nippon Expressway Company. It consists of upward line and downward line, which are separated as independent structures.

(a) Photo of Chino PC viaduct

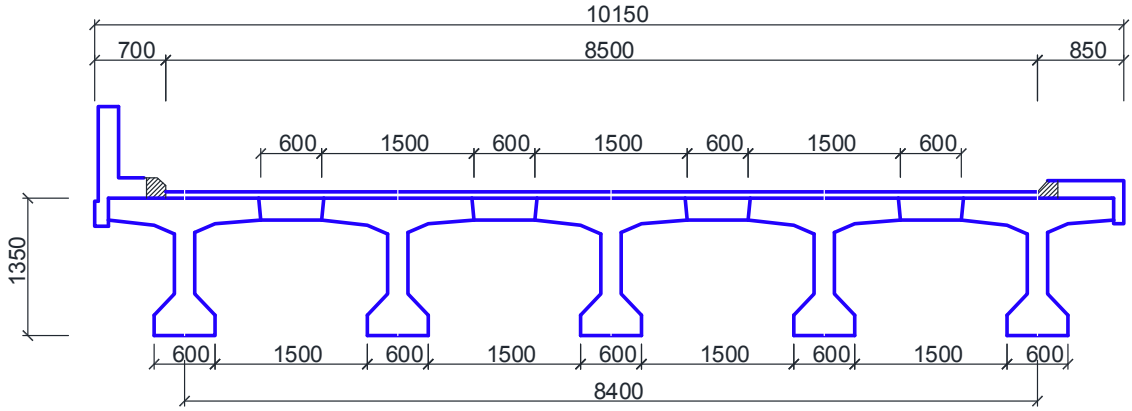

(b) Bridge cross-section

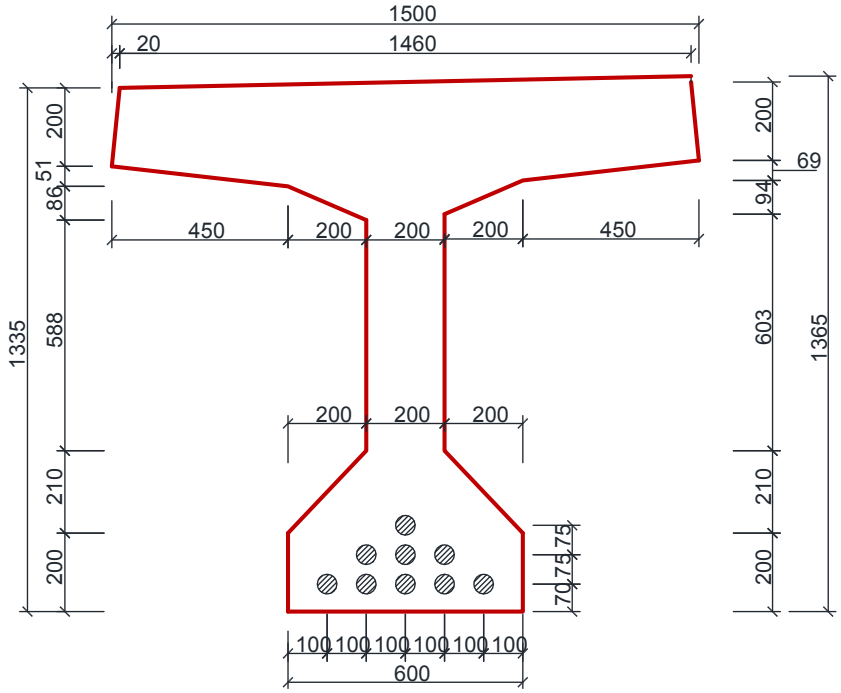

(c) T-girder cross-section

Fig 4.13 Chino viaduct (Unit: mm)

4.3.2 Test preparation introduction

A 3-axle truck (Fig 4.14) is used in the field test, and the truck configurations are shown in Table 4.4. Wight on each axle was measured before and after the test as listed in Table 4.5. It is shown that the total weight and front axle weight before and after the field test are the same. There is only slight difference in the rear axles1.31 m apart, which has little effects on the test results.

Fig 4.14 Truck used in the test

Table 4.4 Truck configuration

Truck Length (m)	Truck Width between Outside of Tires (m)	Distance between front axle and second rear axle (m)	Distance between two rear axles (m)
9.89	2.49	5.55	1.31

Table 4.5 Truck Weight

Weight	Total (Kg)	Front Axle(Kg) (Kg)	First Rear Axle (Kg)	Second Rear Axle (Kg)
Before Test	21600	6350	7350	7900
After Test	21600	6350	8050	7200

There were two test scenarios, which are the truck pass-by test and the static loading test. In truck pass-by test, the truck ran from P20 to P19 at speed of 5km/h and 30km/h. The displacement at T4 with the Radar device and Laser RSV at the same time, with the

objective to verify the precision of Radar device. In static loading test, the truck was stopped with the front axle 0.6 m away from P19, which was intended to investigate the merits of utilizing multi-point measurement. The scenarios are illustrated in Fig 4.15 (a) and (b) respectively.

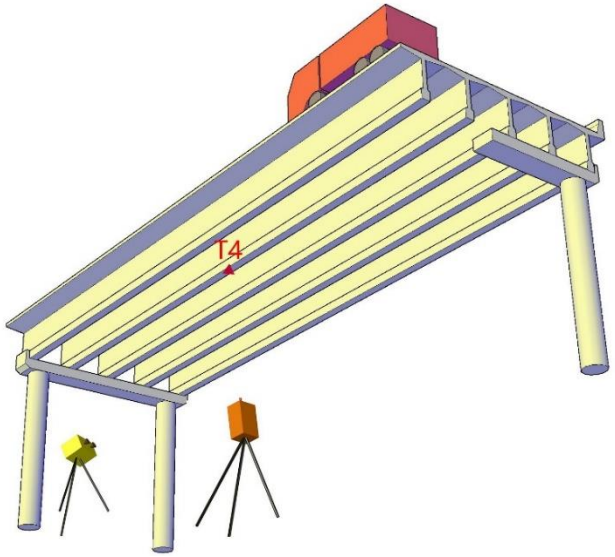

(a) Truck pass-by test

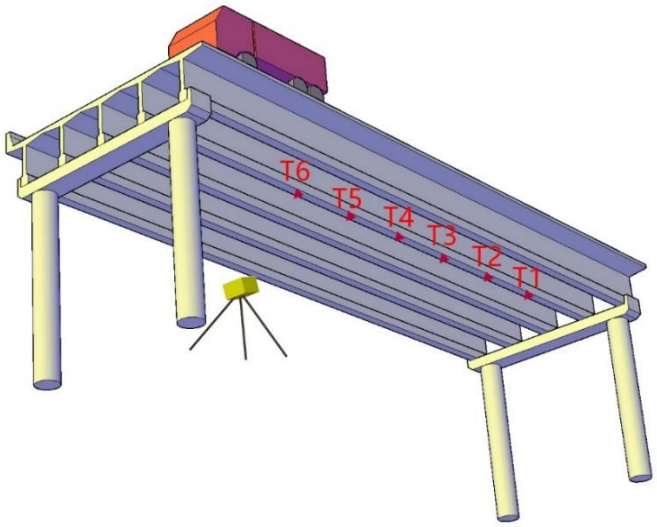

(b) Static loading test

Fig 4.15 Test scenarios

Truck pass-by test was conducted on the second span (P19 ~ P20), which ran from pier P22 to pier P18. For displacement measurement, the interferometric radar device was used simultaneously with a Remote Sensing Vibrometer (RSV), which has a precision of 0.003 mm. The objective of this test is to verify the precision and reliability of Radar device in application on real bridges.

The reflector was attached to the girder before the test, with the help of an inspection vehicle with elevating work platform. The aluminum reflector (Fig 4.16) was installed to the girder bottom surface using strong adhesive, with the center directing toward the radar device to obtain good signal.

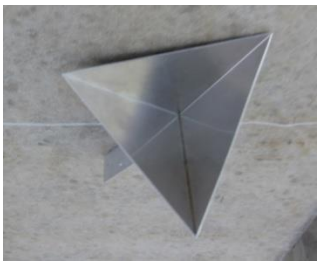

Fig 4.16 The installed refelctor

4.3.3 Verification of Radar device precision

The truck pass-by test was conducted in the inner lane which was closed to traffic. The passing lane was still open to traffic, and the truck pass-by test was conducted when there was no other vehicle on the four-span viaduct. Two humps were placed at 6 m from P19 on P18 ~ P19 span as in Fig 4.17, which excited vibration when truck passed by. It served as a reference for calculating the truck position.

Fig 4.17 Hump Position on the viaduct deck

A total station was used to measure three-dimensional coordinates of the Radar device and the reflector, which provides relative positions for calculating the actual displacement. The elevation angle was calculated as 46.2°, and the actual displacement in vertical direction was calculated with this angle.

The dynamic displacements at target T4 were measured both with the Radar device and RSV-150, as illustrated in Fig 4.15 (a). The comparison of displacement measurements with two devices for truck speed at 5 km/h and 30 km/h are shown in Fig 4.18 and Fig 4.19. It is indicated that the discrepancy is 0.05 mm and 0.06 mm respectively, which should be due to mainly two reasons. First, the RSV measurement is concentrated at one point, which is not exactly the same point with the Radar target. Second, the Radar device measures the displacement in microwave transmission direction, which was converted to vertical direction considering Radar antenna elevation angle. Considering that the precision of traditional displacement sensor LVDT has a precision of 0.1 mm, the Radar device has enough precision for application in practice.

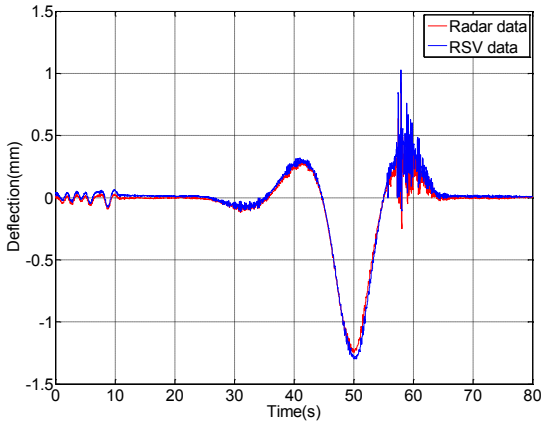

Fig 4.18 Comparison of Radar device and RSV measurement (5 km/h)

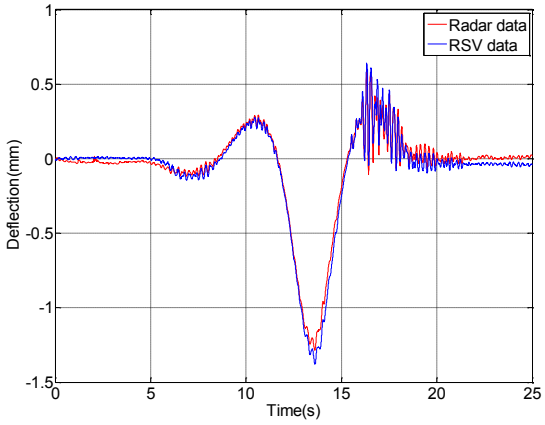

Fig 4.19 Comparison of Radar device and RSV measurement (30 km/h)

4.3.4 Utilization of multi-point measurements

In static loading test, displacement were measured totally 4 times, which include displacement at six points from P1 to P6 as shown in Fig 4.20. .

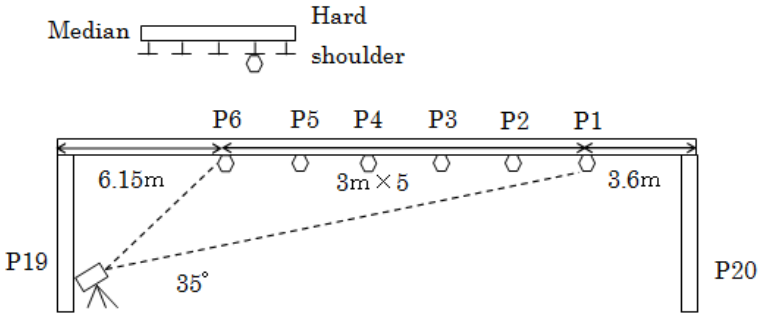

Fig 4.20 Configuration of measurement

All three coordinates for the Radar device and the six reflectors were measured by a total station, and the elevation angle at each reflector was calculated and shown in Table 4.6. It is indicated that the distances between adjacent targets are all larger than the resolution of 1 m, with the smallest as 1.39 m between reflector T5 and T6.

Table 4.6 Elevation angle of the targets

Points	T1	T2	T3	T4	T5	T6
Distance to Radar (m)	20.18	17.60	15.11	12.79	10.86	9.47
Elevation angle (Degree)	28.02	32.29	38.08	46.20	57.26	72.34

The measurement are shown in Fig 4.21, and the maximum displacement is 0.5 ~ 0.6 mm at target T5.

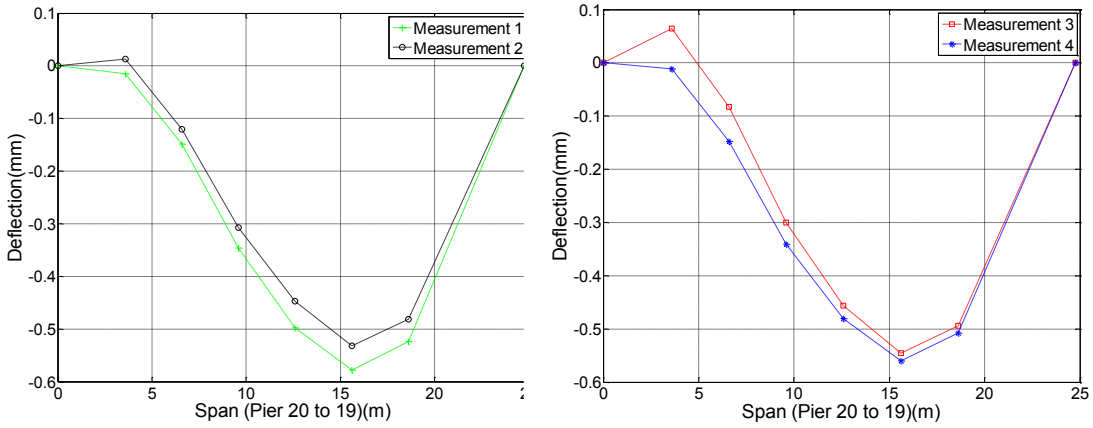

(a) Static test 1 (b) Static test 2

Figure 4.21 Displacement results in static loading tests

As introduced in Chapter 3, beam displacement formula is a three-order polynomial, which could be expressed as below.

$$w(x) = ax^3 + bx^2 + cx + d$$

Four coefficients a,b,c,d could be determined from displacement measurements in a least squire sense. Taking the origin of coordinate to make d zero. The other three coefficients could be calculated with the following equations.

$$\begin{cases} a = \left(\frac{1}{2} w_2 - \frac{1}{2} w_3 + \frac{1}{6} w_4 \right) \frac{1}{\Delta x^3} \\ b = \left(-\frac{5}{2} w_2 + 2 w_3 - \frac{1}{2} w_4 \right) \frac{1}{\Delta x^2} \\ c = \left(3 w_2 - \frac{3}{2} w_3 + \frac{1}{3} w_4 \right) \frac{1}{\Delta x} \end{cases}$$

After knowing the four coefficients, the displacement at unmeasured positions could be predicted with the deflection formula. In this test, displacement at T4 is taken as the prediction point. The results is shown in Table 4.7, which indicates that the largest difference between prediction and measurement is 5%. In practice, this multi-point measurement merit of the Radar device could be utilized to get more information on bridge displacement response.

Table 4.7 Measurement and prediction of T4 displacement

Test	Test 1	Test 2	Test 3	Test 4
Displacement result (mm)	-0.4973	-0.4472	-0.4558	-0.4801
Prediction (mm)	-0.4804	-0.4333	-0.4328	-0.4667
Error (%)	3.4	3.1	5.0	2.8

4.4 Conclusions

In this chapter, the basic principle of Radar device is introduced, and its precision is verified in laboratory experiments and a bridge field test. The device can also measure multi-point simultaneously, which can be utilized to predict displacement at position of interest. It can be applied in practice to measure bridge displacement efficiently with reliable performance.

For practical application on bridges, the information below is summarized.

(1) The device could achieve non-contact measurement, which saves much time and labor work, and it has little effect on the normal traffic.

(2) Measurement of displacement at high sampling frequency of 200 Hz, which is suitable for displacement measurements during truck pass-by test.

(3) Prior knowledge of relative position information of the device and the reflector targets is required for actual displacement measurement.

For displacement measurements with the Radar device in a field test, the following are recommended.

(1) Four personnel are needed;

(2) Tests are performed when there is less traffic, such as during night;

(3) The truck run at constant speeds, 10 ~ 30 km/h is recommended;

(4) Elevation angle of each reflector target (with regard to the Radar device antenna) is measured accurately, as the displacement should be converted to vertical direction;

(5) Elevation angle is set larger than 20° for all reflector targets.

Chapter 5 Load carrying capacity estimation for girder bridges: applications

In recent year, there is more and more concern over load carrying capacity of aging bridges. A proof load test is often applied to an existing bridge for the purpose of checking that it has adequate strength for continued or modified service conditions (Fujino Y., and Lind N.C, 1977). In order to investigate the feasibility and reliability of the proposed method, field tests were carried out on a simply supported PC T-girder bridge and a four-span continuous PC viaduct respectively. Radar device was used to measure displacements under truck pass-by tests. In the first bridge example, the viaduct is in healthy condition, and the curvature results demonstrated no observable stiffness loss. Subsequently, the test results were used to calibrate a detailed finite element (FE) model of this viaduct. Artificial damages were created, and stiffness loss estimation was performed on the FE model with the proposed curvature method. In the second bridge example, both static proof load test and the truck pass-by test were conducted, and the results from them generally agree, which illustrated the feasibility of the proposed method in practical application.

5.1 Introduction

5.1.1 Introduction on durability of PC bridge

In PC bridges, permanent stresses are created for the purpose of improving its

behavior and strength under various service conditions (Lin, 1955). The principle of prestressing technology improved structural performance of concrete greatly. The earliest investigations of prestressed concrete beams were conducted in the nineteenth century in Germany. In 1888, the German engineer W. Doring patented a system for construction of slabs, planks, and beams, by which cracking was reduced through the use of prestressed wires. The first PC bridge was constructed in Aue, Germany in 1937. After that, the French engineer, Eugene Freyssinet (Menn, 1990) made great efforts in further development of PC bridges for practical application. After the Second World War, rapid economic growth triggered a boom in bridge construction, and new design and construction techniques were tested and improved for PC bridges.

For internal tendon PC bridges, the tendons are inside the concrete and invisible, and rupture of tendons may cause sudden collapse of bridges. There were reported collapses of PC bridges occurred without warning. One early example of bridge collapse was 15 years old Bickton Meadows footbridge in Hampshire, UK in 1967 (The Concrete Society, 2002). It was a prestressed concrete bridge, and the collapse was caused by severe corrosion of the top tendons and poor quality in the precast units and the thin mortar joints. In 1985, Ynys-y-Gwas Bridge, which is a post-tensioned segmental bridge in South Wales, UK, collapsed without any warning after 32 years of operation. The direct cause was found to be corrosion of post-tensioned tendons. There was regular inspection but no evidence of obvious deterioration was found before the failure. A detailed investigation (Woodward and Williams, 1988) concluded that chlorides from deicing salt were the primary cause of corrosion of tendons. Segmental joints were found to be the locations susceptible to corrosion. Ineffective waterproofing, inadequate grouting, opening of the

joints under live loads, and the wet environment induced the corrosion, which finally caused the collapse.

Fig 5.1 Collapse of Ynys-y-Gwas Bridge (From 青木圭一, 2015)

In 1992, the bridge across the River Schelde in Belgium collapsed without warning after 36 years of service. It was reported that corrosion of the post tensioning through the hinged joint of the end tie-down member were found after the collapse (Mathy et al. 1996). In 1999, Saint Stefano bridge in Italy collapsed as a result of pitting corrosion near the box girder joint (Proverbio et al. 2000). The bridge was located near the sea, and chloride contamination was considered to be the main cause of corrosion.

In Japan, the deterioration of PC bridges is also a severe issue, and examples of two collapsed PC bridges are described in Section 1.1. PC bridges near the sea often suffer from chloride taken by the wind. According to a questionnaire by NEXCO (Aoki, 2015), 27 severe damage examples of PC bridges were found, and the main damages were corrosion (6), concrete crack (2) and transvers prestress tendon rupture (7) and main tendon rupture (12). There have been several PC bridges which were removed and

reconstructed because of severe tendon corrosion.

The bridge operators in NEXCO are concerned about the deterioration problem of PC bridges, and carried out experimental study on load carrying behavior of PC girder taken from demolished bridges (Osada et al. 2006; 寺田典生, 2015). A PC girder was loaded at two points in the mid-span, which has a span of 17.6 m with simply supported boundary condition. Four tendons out of five were cut off one by one near mid-span to investigate the effects of local tendon rupture on load carrying capacity. The loading force was applied until 149.1 kN, which is equivalent to the design live load. It was loaded in 20 kN interval from 0 kN to 140 kN, and finally loaded at 149.1 kN. The force was plotted against the mid-span displacement. When 1 and 2 tendons were cut off, the load-deflection curve was almost linear, with stiffness loss of around 2.5 % and 13 % respectively. When 3 tendons were cut off, there was clear stiffness decrease of around 30 %. And the load-deflection curve became nonlinear at around 118 kN, then the load was applied until 130 kN. When 4 tendons were cut off, the load-deflection curve became nonlinear at 60 kN, The stiffness decrease was around 40 %. The girder was loaded until 150 kN, with deflection increasing largely until almost 200 mm. These experiments provided important information on the structural performance of PC bridges.

5.1.2 Procedure for field test with the proposed method

The procedure for implementation of the proposed load carrying capacity estimation method is described as follows.

1) Evaluation of the inspection and condition rating results, and determine the candidate bridges for load carrying capacity estimation from bridges rated as Level 3 and

Level 4.

2) Development of truck pass-by test program, with detailed testing schedule and testing scenarios, such as truck speeds and running lanes.

- For stiffness loss estimation at severe damage locations, truck pass-by test is conducted over the corresponding lane over the damaged location, and displacement is measured on the relevant girder.

- For live load carrying capacity evaluation of the bridge, truck pass-by test is conducted over all lanes corresponding to regulated static proof load positions, and displacement is measured at mid-span of the relevant girders.

3) Preparation for the test, which include bridge field survey, testing truck determination and weight measuring. A 20 ~35 ton truck is chosen according to design documents and current traffic weight regulation, which is around 10% ~ 20% of the design loading.

4) Sensor installation. Mid-span is often selected as the displacement measurement position. Radar device location is determined, and reflectors are installed. The distance between the antenna and the reflector target, and the distance between the antenna and the deck are measured for calculation of the Radar wave propagation direction.

5) Test implementation. To minimize the influence on traffic, non-rush hour time is selected such as mid-night. Generally for a bridge with a span between 20 m and 40 m, test truck speed below 30 km/h is preferred (such as 10 km/h, 20 km/h and 30 km/h).

6) Displacement measurement analysis. The measured displacement is converted to

vertical direction, and the dynamic component is filtered. The influence line is obtained for test truck over each lane.

7) Curvature-based stiffness loss estimation is performed on the severely damaged bridge girder using the displacement measurements. It will gives information on stiffness loss estimation of local damage on the bridge.

8) Static load test is simulated on the influence line, and the displacement result is calculated. The result is compared with displacement response under design loads of FE analysis. A smaller value indicates healthy condition of the bridge, and a larger value provides information on the load carrying capacity of the bridge.

5.2 Field test for local stiffness loss estimation

5.2.1 Introduction on the test

Full-scale dynamic testing of structures can provide valuable information on the service behavior and performance of structures. With the growing interest in the structural condition of highway bridges, truck pass-by tests can be used as a tool for assessing the integrity of bridges (Salawu and Williams, 1995). And a vehicle has been used for assessment of bridge condition in different ways, such as identification of natural frequencies of bridge (Dionysius and Fujino, 2012) or determination of dynamic impact factor (Deng and Cai, 2010).

Chino Viaduct is a two-lane four-span continuous PC bridge, which was introduced in details in Section 4.3. The interferometric radar device was used for displacement measurement, as shown in Fig 5.1.

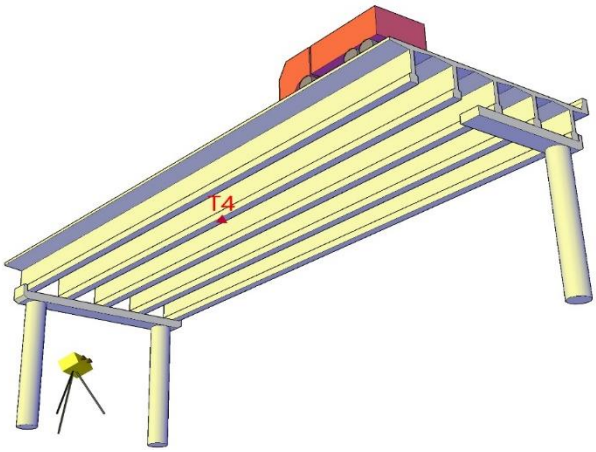

Fig 5.1 Displacement measurement with Radar device

As the tested span is one of the four-span continuous PC viaduct, it is important to identify the location of the truck corresponding to the measurement of displacement time history. A GPS was put on the truck for synchronization of the truck location with the displacement response. It identifies the position of the truck at 1 Hz during the truck pass-by test. These data are stored in the laptop computer. Another GPS was connected with the other laptop computer with the Radar displacement measurement. When the truck passes over the hump, the effects can be located on the displacement time history. In this way, the two GPS can synchronize the truck location with the bridge displacement response.

The truck pass-by test was conducted at a speed of 5km/h and 30km/h respectively, and twice were performed at each speed. The test took less than 1 minute for each running, which has little effect on the traffic.

5.2.2 Truck pass-by test results

After conversion to vertical direction, the dynamic displacement measurement of the target was obtained. As explained in Section 4.3.3, the hump was placed at 6 m from pier

P19. Taking the vibration caused by hump as reference, the time history when the truck was on the instrumented span in each test is extracted.

Mode frequencies of the viaduct are obtained using displacement measurements of the viaduct in the truck pass-by tests. The first three frequencies are obtained as 4.227 Hz, 4.996 Hz and 6.149 Hz, which are illustrated in Fig 5.2.

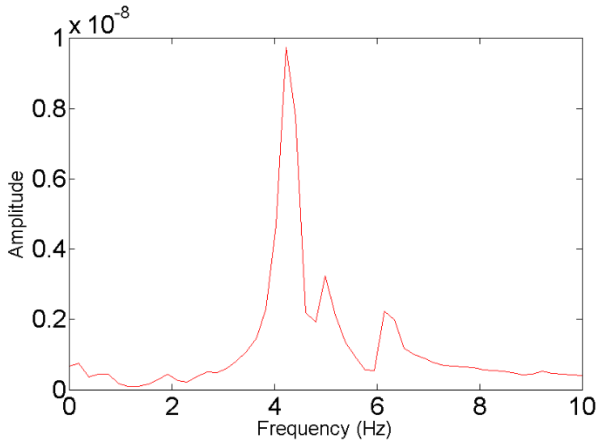

Fig 5.2 Frequency components of the viaduct

A low pass filter is applied to the dynamic displacement data to eliminate the high frequency dynamic components, and the cut-off frequency is taken as 1.0~2.0 Hz. Dynamic displacements in the four truck pass-by tests were filtered, and results of target T4 before and after filtering are shown in Fig 5.3 ~ Fig. 5.6.

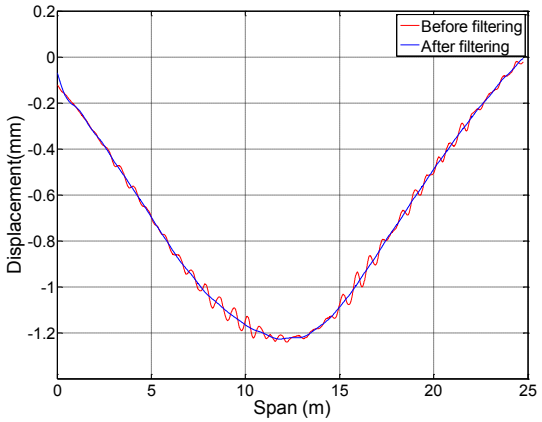

Fig 5.3 Dynamic displacements before and after filtering for test 1

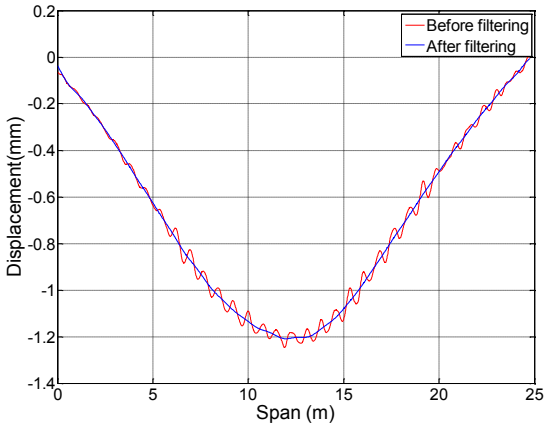

Fig 5.4 Dynamic displacements before and after filtering for test 2

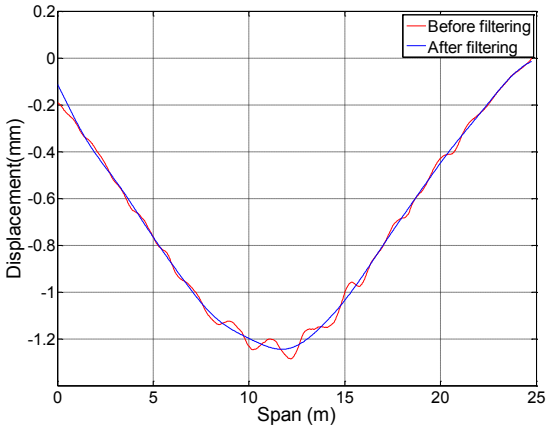

Fig 5.5 Dynamic displacements before and after filtering for test 3

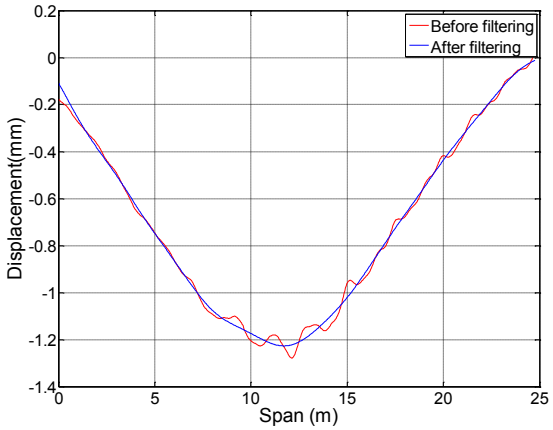

Fig 5.6 Dynamic displacements before and after filtering for test 4

5.2.3 Curvature calculation and stiffness estimation

After filtering, curvature is calculated according to the following formula.

$$\kappa = \frac{y_1 - 2y_2 + y_3}{\Delta x^2}$$

In the four truck pass-by tests, the calculated results of curvature are shown in Fig 5.7 ~ Fig 5.10 respectively.

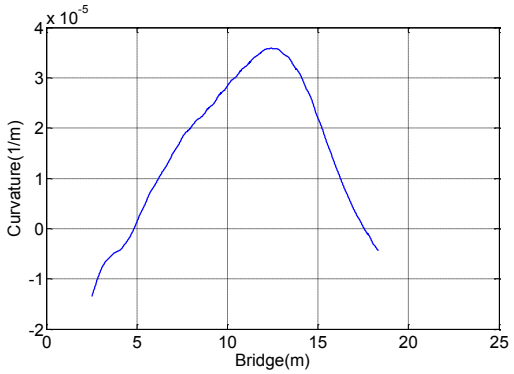

Fig 5.7 Curvature results in Test 1

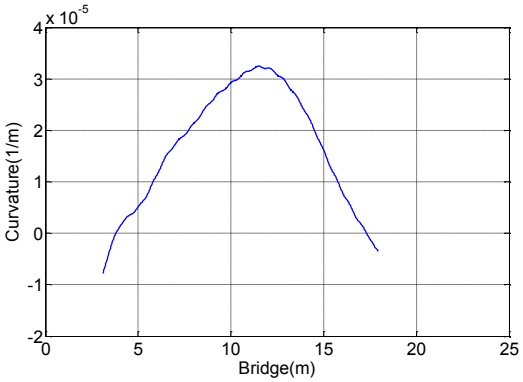

Fig 5.8 Curvature results in Test 2

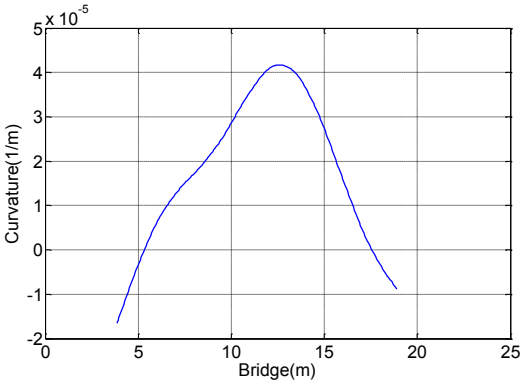

Fig 5.9 Curvature results in Test 3

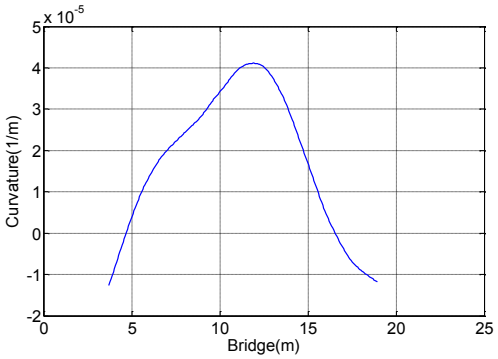

Fig 5.10 Curvature results in Test 4

It is noted that the position target T4 is 12.6m. Inspection results indicated that there is no observable defects in the viaduct, and the curvature results in all the four tests indicate that there is no stiffness loss.

In the following section, a finite element model is calibrated with the field measurement to investigate reliability of the proposed curvature-based local stiffness estimation method.

5.3 Numerical investigation with a finite element model

5.3.1 Calibration of finite element model of the viaduct

In order to further investigate the proposed method, a finite element model of the viaduct is established in commercial software ABAQUS for further analysis. The viaduct model is illustrated in Fig 5.11. The material properties of the concrete and steel are given in Table 5.1. The deck and girders are modeled with solid elements, and the rebars and tendons are modeled with truss elements. The continuous viaduct model contains totally 52343 elements and 79158 nodes. The mesh size is 0.2 m×0.2 m, and there are totally

495 meshes along the longitudinal direction of the viaduct. The prestress is applied through decrease of temperature, and the shrinkage of tendon transfers the prestressing force to adjacent concrete. The thermal expansion coefficient is defined as $1.2\times10^{-5}/℃$.

Fig 5.11 ABAQUS model of the viaduct

Table 5.1 Concrete and steel properties in bridge model

Material	Concrete	Steel
Density	2400 kg/m3	7890 kg/m3
Young's modulus	2.33×10^{10} Pa	2.0×10^{11} Pa
Poisson's ratio	0.15	0.3

Mode frequency analysis is conducted on the viaduct model in ABAQUS, and the first three bending frequencies are obtained as 4.349, 4.895 and 6.167. The corresponding mode shapes are illustrated in Fig 5.12. Comparison between simulation results and measurements is summarized in Table 5.2. It is shown that the extracted three bending frequencies are in good agreement with measurement results. The largest difference of the first three bending mode frequencies between the model and the real viaduct is below

3%.

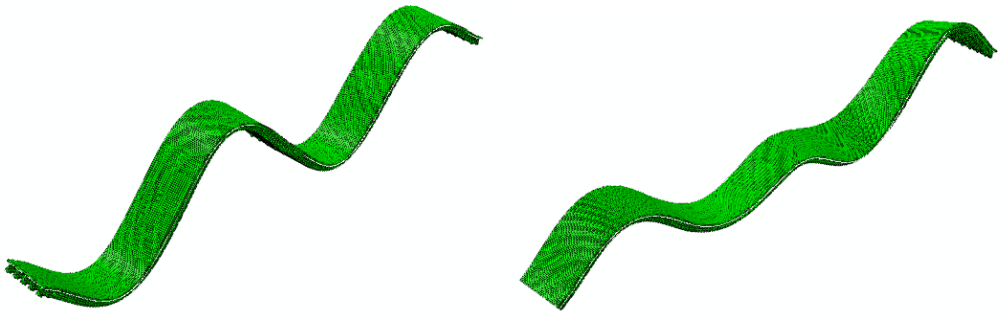

(1) First bending mode (2) Second bending mode

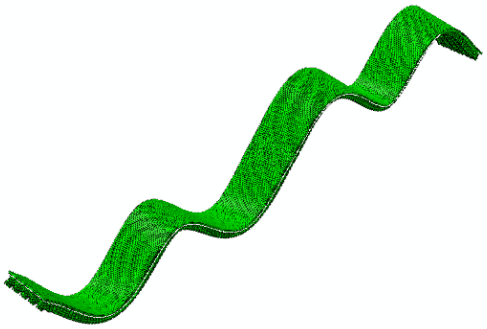

(3) Third bending mode

Fig 5.12 Frequency of the viaduct

Table 5.2 Comparison of mode frequencies between simulation and measurement

Identified frequency from measurement（Hz）	4.227	4.996	6.149
Frequency from FE model（Hz）	4.349	4.895	6.167
Difference	2.9 %	2.0 %	0.3 %

5.3.2 Stiffness loss estimation on the FE viaduct model

The same model in the last subsection is adopted for the stiffness loss estimation. As concrete spalling and tendon corrosion/rupture are possible damages, artificial damage of concrete crack and tendon rupture is created. The damage is created in the second girder at position of 35 m. The concrete spalling is 0.86 m long, 0.2 mm wide and 0.01 m deep, which is equivalent to 2.2% stiffness loss of the girder. They are illustrated in Fig 5.13. The tendon rupture (Fig 5.14) is simulated as 1 m long, where no tendon is simulated in this area.

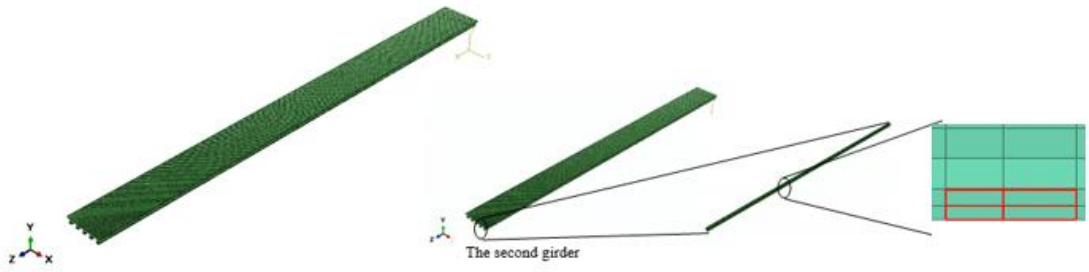

Fig 5.13 Damage in the viaduct model

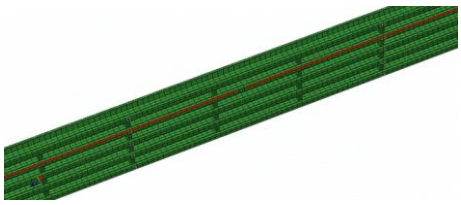

Fig 5.14 Tendon rupture simulation

The vehicle is simulated with a one-wheel quarter car model. The vehicle body is represented by a 20 ton mass supported by a linear spring and a dashpot. The stiffness coefficient is 3.8×10^{6} N/m , and the damping coefficient is 3.4×10^{4} N·s/m .

Modal dynamic analysis in ABAQUS is conducted, and superposition of the first 7 modes (below 10 Hz) is used in this example. Damping ratio for each mode is set as 0.05. The analysis step is conducted for 12 s, including two parts: vehicle passing the bridge (9.9 s) and free-vibration after vehicle passing (2.1s).

As illustrated before, a global iteration method is used for contact force calculation. To achieve geometric compatibility conditions at the contact points, the convergence criterion is set that the maximum contact force difference between successive iterations is smaller than 0.1% of the dynamic displacement at mid-point of the span. Once the convergence criterion is satisfied, the calculation is completed, and response of the bridge is retrieved. The computation is conducted on a personal computer, which takes only around 10 minutes to complete whole analysis

After the third iteration, displacement at 40m position of the loaded girder is extracted, and it is shown in Fig 5.15. The fundamental natural frequency is 4.349 Hz, and fundamental natural period is 1/4.349 s. The vehicle passes through 496 nodes over the bridge in 9.9 s, and the sampling frequency is calculated as 50.1 Hz. Therefore the curvature calculation interval is obtained as 11. For comparison, the intact model is also analyzed, and the displacement is calculated. The curvatures of displacements in intact and damaged model are shown in Fig 5.16. It is illustrated that damage caused by concrete crack and tendon rupture near 35 m can be located and evaluated. The stiffness loss is estimated as 22.3%.

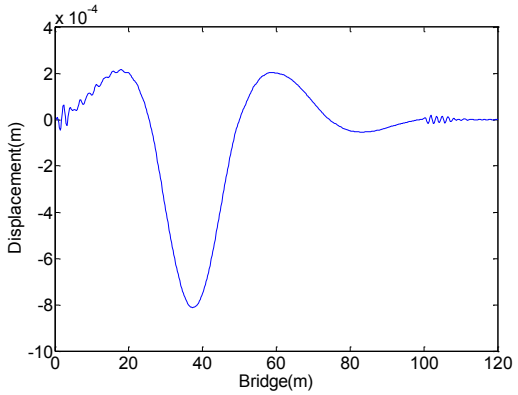

Fig 5.15 Displacement at 40 m position

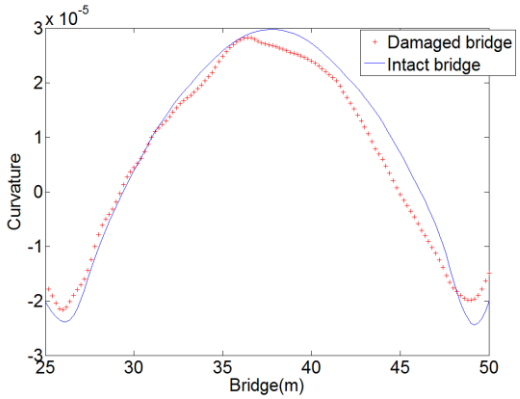

Fig 5.16 Curvatures of intact and damaged girder

Concrete spalling and tendon rupture are simulated as the damage in this PC viaduct model, and it is shown that the defects of tendon rupture and concrete crack can be estimated reliably with the proposed method. With carefully prepared field test and measurement plan, this proposed method has a potential to be applied to real bridges.

5.4 Field test for load carrying capacity evaluation

5.4.1 Introduction on Wenxi Bridge

Wenxi Bridge is a PC T-beam bridge opened to traffic in 2007, which consists of nine simply supported spans with a total span of 9×30 m. It has a total width of 12.5 m with two lanes of traffic in the middle. There are 1.75 m wide pedestrian walkways on both sides of the bridges. The bridge has a 15.7-cm thick concrete deck on five prestressed concrete T-beams. The cross section of the bridge is presented in Fig 5.17 (a) and (b). The photo of the bridge is illustrated in Fig 5.18. The reflectors were installed at mid-span of T1 and T2 respectively Fig 5.19 (a), and the photo of one installed reflector is shown in Fig 5.19 (b).

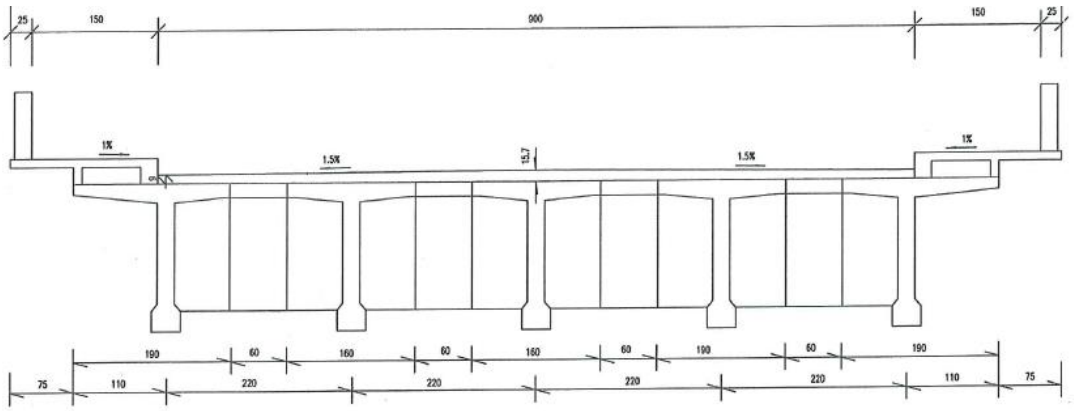

(a) Bridge cross sections

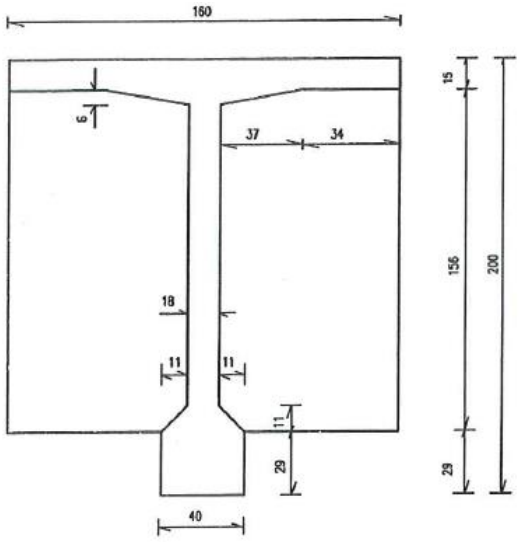

(b) T-beam

Fig 5.17 Cross section of Wenxi Bridge（Unit: cm）

Fig 5.18 Photo of Wenxi Bridge

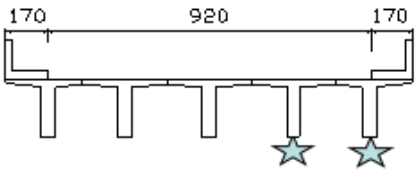

(a) Layout of displacement reflector

(b) Reflector

Fig 5.19 Installed reflector

5.4.2 The static proof load test

The proof load testing was performed on both lanes, and the locations of the four loading trucks are shown in Fig 5.20. During the test, the traffic was closed in both directions, and the four trucks were stopped in place one by one, as illustrated in Fig 5.21. It is noted that the static test takes around 3 hours with total traffic closure, and 12 personnel participated in the test. The traffic closure was possible because the traffic was not busy in that area. The traffic closure regulation was admitted by the local traffic administration, and announced to local people in advance.

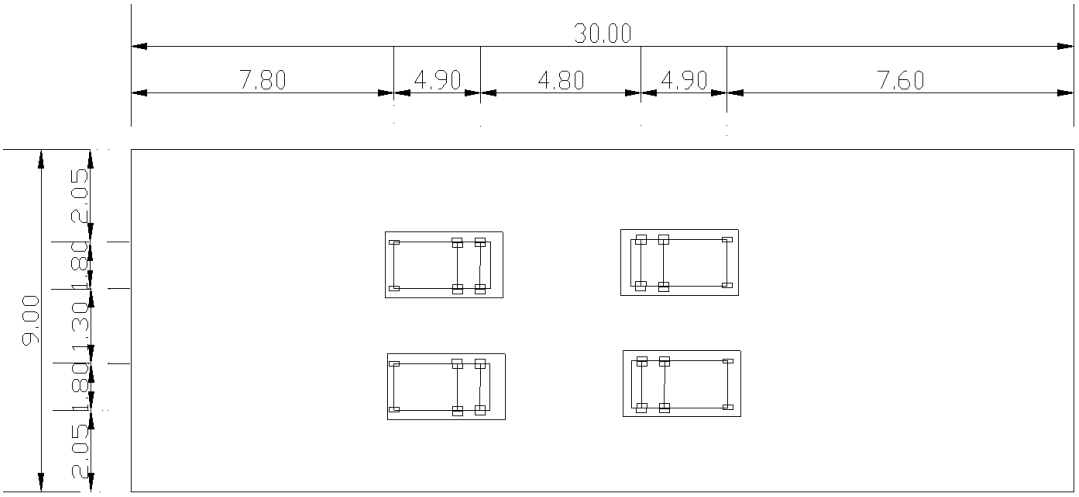

Fig 5.20 Loading truck configuration (Unit: m)

Fig 5.21 Static proof load test

Each truck weighs around 30 ton, and the configurations and the axle loads of the four trucks are presented in Fig 5.22 and Table 5.3 respectively. Digital level Leica DNA-03 is used to measure the displacement, which has a precision of 0.1 mm. The displacement results at mid-span of the four T beams are shown in Table 5.4.

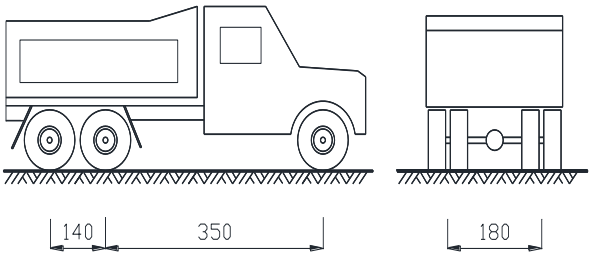

Fig 5.22 Test truck configuration (Unit: cm)

Table 5.3 Truck axle weights

Truck No.	Axle weight (ton)		
	Total weight	**Front axle**	**Two rear axles**
1	30.69	6.14	24.55
2	30.17	6.03	24.14
3	29.62	5.92	23.70
4	29.55	5.91	23.64

Table 5.4 Displacement measurements

T girder no.	Displacement (mm)
T1	6.66
T2	7.18
T3	7.17
T4	6.80
T5	6.64

5.4.3 The truck pass-by test

For the dynamic test, the bridge was tested in both directions with one pass-by truck. The truck configuration is the same as Fig 5.22.

In order to obtain the displacement at mid-span of T1 and T2 beams under static proof load test configuration as shown in Fig 5.20 with one running truck, the pass-by tests should be conducted on two lanes respectively. The truck was moving at three different speeds, 10 km/h, 20 km/h and 30 km/h respectively. A schematic view is

illustrated in Fig 5.23. The distance between the Radar device and T1 is 14.2 m with an elevation angle of 24°. The traffic lane over T1 and T2 is denoted as lane 1, and the other as lane 2.

The truck pass-by test was conducted for 6 running times from 22:46 to 22:58, which took 12 minutes in total. Four personnel joined the test with 1 testing truck. Compared with the static proof load test, it saves much time and labor force in field application.

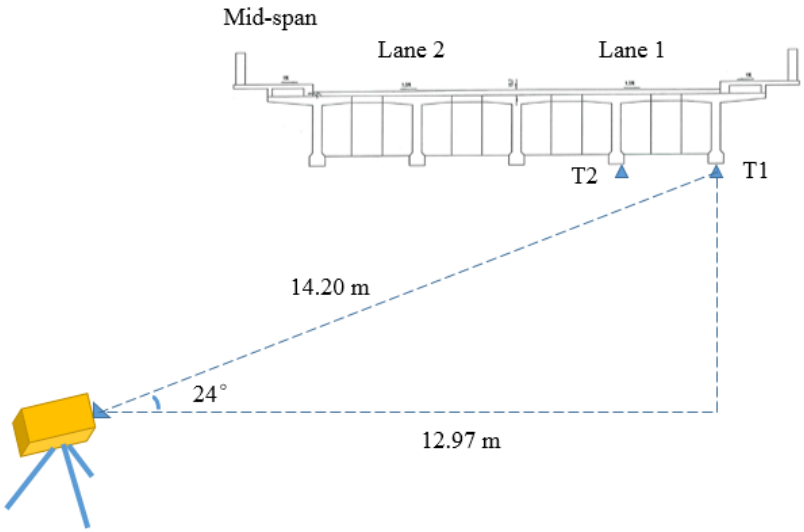

Fig 5.23 Schematic view of truck pass by test

The displacements were measured, and the fundamental natural mode frequency is obtained 4.41 Hz. A low-pass filter is used to eliminate the dynamic components in the signal, and the cut-off frequency is chosen as 0.5 Hz after sensitivity analysis. The results are summarized below.

（1）Truck speed of 10 km/h

When the truck ran over lane 1 and 2, the displacement time history at T1 are shown in Fig 5.24 (a) and (b) respectively.

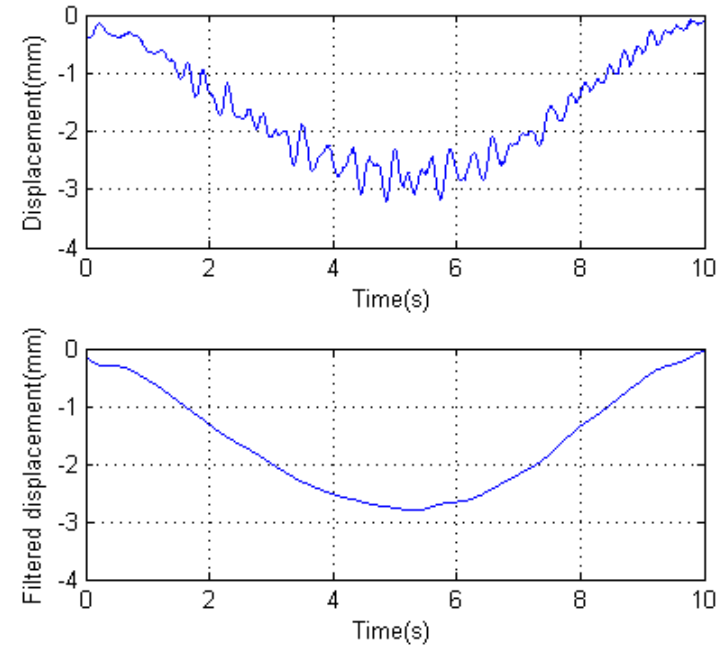

(a) The truck over lane 1

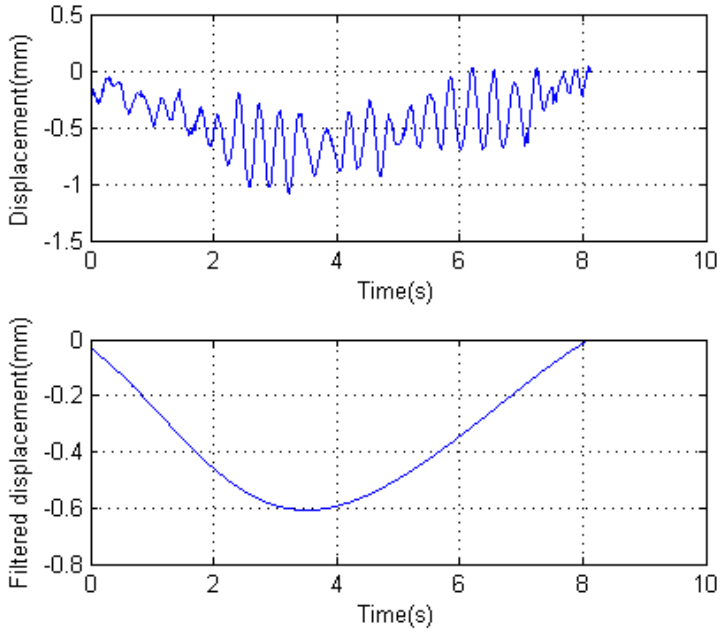

(b) The truck over lane 2

Fig 5.24 Displacement time history at T1 mid-span under truck speed of 10 km/h

When the truck ran over lane 1 and 2, the displacement time history at T2 are shown in Fig 5.25 (a) and (b) respectively.

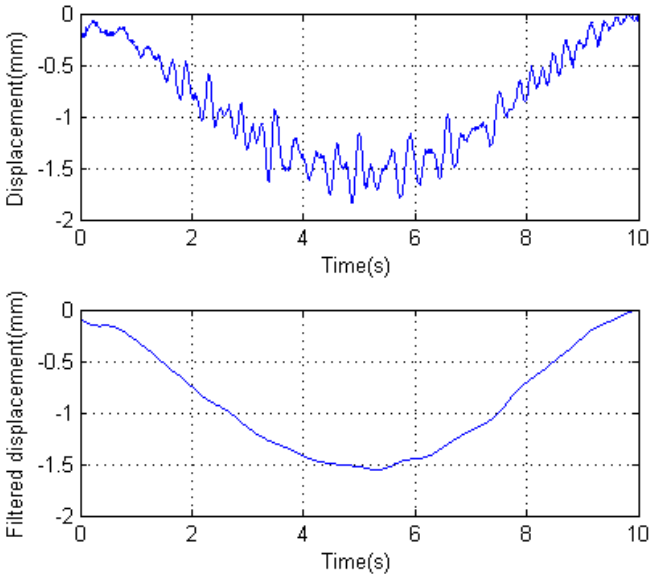

(a) The truck over lane 1

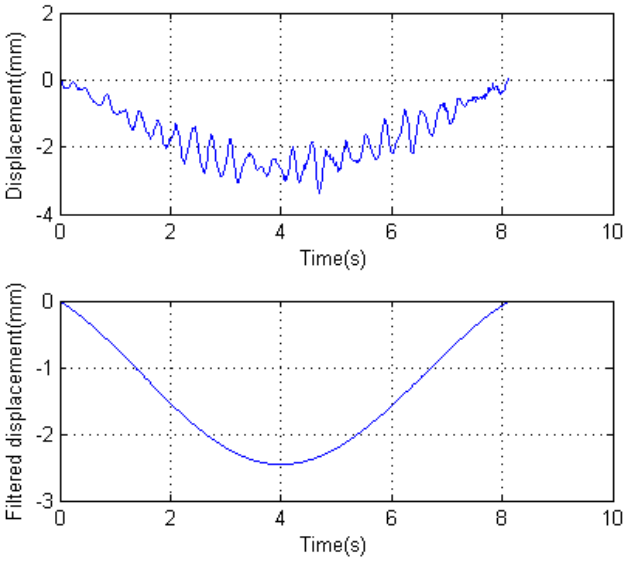

(b) The truck over lane 2

Fig 5.25 Displacement time history at T2 mid-span under truck speed of 10 km/h

(2) Truck speed of 20 km/h

When the truck ran over lane 1 and 2, the displacement time history at T1 are shown in Fig 5.26 (a) and (b) respectively.

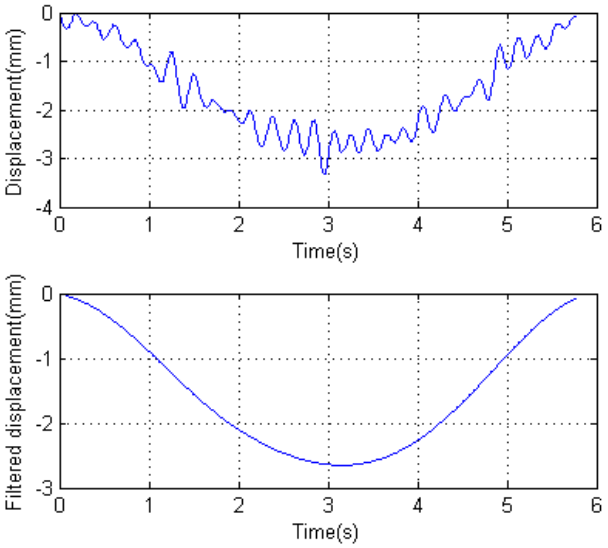

(a) The truck over lane 1

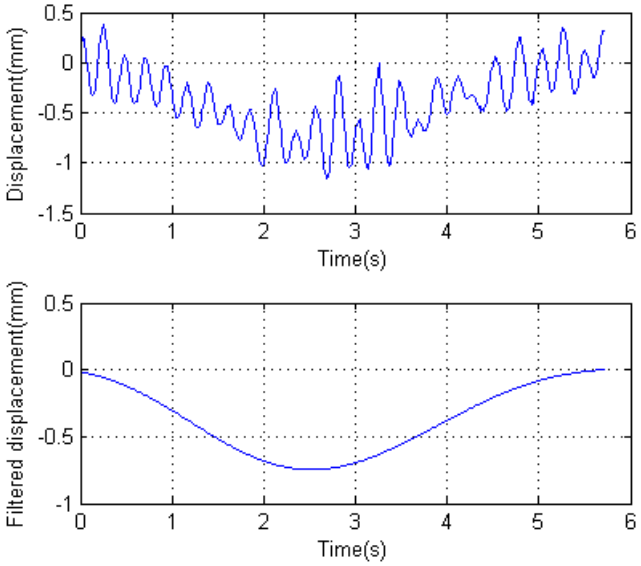

(b) The truck over lane 2

Fig 5.26 Displacement time history at T1 mid-span under truck speed of 20 km/h

When the truck ran over lane 1 and 2, the displacement time history at T2 are shown in Fig 5.27 (a) and (b) respectively.

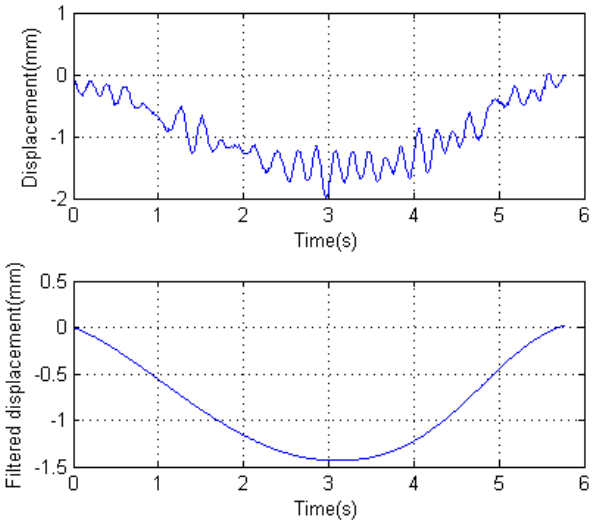

(a) The truck over lane 1

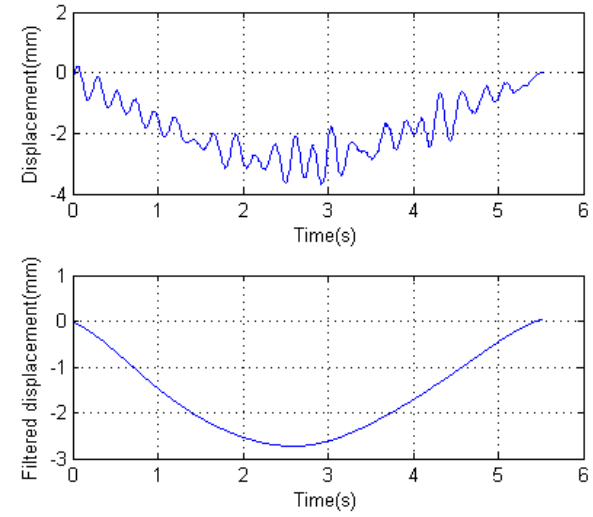

(b) The truck over lane 2

Fig 5.27 Displacement time history at T2 mid-span under truck speed of 20 km/h

(3) Truck speed of 30 km/h

When the truck ran over lane 1 and 2, the displacement time history at T1 are shown in Fig 5.28 (a) and (b) respectively.

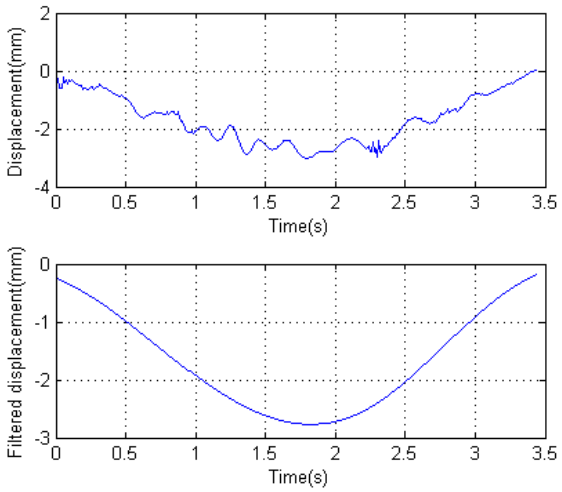

(a) The truck over lane 1

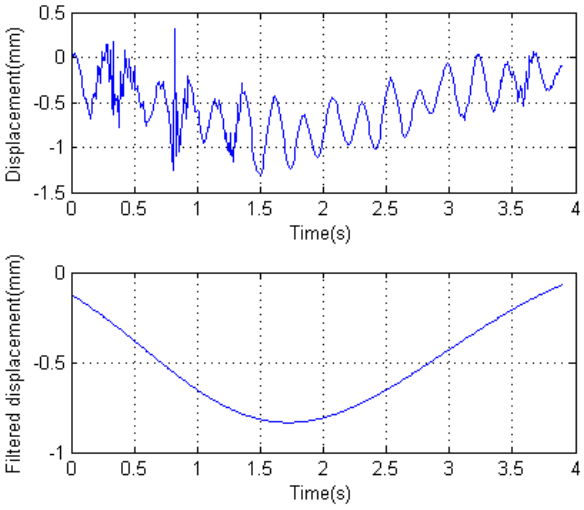

(b) The truck over lane 2

Fig 5.28 Displacement time history at T1 mid-span under truck speed of 30 km/h

When the truck ran over lane 1 and 2, the displacement time history at T2 are shown in Fig 5.29 (a) and (b) respectively.

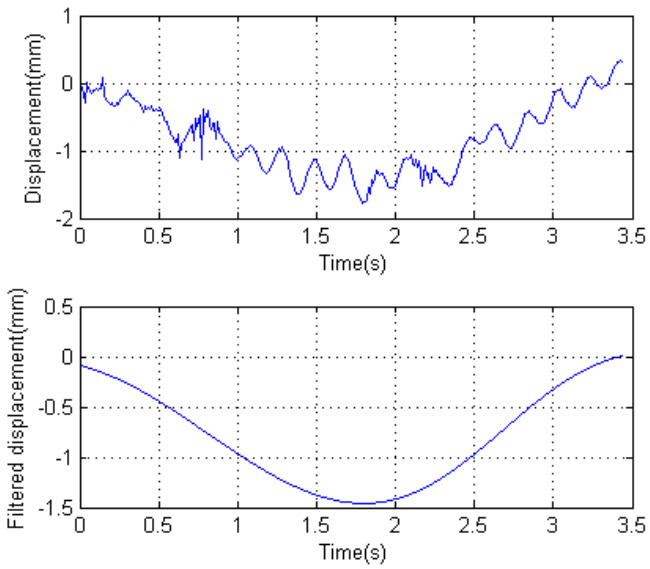

(a) The truck over lane 1

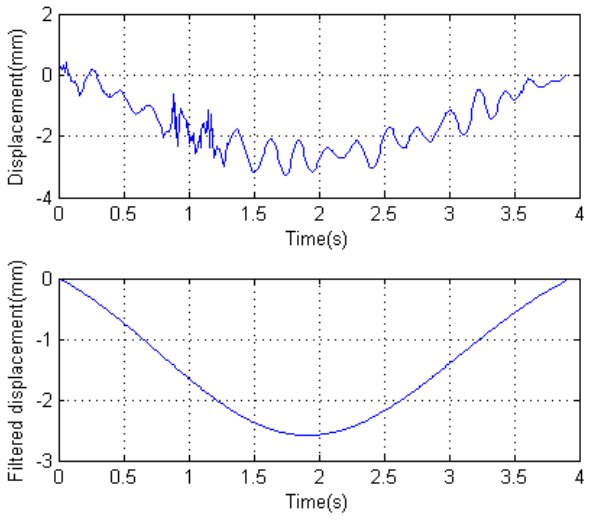

(b) The truck over lane 2

Fig 5.29 Displacement time history at T2 mid-span under truck speed of 30 km/h

5.4.4 The result analysis

From static loading truck configuration shown in Fig 5.20, it is known that truck 1 and 3 are at position of 22.4 m, and truck 2 and 4 are at position of 22.2 m. The values on the displacement time history at the corresponding positions are extracted and added

together. The mid-span displacement at T1 is obtained for three different truck speeds, as shown in Table 5.5. It is illustrated that they are all smaller than the static proof load test results, with the largest discrepancy of 10.3 %.

Table 5.5 Obtained displacement at mid-span of T1

Scenario	10 km/h	20 km/h	30 km/h	Static results
Obtained displacement (mm)	5.97 (10.3 %)	6.09 (8.6 %)	6.11 (8.3 %)	6.66

The mid-span displacement at T2 is also obtained for three different truck speeds, as shown in Table 5.6. It is illustrated that they are all smaller than the static proof load test results, with the largest discrepancy of 5.3 %.

Table 5.6 Obtained displacement at mid-span of T2

Scenario	10 km/h	20 km/h	30 km/h	Static results
Obtained displacement (mm)	6.8 (5.3 %)	6.97 (2.8%)	6.81 (5.0%)	7.17

The mid-span displacements at T1 and T2 are all smaller than the results in static proof load test, which is probably due to the fact that the load-deflection curve is not linear as the loading amplitude increases (Budette and Goodpasture, 1972). As the loading increases, it is possible that some cracks in the girder opened, which reduced the stiffness of the girder, as pointed out by Saiidi et al. (1994). It is recommended that an amplification factor of 1.15 is adopted when using the proposed method to calculate the displacement.

Suppose RF_0, the load carrying capacity based on calculation is 1, the load rating factor is calculated. After multiplying the amplification factor 1.15, the obtained displacement from test is 6.97 and 7.89 for girder T1 and T2 respectively. Based on design, calculated displacement in FE analysis is 8.80 and 9.00 for girder T1 and T2 respectively.

Therefore, the load rating factor is obtained as 1.26 and 1.14 for the two girders, which demonstrates that load carrying capacity of the two girders can satisfy the design requirement. No truck weight limitation nor repair is needed.

5.5 Conclusions

In this Chapter, truck pass-by tests were conducted on two PC bridges. The test results are introduced with details, and the first test was used to estimate potential local stiffness loss and calibrate a FE bridge model. The second test was used to evaluate load carrying capacity as a substitute of traditional static proof load test. Results of the two bridge examples verified applicability of the load carrying capacity estimation method. The conclusions can be drawn as follows.

(1) Field test on a four span continuous viaduct model is performed. An FE model is calibrated by the field test, and artificial damage of tendon rupture and concrete crack is created to investigate curvature-based stiffness loss estimation method. The artificial damage was estimated to be 22.3% stiffness loss. This can provide reference for decision-making on repair or strengthening for the bridge operators.

(2) Truck pass-by test results is conducted on a PC bridge with testing time decreased from 3 hours to 12 minutes. And it has very little requirement on traffic closure time. The obtained displacement is around 10 % or less smaller than traditional static proof load test. An amplification factor of 1.15 is recommended, and load rating factor is calculated as 1.26 and 1.14 for the two girders. It is demonstrated that the proposed method could serve as an efficient substitute of the traditional static proof load test, which is especially suitable for expressway bridges or rural bridges.

Chapter 6 Conclusions and future work

6.1 Conclusions

In this dissertation, a systematic study on development and application of displacement-based load carrying capacity estimation method for girder bridges is performed. It uses the displacement induced by truck pass-by test with a Radar device for high-frequency and non-contact displacement measurement. Compared with traditional static proof load test, it can significantly reduce the testing time and labor cost. The method comprises two major tasks: local stiffness loss estimation and live load carrying capacity evaluation.

In the first task, for damaged bridges rated as Level 3 and 4, the damage locations are already detected by visual inspection and NDTs, but the stiffness loss is unknown. The truck pass-by test is used to estimate the local stiffness loss with no need of a base-line from previous tests. The stiffness loss estimation is of significant value for decision making on repairing and strengthening methodologies.

In the second task, a method is established to use truck pass-by test for live load carrying capacity evaluation, which can be a substitute to the traditional static proof-load test. As it can be conducted more frequently with less labor and time, it's especially useful for expressway bridges and rural road bridges. In the former, traffic closure time required by static proof load test is almost impossible; in the latter, traditional static proof load test is too costly in labor and time, considering the large bridge volume and less maintenance

budget.

The contribution of the research is four-fold.

First, the load carrying capacity estimation method is proposed, which includes stiffness loss estimation in a local scale, and live load carrying capacity evaluation in a global scale. Curvature (second derivative of displacement) is used as the indicator for stiffness loss estimation. Truck pass-by test is selected for field application, and a method is proposed to eliminate the dynamic part in the dynamic displacement for stiffness loss estimation, which is verified with numerical investigation.

Second, investigation and treatment of noise in displacement measurement are performed. A laboratory experiment showed the properties of noise in displacement measurement. A noise/damage effect ratio is defined to illustrate the effect of noise on curvature calculation results. Two approaches are proposed to reduce noise effects, and they are verified with the laboratory experiment.

Third, a Radar device is chosen to measure displacement in the proposed load carrying capacity estimation framework. Both laboratory and field tests were conducted to verify the precision of the Radar device. And multi-point measurements are utilized to predict displacement of unmeasured positions.

Fourth, the proposed load carrying capacity estimation method is verified with two examples of PC girder bridges. In the first PC girder bridge test, results showed no observable stiffness loss. And a calibrated FE model of the bridge with realistic artificial damage is investigated numerically, which estimated local stiffness loss of 22.3 %. The second PC bridge test indicates that the displacement obtained from the truck pass-by test

is around 2% ~ 10% smaller than result of the traditional static proof load test. With an amplification factor, it can efficiently substitute the traditional static proof load test, especially for expressway and rural bridges.

6.2 Future work

After Sasago Tunnel Accident in December, 2012, more and more emphasis have been put on infrastructure safety in Japan. The year of 2013 was called 'メンテナンス元年'(The start year of maintenance), and between 2014 and 2018, the percentage of inspection implementation for all the bridges is 99.9% (国土交通省道路局, 2019).

Once constructed, bridges are deteriorating due to harsh environment, increased traffic volume and heavy trucks year by year. As the bridges deteriorate, they bring more and more burden for bridge management and maintenance. Therefore, more efficient methodologies should be adopted in practice. The proposed load carrying capacity estimation method utilizes displacement induced by a truck pass-by test to evaluate the bridge capacity in both local and global scales. Though verification tests have been conducted on two PC bridges, full-scale tests on more bridge types, such as slab bridges and box girder bridges, are still advised to further widen the application of the proposed method.

From a broader perspective, inspection, online health monitoring and load carrying capacity evaluation methods are all means to achieve a better understanding of the bridges' status as a whole. They should be integrated and utilized to exploit the potential practical merits. One objective in this dissertation is intended to correlate inspection results (severe damages) with local stiffness loss and load carrying capacity of bridges. Likewise, online

health monitoring should be utilized together with inspection and load carrying capacity evaluation, to constitute a more reliable and sustainable bridge maintenance framework. Especially for rural bridges usually with less available budget, integration of the three methodologies in a probabilistic way would improve the budget utilization and allocation efficiency. Actions such as repair or strengthening could be taken more reasonably based on the results of these integrated methodologies.

Appendix A. Deduction of beam deflection formula

When there is no damage, there are two different expressions for bending moment, corresponding to two portions of the intact beam (S. Timoshenko, 1955). Deflection curve must therefore be written for each portion.

$$\begin{aligned} EI\frac{d^2y}{dx^2} &= -\frac{Pb}{l}x && 0 < x \le a \\ EI\frac{d^2y}{dx^2} &= -\frac{Pb}{l}x + P(x-a) && a \le x \le l \end{aligned} \tag{A.1}$$

In which, El is the flexural rigidity of the beam; P is the amplitude of the concentrated load; a, b and l are length of the left portion, right portion and the whole beam respectively.

Integrating these equations, we obtain

$$\begin{aligned} EI\frac{dy}{dx} &= -\frac{Pb}{2l}x^2 + C_1 && 0 < x \le a \\ EI\frac{dy}{dx} &= -\frac{Pb}{2l}x^2 + \frac{P(x-a)^2}{2} + C_2 && a \le x \le l \end{aligned} \tag{A.2}$$

Since the two portions of the deflection curve must have a common tangent at the loading point $x = a$, it is concluded $C_1 = C_2$. Perform the integration again, we obtain

$$
\begin{aligned}
EI \cdot y &= -\frac{Pb}{6l}x^3 + C_1 x + C_3 && 0 < x \le a \\
EI \cdot y &= -\frac{Pb}{6l}x^3 + \frac{P(x-a)^3}{6} + C_1 x + C_4 && a \le x \le l
\end{aligned}
\tag{A.3}
$$

At the loading point, $x = a$, the deflection curve has a common deflection, then we obtain $C_3 = C_4$. On the left end of the beam, deflection is zero, we obtain $C_3 = C_4 = 0$. On the right end of the beam, deflection is also zero, Substituting $y = 0$ and $x = l$ in the second expression, we obtain

$$
C_1 = \frac{Pb(l^2 - b^2)}{6l} \tag{A.4}
$$

Substituting all constants, we finally obtain the deflection curve

$$
y = \begin{cases} \dfrac{Pbx(l^2 - b^2 - x^2)}{6lEI}, & 0 \le x \le a \\ \dfrac{Pbx(l^2 - b^2 - x^2)}{6lEI} + \dfrac{P(x-a)^3}{6EI}, & a < x \le l \end{cases} \tag{A.5}
$$

If there is stiffness loss at area $[x_b, x_e]$, then similarly the beam deflection formula can be expressed in four portions on $[0, x_b]$ $[x_b, x_e]$ $[x_e, a]$ $[a, l]$. And the flexural rigidity at damage area is $EI_d = (1-\alpha)EI$.

The expressions are

$$
\begin{aligned}
EI\frac{d^2y}{dx^2} &= -\frac{Pb}{l}x && 0 < x \le x_b \\
EI_d\frac{d^2y}{dx^2} &= -\frac{Pb}{l}x && x_b < x \le x_e \\
EI\frac{d^2y}{dx^2} &= -\frac{Pb}{l}x && x_e < x \le a \\
EI\frac{d^2y}{dx^2} &= -\frac{Pb}{l}x + P(x-a) && a \le x \le l
\end{aligned}
\tag{A.6}
$$

Integrating the first time, we obtain

$$\begin{aligned}
EI\frac{dy}{dx} &= -\frac{Pb}{2l}x^2 + C_1 && 0 < x \le x_b \\
EI_d\frac{dy}{dx} &= EI(1-\alpha)\frac{dy}{dx} = -\frac{Pb}{2l}x^2 + C_2' && x_b < x \le x_e \\
EI\frac{dy}{dx} &= -\frac{Pb}{2l}x^2 + C_3 && x_e < x \le a \\
EI\frac{dy}{dx} &= -\frac{Pb}{2l}x^2 + \frac{P(x-a)^2}{2} + C_4 && a \le x \le l
\end{aligned} \tag{A.7}$$

For calculation convenience, the second equation can be modified,

$$\begin{aligned}
EI\frac{dy}{dx} &= -\frac{Pb}{2l}x^2 + C_1 && 0 < x \le x_b \\
EI\frac{dy}{dx} &= -\frac{Pb}{(1-\alpha)2l}x^2 + C_2 && x_b < x \le x_e \\
EI\frac{dy}{dx} &= -\frac{Pb}{2l}x^2 + C_3 && x_e < x \le a \\
EI\frac{dy}{dx} &= -\frac{Pb}{2l}x^2 + \frac{P(x-a)^2}{2} + C_4 && a \le x \le l
\end{aligned} \tag{A.8}$$

Because adjacent portions have the common tangent at the shared point, we have

$$\begin{aligned}
-\frac{Pb}{2l}x_b^{\,2} + C_1 &= -\frac{Pb}{(1-\alpha)2l}x_b^{\,2} + C_2 \\
-\frac{Pb}{(1-\alpha)2l}x_e^{\,2} + C_2 &= -\frac{Pb}{2l}x_e^{\,2} + C_3
\end{aligned} \tag{A.9}$$

$$C_3 = C_4$$

Integrating the second time, we obtain

$$
\begin{aligned}
EI \cdot y &= -\frac{Pb}{6l}x^3 + C_1 x + C_5 && 0 < x \le x_b \\
EI \cdot y &= -\frac{Pb}{(1-\alpha)6l}x^3 + C_2 x + C_6 && x_b < x \le x_e \\
EI \cdot y &= -\frac{Pb}{6l}x^3 + C_3 x + C_7 && x_e < x \le a \\
EI \cdot y &= -\frac{Pb}{6l}x^3 + \frac{P(x-a)^3}{6} + C_4 x + C_8 && a \le x \le l
\end{aligned}
\tag{A.10}
$$

Because adjacent portions have the common deflection at shared point, we have

$$
\begin{aligned}
-\frac{Pb}{6l}x_b{}^3 + C_1 x_b + C_5 &= -\frac{Pb}{(1-\alpha)6l}x_b{}^3 + C_2 x_b + C_6 \\
-\frac{Pb}{(1-\alpha)6l}x_e{}^3 + C_2 x_e + C_6 &= -\frac{Pb}{6l}x_e{}^3 + C_3 x_e + C_7
\end{aligned}
\tag{A.11}
$$

$$C_7 = C_8$$

On the left end of the beam, deflection is zero, we obtain $C_5 = 0$. On the right end of the beam, deflection is also zero, Substituting $y = 0$ and $x = l$ in the expression of deflection on $[a, l]$, we obtain

$$
-\frac{Pb}{6l}l^3 + \frac{P(l-a)^3}{6} + C_4 l + C_8 = 0 \tag{A.12}
$$

With eight unknowns and eight equations, we are able to obtain

$$
\begin{aligned}
C_1 &= \frac{Pb(l^2-b^2)}{6l} + \frac{\alpha}{1-\alpha}\frac{Pb}{3l^2}(x_b^3 - x_e^3) - \frac{\alpha}{1-\alpha}\frac{Pb}{2l}(x_b^2 - x_e^2) \\
C_2 &= \frac{Pb(l^2-b^2)}{6l} + \frac{\alpha}{1-\alpha}\frac{Pb}{3l^2}(x_b^3 - x_e^3) + \frac{\alpha}{1-\alpha}\frac{Pb}{2l}x_e^2 \\
C_3 &= C_4 = \frac{Pb(l^2-b^2)}{6l} + \frac{\alpha}{1-\alpha}\frac{Pb}{3l^2}(x_b^3 - x_e^3) \\
C_5 &= 0 \\
C_6 &= -\frac{\alpha}{1-\alpha}\frac{Pb}{3l}x_b^3 \\
C_7 &= C_8 = -\frac{\alpha}{1-\alpha}\frac{Pb}{3l}(x_b^3 - x_e^3)
\end{aligned}
\tag{A.13}
$$

Substituting all constants, we finally obtain the deflection curve for a damaged beam,

$$y=\begin{cases}
-\dfrac{Pb}{6lEI}x^3+\dfrac{1}{EI}\left(\dfrac{Pb(l^2-b^2)}{6l}+\dfrac{\alpha}{1-\alpha}\dfrac{Pb}{3l^2}(x_b^3-x_e^3)-\dfrac{\alpha}{1-\alpha}\dfrac{Pb}{2l}(x_b^2-x_e^2)\right)x & 0<x\le x_b \\
-\dfrac{Pb}{(1-\alpha)6lEI}x^3+\dfrac{1}{EI}\left(\dfrac{Pb(l^2-b^2)}{6l}+\dfrac{\alpha}{1-\alpha}\dfrac{Pb}{3l^2}(x_b^3-x_e^3)+\dfrac{\alpha}{1-\alpha}\dfrac{Pb}{2l}x_e^2\right)x-\dfrac{\alpha}{1-\alpha}\dfrac{Pb}{3lEI}x_b^3 & x_b<x\le x_e \\
-\dfrac{Pb}{6lEI}x^3+\dfrac{1}{EI}\left(\dfrac{Pb(l^2-b^2)}{6l}+\dfrac{\alpha}{1-\alpha}\dfrac{Pb}{3l^2}(x_b^3-x_e^3)\right)x-\dfrac{\alpha}{1-\alpha}\dfrac{Pb}{3l}(x_b^3-x_e^3) & x_e<x\le a \\
-\dfrac{Pb}{6lEI}x^3+\dfrac{P(x-a)^3}{6EI}+\dfrac{1}{EI}\left(\dfrac{Pb(l^2-b^2)}{6l}+\dfrac{\alpha}{1-\alpha}\dfrac{Pb}{3l^2}(x_b^3-x_e^3)\right)x-\dfrac{\alpha}{1-\alpha}\dfrac{Pb}{3l}(x_b^3-x_e^3) & a\le x\le l
\end{cases} \tag{A.14}$$

Appendix B. Curvature change for different measurement scenarios

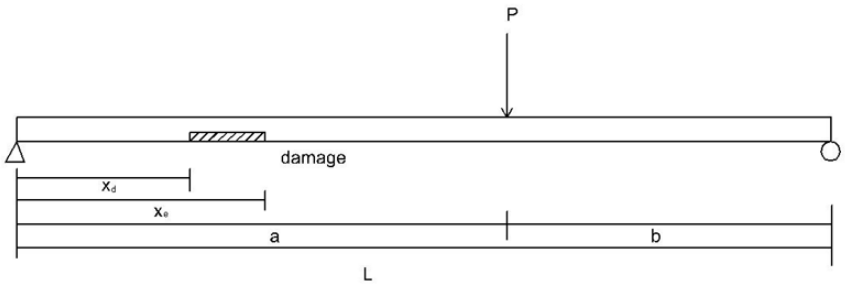

Fig B.1 Simply supported beam with damage

Suppose a simply supported beam with length L as shown in Fig B.1, and the damage range is between x_d and x_e. The stiffness is EI and αEI for the intact and damaged parts respectively. The beam deflection formula can be expressed as Equation (A.14) in four portions on $[0, x_d]$ $[x_d, x_e]$ $[x_e, a]$ $[a, L]$. Here a denotes position of the concentrated load, and $b = L - a$.

When estimating the stiffness loss in damage range, different cases of measurement point configuration should be considered. Suppose there is damage on a beam, and curvature figure is calculated from displacement measurement. It is noted that only the displacement measurements near the damage range are affected. Specifically, in curvature calculation equation, displacement data at three coordinates $x - \Delta x, x, x + \Delta x$ are used. Totally there are five different cases of configuration of measurement points near the damage range (Fig B.2). The three highlighted points in each case refer to the three data positions for curvature calculation.

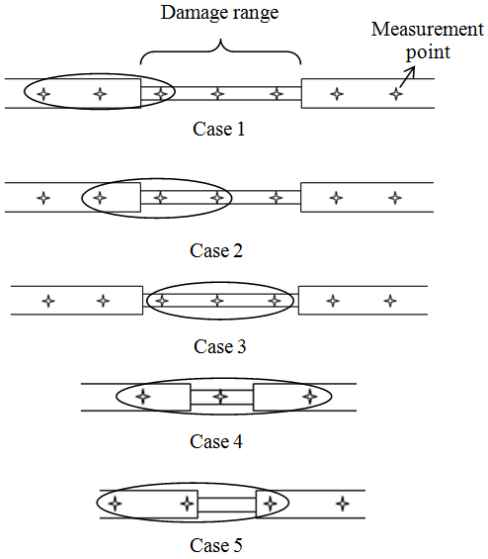

Fig B.2 Different cases of measurement point configuration for curvature calculation

Based on deflection formula of a damaged beam, the relation between curvature change $\frac{\Delta\kappa}{\kappa_i}$ and stiffness loss α is derived as $\frac{\Delta\kappa}{\kappa_i}=\frac{\alpha}{1-\alpha}f_r(x_d,x_e,x_{j-1},x_j,x_{j+1})$. For different cases, the expressions are as follows.

$$\begin{cases} f_r(x_d,x_e,x_{j-1},x_j,x_{j+1})=\dfrac{-2x_d^3+3x_{j+1}x_d^2-x_{j+1}^3}{-\left(x_{j-1}^3-2x_j^3+x_{j+1}^3\right)} & for\ \ case\ \ 1 \\ f_r(x_d,x_e,x_{j-1},x_j,x_{j+1})=\dfrac{2x_d^3+(3x_{j+1}-6x_j)x_d^2+2x_j^3-x_{j+1}^3}{-\left(x_{j-1}^3-2x_j^3+x_{j+1}^3\right)} & for\ \ case\ \ 2 \\ f_r(x_d,x_e,x_{j-1},x_j,x_{j+1})=1 & for\ \ case\ \ 3 \\ f_r(x_d,x_e,x_{j-1},x_j,x_{j+1})=\dfrac{2x_j^3-6x_jx_d^2+3x_{j+1}[x_d^2-x_e^2]+2[x_d^3+x_e^3]}{-\left(x_{j-1}^3-2x_j^3+x_{j+1}^3\right)} & for\ \ case\ \ 4 \\ f_r(x_d,x_e,x_{j-1},x_j,x_{j+1})=\dfrac{3x_{j+1}[x_d^2-x_e^2]-2[x_d^3-x_e^3]}{-\left(x_{j-1}^3-2x_j^3+x_{j+1}^3\right)} & for\ \ case\ \ 5 \end{cases} \quad \text{(B.1)}$$

where $\frac{\Delta\kappa}{\kappa_i}$ denotes curvature change; α denotes stiffness loss level; x_d and x_e denote coordinates of starting point and end point of the damage range; and x_{j-1},x_j,x_{j+1} denote coordinates of the three points in each case. $\Delta\kappa=\kappa_d-\kappa_i$; κ_d is directly obtained from

curvature results; κ_i is calculated from linear fitting of curvature values in the intact section. For case 3, stiffness loss can be calculated directly from the curvature change. For other four cases, damage range coordinates x_d and x_e are needed.

Reference

AASHTO. (2011). The Manual for Bridge Evaluation, American Association of State Highway and Transporation Officials, Washington.DC

AASHTO LRFR, Guide Manual for Condition Evaluation and Load and Resistance Factor Rating (LRFR) of Highway Bridges, American Association of State Highway and Transportation Officials, US, 2003.

Alfredo H-S. Ang; Wilson H. Tang. (1975). Probability Concepts in Engineering Planning and Design, Volume 1 Basic Principles. Newyork: John Wiley & Sons, Inc.

Asta, A. D., & Dezi, L. (1996). Discussion on Prestressed force effect on vibration frequency of concrete bridges. Journal of Structural Engineering , 458-460.

Bakht B, Jaeger LG. (1990). Bridge testing-a surprise every time. J Struct Engng, ASCE 116(5):1370–83.

Banan, M., Banan, M., & Hjelmstad, K. (1994). Parameter estimation of structures from static response. I: Computational aspects. ASCE, Journal of Structural Engineering , 120, 3243-3258.

Banan, M., Banan, M., & Hjelmstad, K. (1994). Parameter estimation of structures from static response. II: Numerical Simulation Studies. ASCE, Journal of Structural Engineering , 120, 3259-3283.

Bilello C. and Bergman L.A.. (2004). Vibration of damaged beams under a moving mass: theory and experimental valdation. Journal of sound and vibration , 274, 567-582.

Brownjohn, J.M.W., Xia, P.Q., Hao, H. and Xia, Y. (2001). Civil structure condition assessment by FE model updating: methodology and case studies, Finite Elements in Analysis and Design, Vol. 37, No. 10, pp. 761–775.

Budette E.G; Goodpasture D.W. （1974）. Test to failure of a prestressed concrete bridge. PCI Journal. 19(3):92-103. DOI: 10.15554/pcij.05011974.92.103.

Cai, C.S. and Shahawy, M. (2003). Understanding capacity rating of bridges from load tests, Practice Periodical on Structural Design and Construction, Vol. 8, No. 4, pp. 209–216.

Casas, J. R., and Gómez, J. D. (2013). Load rating of highway bridges by proof-loading. KSCE J. Civil Eng. 17, 556–567. doi: 10.1007/s12205-013-0007-8

Chajes, M.J., Mertz, D.R. and Commander, B. (1997). Experimental load rating of a posted bridge, Journal of Bridge Engineering, ASCE, Vol. 2, No. 1, pp. 1–10.

Cheng, C.-C., Yu, C.-P., Ke, Y.-T., & Hsu, K.-T. (2012). Evaluation of bridge span by recovered stiffness data obtained with moving vehicle loadings. Proceedings of SPIE, Health Monitoring of Structural and Biological Systems. San Diego, California, USA.

Choi, I.-Y., Lee, J. S., Choi, E., & Cho, H.-N. (2004). Development of elastic damage load theorem for damage detection in a statically determinate beam. Computers and Structures , 82, 2483-2492.

Danish Road Directorate, Calculation of Load Carrying Capacity for Existing Bridges, Guideline Document, Ministry of Transport—Denmark, 1996.

Danish Road Directorate, Reliability Based Classification of the Load Carrying Capacity of Existing Bridges, Guideline Document, Report 291, Ministry of Transport—Denmark, 2004.

David K. Barton, Sergey A. Leonov. (1998). Radar Technology Encyclopedia. Boston. London. : Artech House.

Deng, L; Cai, C.S. (2010). Development of dynamic impact factor for performance evaluation of existing multi-girder concrete bridges. Engineering Structures , 32, 21-31.

Deng L.; Cai. C.S. (2010). Identification of dynamic vehicular axle loads: theory and simulations. Journal of vibration and Control , 16 (14), 2167-2194.

Dimarogonas, A. (1996). Vibration of cracked structures- a state of the art review.

Engineering fracture mechanics , 55 , 831-857.

Ding, L., Hao, H., Xia, Y., & Deeks, A. J. (2012). Evaluation of Bridge Load Carrying Capacity Using Updated Finite Element Model and Nonlinear Analysis. Advances in Structural Engineering, 15(10), 1739–1750. https://doi.org/10.1260/1369-4332.15.10.1739

Dionysius, M., & Fujino, Y. (2012). Estimating bridge fundamental frequency from vibration response of instrumented passing vehicle' analytical and experimental study. Advances in structural engineering , 15 (3), 443-459.

Dionysius, M. S., Fujino, Y., and Nagayama T. (2013). Dynamic Characteristics of an Overpass Bridge in a Full-Scale Destructive Test. Journal of Engineering Mechanics ASCE, 139, 691-701.

Dodds, C. J. and Robson, J. D. (1973). The description of road surface roughness. Journal of Sound and Vibration , 31 (2), 175-183.

Doebling, S. W., Farrar, C. R., & B.Prime, M. (1998). A summary review of vibration-based damage identification methods. The shock and Vibration Digest , 30 (2), 91-105.

Faber M. H., Val D. V., (2000). Stewart M G, Proof load testing for bridge assessment and upgrading. Engineering Structures. (22): 1677–1689.

Farrar, C. R., & K.Worden. (2007). An introduction to structural health monitoring. Philosophical Transactions of The Royal Society A , 365, 303–315.

Farrar, C., Darling, T., Migliori, A., & Baker, W. (1999). Microwave interferometers for non-contact vibration measurements on large structures. Mechanical Systems and Signal Processing , 13 (2), 241-253.

Farrar, C., Scott, W., Doebling, S., & David, A. (2001). Vibration-based structural damage identification. Phyilosophical Transactions of Royal Society , 359, 131-149.

FHWA. National Bridge Inspection Standards (NBIS), Federal Highway Administation.

FHWA. “Bridge Inspector’s Reference Manual” Federal Highway Administation.

Fraden, J. (2010). Handbook of Modern Sensors, the fourth edition. Springer.

Freyermuth, C. (2001). Status of the durability of post-tensioning tendons in the United States. Durability of post-tensioning tendons. Ghent, Belgium.

Fryba, L. (1999). Vibration of solids and structures under moving loads. Prague: Academia Prague.

Fujino, Y. (2005). Developement of vehicle intelligent monitoring system (VIMS). Proceedings of SPIE International Symposia on Smart Structures & Materials/NDE. San Diego.

Fujino Y, Lind NC. (1977). Proof-load factors and reliability. J Struct Engng, ASCE;103(4):853–70.

Ghosn, M., Moses, F. and Gobieski, J. (1986). Evaluation of steel bridge using in-service

testing, Transportation Research Record, No. 1072, pp. 71–78.

Gentile, C. (2010). Radar-based measurement of deflections on bridges and large structures: advantages, limitations and possible applications. IV ECCOMAS Thematic Conference on Smart Structures and Materials.

Gonzalez, A. (2010). Finite Element Analysis: Vehicle-bridge dynamic interaction using finite element modeling. Sciyo.

Gonzalez, A; Hester, D. (2009). The use of wavelets on the response of a beam to a calibrated vehicle for damage detection. The E-Journal & Exhibition of Nondestructive Testing in Civil Engineering. Nantes, France.

Green M.F.; Cebon D. (1997). Dynamic interaction between heavy vehicles and highway bridges. Computers & Structures , 62 (2), 253-264.

Gumbel, E. (1954). Statistical theory of extreme values and some practical applications, Applied Mthematics Series 33. Washington, D.C. : National Bureau of Standards.

Harik, I. E., Shaaban, A. M., Gesund, H., Valli, G. Y. S., and Wang, S. T. (1990). United States bridge failures, 1951–1988. J. Perform. Constr. Facil., 10.1061/(ASCE)0887-3828(1990)4:4(272), 272–277.

Hester D.; Gonzalez A. (2012). A wavelet-based damage detection algorithm based on bridge acceleration response to a vehicle. Mechanical systems and signal processing , 28, 145-166.

Henchi,K.; Fafard, M.; Talbot, M.& Dhatt, G. (1998). An efficient algorithm for dynamic analysis of bridges under moving vehicles using a coupled modal and physical components approach. Journal of Sound and Vibration , 212 (4), 663-683.

Henderson F. M and Lewis A. J. (1998). Principles and applications of imaging radar. Manual of remote sensing. Wiley & Sons.

Highways Agency, Design Manual for Road and Bridges, Highway Structures: Inspection and Maintenance—Assessment, Vol. 3, Sec. 4, UK, 2006.

Hoon Sohn et al. (1999). An experimental study of temperature effect on modal parameters of teh Alamosa Canyon bridge. Earthquake engineering and structural dynamics , 28, 879-897.

Huang, K. (2001). Patent No. US 6192758 B1. United States.

Inglis, C. E. (1934). A Mathematical treatise on vibration in railways bridges. Cambridge At The University Press.

Iwaki, I. (2010). Properties of concrete and reinforcing steel in PC bridges girders severely damaged in coastal environment. Safety, reliability and risk of structures, infrastructures and engineering systems. London: Taylor & Francis Group.

Jang, J. B., Lee, H. P., & Song, K. M. (2010). A sensitivity analysis of the key parameters for the prediction of the prestress force on bonded tendons. Nuclear Engineering and technology , 42 (3), 319-328.

Jauregui, D.U. and Barr, P.J. (2004). Nondestructive evaluation of the I-40 Bridge over the Rio Grande River, Journal of Performance of Constructed Facilities, Vol. 18, No. 4, pp. 195–204.

Jekins, C., Kjerengtroen, L., & Oestensen, H. (1997). Sensitivity of parameter changes in structural damage detection. Shock and Vibration , 4 (1), 23-37.

Jungwirth, D. (2001). Problems, solutions and developments for post-tensioning tendons from the German point of view. Durability of post-tensioning tendons. Ghent, Belgium.

Kim, C.W.; Kawatani, M. & Kim, K.B. (2005). Three-dimentional dynamic analysis for

bridge-vehicle interaction with roadway roughness. Computers and Structures , 83, 1627-1645.

Kwasniewski, L.; Li, H.; Wekezer, J. & Malachowski, J. (2006). Finite element analysis of vehicle-bridge interaction. Finite elements in analysis and design , 42, 950-959.

Law S.S.; Zhu X.Q. (2004). Dynamic behavior of damaged concrete bridge structures under moving vehicular loads. Engineering Structures , 26, 1279-1293.

Lee, J., Kim, J., Yun, C., Yi, J., Shim, J. (2002). Health-monitoring method for bridges under ordinary traffic loadings. Journal of Sound and Vibration , 257 (2), 247-264.

Lin, T. Y. (1955). Design of prestressed concrete structures. New York, London: John Wiley & Sons, Inc.

Majumder L.; Manohar C.S. (2003). A time-domain approach for damage detection in beam structures using vibration data with a moving oscillator as an excitation source. Journal of Sound and Vibration , 268, 699-716.

Mahamound, M. (2001). Stress intensity factors for single and double edge cracks in a simple beam subjected to a moving load. International Journal of Fracture , 111, 151-161.

Mahamound M. A.; Zaid. M.A. (2002). Dynamic response of a beam with a crack subject to a moving mass. Journal of Sound and Vibration , 256, 591-603.

Mathy, B.; Demars, P.; Roisin, F. and Wouters, M. (1996). Investigation and strengthening study of twenty damaged bridges: A Belgium Case history. Proceedings of the 3rd International Conference on Bridge Management, (pp. 658-666). London.

Mazurek, D., & Dewolf, J. (1990). Experimental study of bridge monitoring technique. Journal of Structural Engineering , 116 (9), 2532-2549.

Menn, C. (1990). Prestressed Concrete Bridges. Basel Bostion Berlin: Birkhauser Verlag.

Meredith J. and Gonzalez. A. (2012). Theoretical testing of an empirical mode decomposition damage detection approach using a spatial vehicle-bridge interaction model. Bridge Maintenance, Safety, Management, Resilience and Sustainability (pp. 438-445). Taylor & Francis Group, London.

Ministry of Land, Infrastructure, Transportation, and Tourism (2014). Manual for Bridge Periodic Inspection. Tokyo: Ministry of Land, Infrastructure, Transportation, and Tourism.

Ministry of Transport, China. Specifications for Inspection and Evaluation of Load-bearing Capacity of Highway Bridges, JTG /T-J21–2011, 2011

Nabil F. Grace; Brian Ross. (1996). Dynamic characteristics of post-tensioned girders with web openings. Journal of Structural Engineering , 122 (6), 643-650.

Nguyen K. V., Tran H.T. (2010). Multi-cracks detection of a beam-like structure based on the on-vehicle vibration signal and wavelet analysis. Journal of Sound and Vibration. 329, 4455-4465.

Nowak, A.A. and Tharmabala, T. (1988). Bridge reliability evaluation using load tests,

Journal of Structural Engineering, ASCE, Vol. 114, No. 10, pp. 2268–2279.

Osada, K., Fujioka, A., Nojima, S., Ikeda, S. (June 5-8, 2006). Strengtheing of deteriorated prestressed concrete bridges with additional prestressing. Proceedings of the 2nd international congress. Naples, Italy.

Pandey, A., Biswas, M., & Samman, M. (1991). Damage detection from changes in curvature mode shapes. Journal of Sound and Vibration , 145 ((2)), 321-332.

Park, J.-H., Kim, J.-T., Ryu, Y.-S., & Lee, J.-M. (2007). Monitoring of cracks and prestress-loss in PSC girder bridges using vibration-based damage detection techniques. Proceedings of SPIE, 6532, 65321V.

Pesterev, A. V., Yang, B., Bergman, L., & Tan, C. (2003). Revisiting the moving force problem. Journal of Sound and Vibration , 261, 75-91.

Philip R. Bevington, D. Keith Robinson. (2003). Data reduction and error analysis for the physical sciences. New York: McGRAW- Hill book company. .

Proverbio, E. and Ricciardi, G. (2000). Failure of a 40 Year Old Post-tensioned Bridge Near Seaside. Proc. Int. Conf. Eurocorr 2000, (pp. 10-14). London.

Rens, K.L., Nogueira, C.L. and Transue, D.J. (2005). Bridge management and

nondestructive evaluation, Journal of Performance of Constructed Facilities, ASCE, Vol.

19, No. 1, pp. 3-16.

Saiidi M.; Douglas B.; Feng S. (1994). Prestress force effect on vibration frequency of

concrete bridges. Journal of Structural Engineering , 120 (7), 2233-2241.

Salawu O.S. and Williams C. (1995). Review of full-scaled dynamic testing of bridge structures. Engineering Structures , 17 (2), 113-121.

Salawu, O.S. (1997). Detection of structural damage through changes in frequency: a review. Engineering Structures , 19 (9), 718-723.

Sanayei, M., & onipede, O. (1991). Damage assessment of structures using static test data. AIAA Journal , 29 (7), 1174-1179.

Saraf V, Nowak AS. (1998) Proof load testing of deteriorated steel girder bridges. J Bridge Engng, ASCE; 3(2):82–9.

Shi ZY, Law SS, Zhang LM. (1998) Structural damage localization from modal strain energy change. J Sound Vib 218(5): 825–844.

Simmons, C. J. (1847). Report to the Commisioners of the railways. Chester and Holyhead Railway.

Sohn, H. (2007). Effects of environmental and operational variability on structural health monitoring. Philosophical transactions of the Royal Society of London. Series A: Mathematical, physical, and engineering sciences , 365, 539-560.

Stohr, S., Link, M., Rohrmann, R., & Rucker, W. (2006). Damage detection based on static measurements on bridge structures. Conference & Exposition on Structural Dynamics. St Louis, Missouri, USA.

Stokes, G. (1849). Discussion of a differential equation relating to the breaking of railway bridges. Transactions of the cambridge philosophical society , 8, 707-735.

Sun Z., Zou Z. and Zhang Y. (2017) Utilization of structural health monitoring in long-span bridges: case studies, *Structural Control and Health Monitoring*, e1979. doi: 10.1002/stc.1979.

Taylor, J. D. (2001). Ultra-wideband radar technology. . CRC Press.

The Concrete Society. (2002). Concrete Society Technical Report No. 47.

Timoshenko S.P, J.N Goodier. (1951). Theory of Elasticity. New York: McGRAW- Hill book company.

Timoshenko, S. P. (1953). History of the strength of materials. New York: D. Van Nostrand Company.

Timoshenko, S. P. (1955). Strength of Materials. New York: D.Van Nostrand Company.

Wardhana, K., and Hadipriono, F. C. (2003). Analysis of recent bridge failures in the United States. J. Perform. Constr. Facil., 10.1061/(ASCE)0887-3828(2003)17:3(144), 144–150.

Weaver W.; Timoshenko S. P.; Young D. H. (1990). Vibration problem in engineering. New York: John Wiley and Sons.

Wenzel, H. (2009). Health monitoring of bridges. John Wiley and Sons.

Willis, R. (1849). Appendix to the report of the commissioners appointed to inquire into the application of iron to railway structures. London: H. M. Stationery office.

Wisniewski, D., Casas, J. R., and Ghosn, M. (2012). Codes for Safety assessment of existing bridges - current state and further development. Struct. Eng. Int. 22:2. doi: 10.2749/101686612X13363929517857

Woodward, R., & Williams, F. (1988). Collapse of Ynys-s-Gwas bridge, West Glamorgan. Proceedings of Institute of Civil Engineers, 84, pp. 635-669.

Wyss J. C., Su D., Fujino Yo. (2011). Prediction of vehicle-induced local responses and application to a skewed girder bridge. Engineering Structures , 33 (4), 1088-1097.

Xia Yong et al. (2011). Temperature effect on variation of structural frequencies: from laboratory testing to field monitoring. The 6th international workshop on advanced smart materials and smart structures technology. Dalian, China.

Xu F. Y., Zhang M. J., Wang L. and Zhang J. R. (2016). Recent Highway Bridge Collapses in China: Review and Discussion. Journal of Performance of Constructed Facilities. 30(5): 04016030

Yam, L. H., Li, Y., & Wong, W. (2002). Sensitivity studies of parameters for damage detection of plate-like structures using static and dynamic approaches. Engineering Structures , 24, 1465-1475.

Yang, Y. B. & Lin B.H. (1995). Vehicle-bridge interaction analysis by dynamic

condensation method. Journal of Structural Engineering , 121 (11), 1636-1643.

Yang, Y.B. & Yau, J.D. (1997). Vehicle-bridge interaction element for dynamic analysis. Journal of Structural Engineering , 123 (11), 1512-1518.

Zhu, X.Q., Law, S.S. (2002). Dynamic load on continuous multi-lane bridge deck from moving vehicles. Journal of Sound and Vibration , 251 (4), 697-716.

Zhu X.Q., Law S.S. (2006). Wavelet-based crack identification of bridge beam from operational deflection time history, International Journal of Solids and Structures, 43, 2299-2317.

青木圭一 プレストレストコンクリート橋におけるPC鋼材破断とその調査および性能評価に関する研究，2015

国土交通省道路局. (2019). 道路メンテナンス年報.　令和元年８月.

国土交通省(2007) 道路橋の予防保全に向けた有識者会議（第 1 回）参考資料、平成 19 年 10 月 24 日

土木研究所. (2001). 塩害を受けた PC 橋の耐荷力評価に関する研究(Ⅰ): プレテンション PC 桁の載荷試験. 土木研究所資料第 3808 号.

土木研究所. (2001). 塩害を受けた PC 橋の耐荷力評価に関する研究(Ⅰ): プレテンション PC 桁の載荷試験. 土木研究所資料第 3808 号.

土木研究所. (2001). 塩害を受けた PC 橋の耐荷力評価に関する研究（ＩＩ）旧暮坪陸橋の載荷試験. 土木研究所資料第 3809 号.

土木研究所. 塩害を受けた PC 橋の耐荷力評価に関する研究（ＩＶ）　旧芦川橋の載荷試験. 土木研究所資料第 3816 号.

寺田典生（2015）プレストレストコンクリート橋における PC グラウト充填状況に着目した維持管理のあり方に関する研究，京都大学